# Noise-Free Dynamic Rank-Adaptation via Riemannian Methods in Federated Fine-Tuning

**Zihan Zhou**[1] **Yang Zhou**[1*] **Tianshi Che**[1] **Zeru Zhang**[1] **Jiaxiang Ren**[1]
**Da Yan**[2] **Zhe Jiang**[3] **Yelong Shen**[4] **Ruoming Jin**[5] **Jianfeng Gao**[4]
[1]Auburn University [2]Indiana University Bloomington [3]University of Florida
[4]Microsoft Research [5]Kent State University *Corresponding author: yangzhou@auburn.edu

## Abstract

Rank-adaptive low-rank adaptation (LoRA), a parameter-efficient fine-tuning (PEFT) technology, has achieved state-of-the-art performance in fine-tuning foundation models (FM). Directly transplanting the rank-adaptive LoRA methods from centralized learning to federated learning raises two critical issues: aggregation noise and rank drift. We presents Riemannian LoRA algorithm with adaptive rank for federated fine-tuning of foundation models (FFT-FM), RAFFT, which resolves both issues and significantly improves the computational cost. First, by utilizing Riemannian Procrustes analysis, we propose a Riemannian parameter matching method to avoid aggregation noise and ensure effective FFT-FM with rank-adaptive LoRA while cutting SVD cost by decomposing only low-dimensional $r \times r$ matrices, where $r$ is the rank parameter in the LoRA. We theoretically derive the equivalence between our RAFFT algorithm with rank-adaptive LoRA for the FFT-FM and the standard FFT-FM on the full parameter matrices based on FedAvg and verify the bounded error introduced by approximation. Second, by leveraging Riemannian manifold theory, we develop a Riemannian gradient descent (RGD) method to guarantee the local full parameter matrices on clients in the form of low-rank ones with fixed rank optimized by the server in each FFT-FM round, for alleviating the rank-drift issue to speed up the convergence of RAFFT. We theoretically demonstrate that the RGD optimization on the Riemannian manifold ensures the rank invariance during the local update process and the RGD optimization can converge in the FFT-FM context. Our source code is available at `https://github.com/zzz0134/RAFFT`.

Proceedings of the 29[th] International Conference on Artificial Intelligence and Statistics (AISTATS) 2026, Tangier, Morocco. PMLR: Volume 300. Copyright 2026 by the author(s).

## 1 INTRODUCTION

Parameter-efficient fine-tuning (PEFT) for fine-tuning of foundation models (FT-FM) has attracted active research in recent years, such as adapter tuning (Houlsby et al., 2019; Lin et al., 2020; Pfeiffer et al., 2021; Rücklé et al., 2021; He et al., 2022), prefix tuning (Li and Liang, 2021), P-Tuning (Liu et al., 2021b), P-Tuning V2 (Liu et al., 2021a), low-rank adaptation (LoRA) (Hu et al., 2022), and prompt tuning (Lester et al., 2021; Li and Liang, 2021). These methods freeze the backbone parameters (i.e., original weights of pre-trained FMs) and adjust only a small portion of parameters (i.e., adapter weights during the FT phase), to improve the efficiency. Among the above PEFT approaches, LoRA has achieved the state-of-the-art FT performance (Hu et al., 2022). The idea of the LoRA method can be illustrated as follows: $\mathbf{W} = \mathbf{W}_0 + \Delta\mathbf{W} = \mathbf{W}_0 + \mathbf{BA}$, where $\mathbf{W} \in \mathbb{R}^{m\times n}$ is the complete parameter of a FM. $\mathbf{W}_0$ and $\Delta\mathbf{W}$ are the backbone (pre-trained FM parameters) and adapter parameters respectively. A low-rank decomposition $\Delta\mathbf{W} = \mathbf{BA}$ where $\mathbf{B} \in \mathbb{R}^{m\times r}$, $\mathbf{A} \in \mathbb{R}^{r\times n}$, and rank $r << \min(m, n)$. During the FT phase, only $\mathbf{B}$ and $\mathbf{A}$ are trained while freezing $\mathbf{W}_0$ on the clients. Notice that in the LoRA-style methods, rank $r$ is often user-defined and keeps unchanged during the entire FT process.

In order to further enhance the performance of the LoRA-style methods, various rank-adaptive LoRA methods have been recently proposed to dynamically allocate the ranks among parameter matrices based on their importance: assigning more/less trainable parameters with higher/lower ranks to the criti-

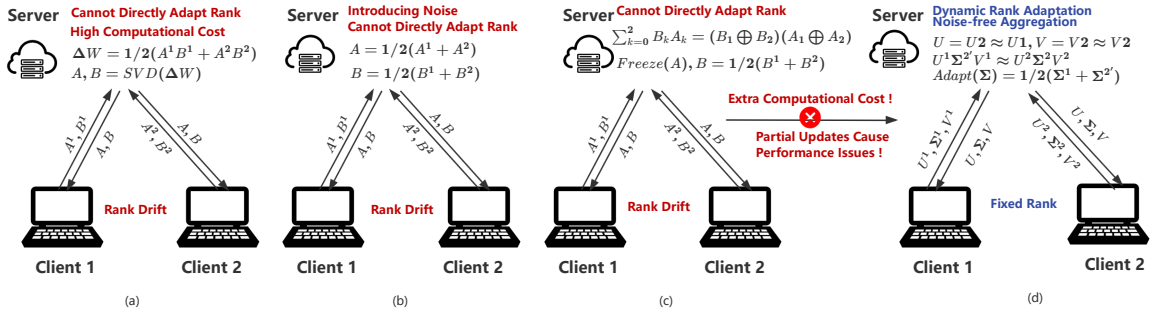


Figure 1: FFT-FM aggregation approaches: (a) full-matrix FedAvg; (b) noisy low-rank aggregation; (c) noise-free existing methods; (d) RAFFT noise-free dynamic-rank adaptation.

$$\underbrace{\frac{1}{2}\left(\mathbf{U}^1+\mathbf{U}^2\right)\times\frac{1}{2}\left(\mathbf{\Sigma}^1+\mathbf{\Sigma}^2\right)\times\frac{1}{2}\left(\mathbf{V}^1+\mathbf{V}^2\right)}_{\text{Parameter aggregation with SVD-based rank-adaptive LoRA + FedAvg}} \neq \underbrace{\frac{1}{2}\left(\mathbf{U}^1\mathbf{\Sigma}^1\mathbf{V}^1+\mathbf{U}^2\mathbf{\Sigma}^2\mathbf{V}^2\right)=\frac{1}{2}(\Delta\mathbf{W}^1+\Delta\mathbf{W}^2)=\Delta\mathbf{W}}_{\text{Ideal parameter aggregation with FedAvg on full parameter matrices}} \quad (1)$$

cal/insignificant parameter matrices for better model performance/efficiency. These methods can be broadly classified into two categories: (1) SVD-based approaches in centralized fine-tuning (CFT) dynamically adjust the ranks by truncating singular values in the form of SVD (Zhang et al., 2023b; Ding et al., 2023; Zhang et al., 2023a); (2) Rank sampling-based algorithms in both CFT and federated fine-tuning (FFT) search for the best rank by sampling a range of ranks and sorting the representations learnt by the model at different ranks during training (Valipour et al., 2023; Rajabzadeh et al., 2024; Xu et al., 2024). They need to fine-tune the model multiple times at different ranks, raising non-trivial cost. Several pioneering rank-adaptive LoRA algorithms for FFT-FM iteratively aggregate local full parameter metrics into a global one and perform the SVD on the latter to find the optimal rank (Chai et al., 2022; Wu et al., 2021; Niu et al., 2023). However, iterative SVD on the high-dimensional full parameter matrices is prohibitive.

Figure 1 (a) shows ideal FedAvg (McMahan et al., 2017) aggregation over the full parameter matrices, but this approach has prohibitive computational cost and cannot adjust the rank dynamically. In Figure 1 (b) a straightforward idea is to aggregate each client's low-rank update matrix, but recent work (Sun et al., 2024; Wang et al., 2024a; Singhal et al., 2025; Guo et al., 2025; Koo et al., 2024; Nguyen et al., 2024) shows this injects aggregation noise, so we cannot apply the SVD-based rank-adaptive LoRA directly in federated fine-tuning. Meanwhile, dynamic rank adaptation makes the problem even harder. Figure 1 (c) shows that existing methods aggregate only $\mathbf{A}^k$ and $\mathbf{B}^k$ and cannot adjust the rank directly. Extending them to support dynamic rank adaptation requires extra operations such as SVD, which greatly increases computation cost, and approaches that freeze one factor during updates cause performance issues. Figure 1 (d) shows our method adjusts the rank directly from $\mathbf{\Sigma}^k$ without any additional steps. For a detailed analysis, please refer to Appendix A.2. We formalize the mismatch between LoRA-based aggregation and ideal FedAvg in Eq.(1), where the left side denotes the parameter aggregation of FFT-FM with LoRA, while the right side represents the standard parameter aggregation of FFT-FM. The difference between two sides may become more significant when (1) the number of local update steps between aggregations is large and (2) the local datasets are different across clients. In this case, FFT-FM with LoRA may fail to converge and result in poor model performance.

Another significant challenge in FFT-FM with rank-adaptive LoRA is the rank-drift issue, caused by data heterogeneity (McMahan et al., 2017; Smith et al., 2017; Chen et al., 2018; Khodak et al., 2019; Sattler et al., 2019; Liu et al., 2019a; Hsieh et al., 2020), a common problem in federated learning. Rank-drift is defined as the variation in the optimal ranks of local models across clients and training rounds due to Non-IID data, resulting in oscillations during training, misalignment with the global model, and slower convergence. For a detailed analysis, please refer to Appendix A.2.

To address the aggregation noise issue, by utilizing Riemannian Procrustes analysis, we propose a Riemannian parameter matching method to match the local parameter matrices $\mathbf{U}^k$ and $\mathbf{V}^k$ on other clients with pivots $\mathbf{U}^1$ and $\mathbf{V}^1$ on client 1, in terms of their lengths and directions. To maintain the con-

sistency between low-rank parameter metrics before and after the Riemannian parameter matching, i.e., $\Delta\mathbf{W}^k = \mathbf{U}^k\mathbf{\Sigma}^k\mathbf{V}^k = \tilde{\mathbf{U}}^k\tilde{\mathbf{\Sigma}}^k\tilde{\mathbf{V}}^k$, for ensuring the effectiveness of FFT-FM with rank-adaptive LoRA, we derive a modified diagonal matrix $\tilde{\mathbf{\Sigma}}^k$ for the other clients by performing the SVD on low-dimensional $r \times r$ matrices $(\mathbf{U}^1)^T\mathbf{U}^k$ and $(\mathbf{V}^1)^T\mathbf{V}^k$. Based on the global diagonal matrix $\frac{1}{K}\left(\mathbf{\Sigma}^1 + \sum_{k=2}^{K}\tilde{\mathbf{\Sigma}}^k\right)$, it is easy to find the optimal rank of the global parameter matrix, with aggregation on only the local low-rank matrices $\mathbf{U}^k, \tilde{\mathbf{\Sigma}}^k$, and $\mathbf{V}^k$ (See Eq.(10)). We theoretically derive the equivalence between our RAFFT algorithm with rank-adaptive LoRA for the FFT-FM and the standard FFT-FM on the full parameter matrices based on FedAvg and verify the bounded error introduced by approximation.

To address rank drift, we introduce a federated Riemannian gradient descent that operates directly on the fixed-rank manifold $M$, where $M$ denotes the set of matrices of rank $r$. Each client represents its update $\Delta\mathbf{W}^k$ as the low-rank factors $\mathbf{U}^k, \mathbf{\Sigma}^k$, and $\mathbf{V}^k$, constrained to lie on the fixed-rank manifold with rank r (Chakraborty and Vemuri, 2019). In each FFT-FM round, we compute the Riemannian gradient of the local loss $L^k$ at $\Delta\mathbf{W}^k$, split it into components for $\mathbf{U}^k, \mathbf{\Sigma}^k$, and $\mathbf{V}^k$ in the tangent space, take a step of size $\eta_t$ along that direction, and the apply a retraction to return to $M$. This procedure guarantees that the rank of $\Delta\mathbf{W}^k$ remains fixed throughout local training. We theoretically demonstrate that the RGD optimization on the Riemannian manifold ensures the rank invariance during the local update process and the RGD optimization can converge in the FFT-FM context.

To our best knowledge, this work is the first to offer a rank-adaptive low-rank adaptation solution for FFT-FM with Riemannian theory. Our RAFFT method exhibits three compelling advantages: (1) The proposed Riemannian parameter matching removes aggregation noise when adapting centralized LoRA to federated fine-tuning, allows any existing rank-adaptive LoRA to plug in, and requires aggregating only local low-rank factors instead of full parameter matrices; (2) Transforming the SVD of high-dimensional full parameter matrices into the SVD of low-dimensional $r \times r$ matrices can significantly improve the efficiency of FFT-FM with low-rank adaption. In addition, this design avoids the expensive cost of training FFT multiple times at different ranks by rank sampling-based algorithms; and (3) The combination of Riemannian gradient descent and Riemannian manifold theory guarantees the local parameter matrices with fixed rank optimized by the server in each FFT-FM round, for alleviating the rank-drift issue to speed up the convergence of RAFFT.

Empirical evaluation on real datasets demonstrates the superior performance of our RAFFT model against several state-of-the-art federated prompt tuning, federated LoRA, and federated rank-adaptive LoRA methods. More experiments, implementation details, and hyper-parameter setting are presented in Appendices A.7-A.8.

## 2 BACKGROUND

### 2.1 Rank-Adaptive Low-Rank Adaptation

AdaLoRA Zhang et al. (2023b) is a parameter-efficient fine-tuning (PEFT) method in centralized setting that parameterizes full parameter metrics as $\Delta\mathbf{W} = \mathbf{U}\mathbf{\Sigma}\mathbf{V}$ and adaptively allocates the rank $r$ for low-rank parameter metrics $\mathbf{U}$, $\mathbf{\Sigma}$, and $\mathbf{V}$ according to their importance in the form of singular value decomposition (SVD) of $\Delta\mathbf{W}$.

$$\mathbf{W} = \mathbf{W}_0 + \Delta\mathbf{W} = \mathbf{W}_0 + \mathbf{U}\mathbf{\Sigma}\mathbf{V} \tag{2}$$

where $\mathbf{W}, \mathbf{W}_0, \Delta\mathbf{W} \in \mathbb{R}^{m\times n}$ are the complete, backbone, and adapter parameter matrices respectively. $\mathbf{U} \in \mathbb{R}^{m\times r}$ and $\mathbf{V} \in \mathbb{R}^{r\times n}$ are matrices representing the left and right singular vectors of full parameter matrices $\Delta\mathbf{W}$ respectively. $\mathbf{\Sigma} \in \mathbb{R}^{r\times r}$ is a diagonal matrix containing the singular values $\{\mathbf{\Sigma}_{ii}\}_{1\le i\le r}$ with rank $r << \min(m, n)$. AdaLoRA is thus able to dynamically adjust the number of the singular values in $\mathbf{\Sigma}$ and assign more/less trainable parameters with higher/lower rank $r$ to the critical/insignificant parameter matrices for better model performance/efficiency.

### 2.2 Federated Fine-Tuning

First, given a machine learning (ML) task (e.g., image classification), $K$ clients with their local training data $D = \{D_1, \cdots, D_K\}$, and a server, federated learning (FL) based on the FedAvg algorithm McMahan et al. (2017) aims to learn a global ML model on the server by optimizing the problem below.

$$\begin{aligned} &\min_{\mathbf{W}\in\mathbb{R}^{m\times n}} \mathcal{L}(\mathbf{W}) = \sum_{k=1}^{K}\frac{n^k}{n}L^k(\mathbf{W}), \\ &\text{where } L^k(\mathbf{W}) = \frac{1}{n_k}\sum_{\{x_i,y_i\}\in D^k} l_i(\mathbf{W}) \end{aligned} \tag{3}$$

where $l_i(\mathbf{W}) = l(x_i, y_i; \mathbf{W})$ denotes the loss function of the prediction on data example $\{x_i, y_i\} \in D_k$ made with a global model parameter $\mathbf{W}$. $n^k = |D_k|$ denotes the size of local dataset $D_k$. $n$ is the size of total training data $D$, i.e., $n = n^1 + \cdots + n^K$. In the FL, the

global model parameter $\mathbf{W}$ is iteratively updated with the aggregation of all local model parameters $\mathbf{W}^1, \mathbf{W}^K$ on $K$ clients in each round, i.e., $\mathbf{W} = \sum_{k=1}^{K} \frac{n^k}{n} \mathbf{W}^k$.

In the context of federated fine-tuning (FFT), in Eq.(2), the backbone parameter matrices $\mathbf{W}_0$ are frozen and only the adapter parameter matrices $\Delta\mathbf{W}$ are adjusted in each round by updating their low-rank versions $\mathbf{U}$, $\mathbf{\Sigma}$, and $\mathbf{V}$ respectively.

# 3 RIEMANNIAN PARAMETER MATCHING TO AVOID AGGREGATION NOISE ON SERVER

As discussed in Section 1, directly using FedAvg to aggregate the clients' local matrices $\mathbf{U}^k, \mathbf{\Sigma}^k, \mathbf{V}^k$ on the server side leads to aggregation noise, as shown in Eq.(1), which negatively impact the convergence and performance of federated learning. Among three categories of rank-adaptive low-rank approximation techniques, SVD-based methods in centralized learning encounter the dilemma of the aggregation noise, rank sampling-based algorithms and federated rank-adaptive LoRA algorithms raise extremely expensive cost. To address these challenges, we propose a Riemannian parameter matching method to match the local parameter matrices $\mathbf{U}^k$ and $\mathbf{V}^k$ from other clients with the pivot matrices $\mathbf{U}^1$ and $\mathbf{V}^1$ on client 1, i.e., $\tilde{\mathbf{U}}^k \approx \mathbf{U}^1$ and $\tilde{\mathbf{V}}^k \approx \mathbf{V}^1$, preserving both their lengths and directions. Correspondingly, we adjust the diagonal matrix $\mathbf{\Sigma}^k$ to ensure consistency in the low-rank parameter measurements before and after Riemannian parameter matching, i.e., $\mathbf{U}^k\mathbf{\Sigma}^k\mathbf{V}^k = \tilde{\mathbf{U}}^k\tilde{\mathbf{\Sigma}}^k\tilde{\mathbf{V}}^k \approx \mathbf{U}^1\tilde{\mathbf{\Sigma}}^k\mathbf{V}^1$. This approach allows the server to directly aggregate the aligned local low-rank matrices $\mathbf{U}^k$, $\tilde{\mathbf{\Sigma}}^k$, and $\mathbf{V}^k$ while avoiding aggregation noise. Moreover, the global diagonal matrix enables the server to easily identify the optimal rank for the global parameter matrix, enhancing both efficiency and performance.

## 3.1 Riemannian Parameter Matching Objective and Efficient Optimization

Since both $\mathbf{U}^k$ and $\mathbf{V}^k$ are orthogonal matrices, they belong to the Riemann manifold, which is defined as the set of standard orthogonal matrices $S = \{\mathbf{U}^k \in \mathbb{R}^{m\times r} : (\mathbf{U}^k)^T(\mathbf{U}^k) = I\}$ (Chakraborty and Vemuri, 2019; Atiyah and Todd, 1960). Therefore, we can performing the Riemannian parameter matching to ensure that the length and direction of the parameter matrices between clients are as aligned as possible. We adopt the Procrustes distance metric proposed in Kendall et al. (2003) to efficiently compute the parameter matching on the manifold. The procrustes representation $S_p$ on the Riemann manifold $S$ can be defined as follows: an $m \times r$ matrix $\mathbf{U}^k$ on $S_{r,m}$ is identified with the equivalence class of matrices $\mathbf{U}^k\mathbf{R}^k$ in $\mathbf{R}_{m,r}$, for $\mathbf{R} > 0$.

The squared Procrustes distance for each two matrices $\mathbf{U}^k$ and $\mathbf{U}^1$, considering the representation $S_p$ on the Riemann manifold $S$, is defined as the minimum squared Euclidean distance over all pairs of matrices in the respective equivalence classes.

Therefore, we aim to solve the following Riemann distance optimization problem.

$$\begin{aligned} d^2_{S_P}(\mathbf{U}^1, \mathbf{U}^k) &= \min_{\mathbf{R}^k>0} \operatorname{tr}\left((\mathbf{U}^1 - \mathbf{U}^k\mathbf{R}^k)^T(\mathbf{U}^1 - \mathbf{U}^k\mathbf{R}^k)\right) \\ &= \min_{\mathbf{R}^k>0} \operatorname{tr}\left((\mathbf{R}^k)^T\mathbf{R}^k - 2(\mathbf{U}^1)^T\mathbf{U}^k\mathbf{R}^k + I_r\right) \end{aligned} \tag{4}$$

where $I_r$ is an identity matrix. Matrix $\mathbf{R}^k$ is a $r\times r$ symmetric positive constraint that ensures the aggregated points remain on the Riemannian manifold.

Notice that $(\mathbf{U}^1)^T\mathbf{U}^k$ is a low-rank matrix with low dimensions $r \times r$. We perform the SVD on $(\mathbf{U}^1)^T\mathbf{U}^k$ to generate $(\mathbf{U}^1)^T\mathbf{U}^k = \mathbf{P}^k\mathbf{\Lambda}^k\mathbf{Q}^k$. According to the properties of the matrix trace and the symmetry of the Frobenius inner product (Schneider, 2015), the optimization problem in Eq.(4) is further converted to another equivalent optimization problem below.

$$\begin{aligned} &\min_{\mathbf{R}^k} \operatorname{tr}\left((\mathbf{R}^K)^T\mathbf{R}^k - 2(\mathbf{U}^1)^T\mathbf{U}^k\mathbf{R}^k\right) = \min_{\mathbf{R}^k} \|\mathbf{R}^k - \mathbf{P}^k\mathbf{\Lambda}^k\mathbf{Q}^k\|_F^2 \\ &= \min_{\mathbf{R}^k} \|(\mathbf{Q}^k)^T\mathbf{R}^k\mathbf{Q}^k - (\mathbf{Q}^k)^T\mathbf{P}^k\mathbf{\Lambda}^k\|_F^2 \end{aligned} \tag{5}$$

We introduce two auxiliary variable $\mathbf{Y}^k$, $\mathbf{Z}^k$ and let $\mathbf{Y}^k = (\mathbf{Q}^k)^T\mathbf{R}^k\mathbf{Q}^k$,$\mathbf{Z}^k = (\mathbf{Q}^k)^T\mathbf{P}^k$, then we transform the Riemann Procrustes distance optimization problem into an equivalent optimization problem.

$$\begin{aligned} d^2_{S_P}(\mathbf{U}^1, \mathbf{U}^k) \iff \min_{\mathbf{R}^k} \|\mathbf{Y}^k - \mathbf{Z}^k\mathbf{\Lambda}^k\|_F^2 &= \sum_{i=1}^{r}(\mathbf{Y}^k_{ii} - \mathbf{Z}^k_{ii}\mathbf{\Lambda}^k_i)^2 \\ &+ \sum_{j>i}\left((\mathbf{Y}^k_{ij} - \mathbf{Z}^k_{ij}\mathbf{\Lambda}^k_i)^2 + (\mathbf{Y}^k_{ij} - \mathbf{Z}^k_{ji}\mathbf{\Lambda}^k_j)^2\right) \end{aligned} \tag{6}$$

where $\mathbf{Y}^k_{ij}$, $\mathbf{Z}^k_{ij}$ and $\mathbf{Z}^k_{ji}$ represent the elements of the symmetric matrix $\mathbf{Y}^k$ and matrix $\mathbf{Z}^k$, respectively. Additionally $\mathbf{Y}^k_{ii}$, $\mathbf{\Lambda}^k_i$ and $\mathbf{\Lambda}^k_j$ denote the diagonal elements of the symmetric matrix $\mathbf{Y}^k$ and matrix $\mathbf{\Lambda}^k$.

Given the inherent symmetry of Y, the variables $\mathbf{Y}^k_{ij}$ (where j ≥ i ) are uncoupled, allowing us to minimize each term separately. Specifically, we minimize $(\mathbf{Y}^k_{ii} - \mathbf{Z}^k_{ii}\mathbf{\Lambda}^k_i)^2$ and $(\mathbf{Y}^k_{ij} - \mathbf{Z}^k_{ij}\mathbf{\Lambda}^k_i)^2 + (\mathbf{Y}^k_{ij} - \mathbf{Z}^k_{ji}\mathbf{\Lambda}^k_j)^2$ for $j > i$. Since Y is a symmetric matrix, it suffices to compute only the upper triangular part. Then we generate the solution of the optimal problem as follows.

$$\mathbf{Y}^k_{ij} = \begin{cases} \mathbf{Z}^k_{ii}\mathbf{\Lambda}^k_i, & i = j \le \operatorname{rank}((\mathbf{U}^1)^T\mathbf{U}^k), \\ \frac{\mathbf{Z}^k_{ij}\mathbf{\Lambda}^k_i + \mathbf{Z}^k_{ji}\mathbf{\Lambda}^k_j}{2}, & j > i \text{ and } i \le \operatorname{rank}((\mathbf{U}^1)^T\mathbf{U}^k), \\ 0, & \text{otherwise.} \end{cases} \tag{7}$$

Then we generate optimal $\mathbf{R}^k$ below: $\mathbf{R}^k = \mathbf{Q}^k\mathbf{Y}^k(\mathbf{Q}^k)^T$. By following the same approach, we produce an optimal matrix $\mathbf{S}^k$ for another Riemannian parameter matching problem $\min_{\mathbf{S}^k} d^2_{S_P}(\mathbf{V}^1, \mathbf{V}^k)$s.t. $(\mathbf{S}^k)^T = \mathbf{S}^k$. Therefore, the low-rank parameter matrices are aligned together. $\tilde{\mathbf{U}}^k$ and $\tilde{\mathbf{V}}^k$ are the aligned parameter matrices for client $k$. $\tilde{\mathbf{U}}^k = \mathbf{U}^k\mathbf{R}^k \approx \mathbf{U}^1, \tilde{\mathbf{V}}^k = \mathbf{S}^k\mathbf{V}^k \approx \mathbf{V}^1$.

To maintain parameter consistency before and after performing the Riemannian parameter matching, as well as the effectiveness of FFT-FM with rank-adaptive LoRA, i.e., $\tilde{\mathbf{U}}^k\tilde{\mathbf{\Sigma}}^k\tilde{\mathbf{V}}^k = \mathbf{U}^k\mathbf{\Sigma}^k\mathbf{V}^k = \Delta\mathbf{W}^k$, we need to derive a modified version $\tilde{\mathbf{\Sigma}}^k$ of $\mathbf{\Sigma}^k$.

$$\min_{\tilde{\mathbf{\Sigma}}^k} \|\tilde{\mathbf{U}}^k\tilde{\mathbf{\Sigma}}^k\tilde{\mathbf{V}}^k - \mathbf{U}^k\mathbf{\Sigma}^k\mathbf{V}^k\|_F^2 \tag{8}$$

However, it is difficult to directly solve the above optimization problem. We convert it to another equivalent problem below. Since $\mathbf{U}^k$ and $\mathbf{V}^k$ are orthogonal matrices, the problem can be further transformed. Notice that $\tilde{\mathbf{U}}^k = \mathbf{U}^k\mathbf{R}^k$, $\tilde{\mathbf{V}}^k = \mathbf{S}^k\mathbf{V}^k$. Additionally, since $\mathbf{R}^k$ and $\mathbf{S}^k$ are non-singular matrices, an invertible matrix must exist.

$$\begin{aligned}&\min_{\tilde{\mathbf{\Sigma}}^k} \|(\mathbf{U}^k)^T\left(\tilde{\mathbf{U}}^k\tilde{\mathbf{\Sigma}}^k\tilde{\mathbf{V}}^k - \mathbf{U}^k\mathbf{\Sigma}^k\mathbf{V}^k\right)(\mathbf{V}^k)^T\|_F^2 \\ &= \min_{\tilde{\mathbf{\Sigma}}^k} \|\tilde{\mathbf{\Sigma}}^k - (\mathbf{R}^k)^{-1}\mathbf{\Sigma}^k(\mathbf{S}^k)^{-1}\|_F^2\end{aligned} \tag{9}$$

The optimal solution is obtained when $\tilde{\mathbf{\Sigma}}_{\mathbf{ii}}{}^k = (\mathbf{R}_{\mathbf{ii}}{}^k)^{-1}\mathbf{\Sigma}_{\mathbf{ii}}{}^k(\mathbf{S}_{\mathbf{ii}}{}^k)^{-1}$. Next, the server can directly perform the aggregation on local low-rank parameter matrices to generate the global ones without the aggregation noise.

$$\begin{aligned}&\frac{1}{K}\left(\mathbf{U}^1 + \sum_{k=2}^{K}\mathbf{U}^k\mathbf{R}^k\right) \times \frac{1}{K}\left(\mathbf{\Sigma}^1 + \sum_{k=2}^{K}\tilde{\mathbf{\Sigma}}^k\right) \times \frac{1}{K}\left(\mathbf{V}^1 + \sum_{k=2}^{K}\mathbf{S}^K\mathbf{V}^K\right) \\ &= \mathbf{U}^1 \times \frac{1}{K}\left(\mathbf{\Sigma}^1 + \sum_{k=2}^{K}\tilde{\mathbf{\Sigma}}^k\right) \times \mathbf{V}^1 \approx \frac{1}{K}\left(\sum_{k=1}^{K}\mathbf{U}^k\mathbf{\Sigma}^k\mathbf{V}^k\right) \\ &= \frac{1}{K}\sum_{k=1}^{K}\Delta\mathbf{W}^k\end{aligned} \tag{10}$$

Thus, when searching for the optimal rank on the globally low-rank parameter matrix, there is no need to physically generate full parameter matrix $\Delta\mathbf{W}$ and execute iterative SVD on $\Delta\mathbf{W}$.

By following the same idea in existing efforts Falini (2022); Wu et al. (2022), this paper utilizes singular value contribution rate $\Theta(r)$ to determine the rank $\tilde{\mathbf{\Sigma}}^{k'}$ after each round of FFT-FM. $\Theta(r)$ is defined as the cumulative percentage of the first $r$ singular values to all the singular values. We retain the first $r$ singular values such that $\Theta(r)$ is bigger than a threshold value $\varphi$.

$$\Theta(r) = \frac{\sum_{i=1}^{r}\tilde{\mathbf{\Sigma}}'_{ii}}{\sum_{i=1}^{r_{max}}\tilde{\mathbf{\Sigma}}'_{ii}} \geq \varphi \tag{11}$$

where $r_{max}$ is a maximum acceptable rank.

### 3.2 Approximation Error Analysis

To evaluate the impact of the approximation, we derive a bound for the potential errors introduced in Eq. (10). Theorem 1 shows that the approximation error remains bounded and depends only on the model rank and alignment constants, ensuring that the aggregated update stays within a controlled Frobenius-norm distance.

**Theorem 1.** *We assume that the Frobenius norm of $\mathbf{R}^k$ is bounded by a constant $H$, and its eigenvalues lie within the interval $[\lambda_{R_{\min}}, \lambda_{R_{\max}}]$. Similarly, the Frobenius norm of $\mathbf{S}^k$ is bounded by a constant $N$, with eigenvalues in the range $[\lambda_{S_{\min}}, \lambda_{S_{\max}}]$. Additionally, the matrix $\Delta W$ has rank $r$. Given these conditions, the total approximation error bound in Eq.(10) is derived as follows*

$$\begin{aligned}&\|\mathbf{U}^1 \times \frac{1}{K}\left(\mathbf{\Sigma}^1 + \sum_{k=2}^{K}\tilde{\mathbf{\Sigma}}^k\right) \times \mathbf{V}^1 - \frac{1}{K}\left(\sum_{k=1}^{K}\mathbf{U}^k\mathbf{\Sigma}^k\mathbf{V}^k\right)\|_F^2 \\ &= \sum_{k=2}^{K}\left(2r(1-H-N) + (1+(\frac{\lambda_{R_{\max}}}{\lambda_{R_{\min}}})^2)H^2 + (1+(\frac{\lambda_{S_{\max}}}{\lambda_{S_{\min}}})^2)N^2\right)\end{aligned} \tag{12}$$

*Please refer to Appendix A.4 for detailed proof of Theorem 1.*

## 4 RIEMANNIAN GRADIENT DESCENT FOR ALLEVIATING RANK DRIFT ON CLIENTS

The data heterogeneity issue in the FFT-FM may bring the rank-drift challenges. When the server dispatches the low-rank parameter matrix with the appropriate rank $r$ to the clients, the rank of its local full parameter matrix $\Delta\mathbf{W}^k = \mathbf{U}^k\mathbf{\Sigma}^k\mathbf{V}^k$ on each client may significantly change after local training epoch, and so does the appropriate rank of the global parameter matrix. This may slow down the convergence of FFT-FM and degrade the model performance too. We develop a Riemannian gradient descent (RGD) method to guarantee the local full parameter matrices $\Delta\mathbf{W}^k$ in the form of low-rank ones $\mathbf{U}^k, \mathbf{\Sigma}^k$, and $\mathbf{V}^k$ with fixed appropriate rank determined by the server in each iteration of FFT-FM, to speed up the convergence of RAFFT.

### 4.1 Riemannian Gradient Optimization

We introduce a Riemannian manifold containing all fixed-rank matrices, i.e., the set $M$ of all matrices with a fixed rank $r$: $M = \{\Delta\mathbf{W} : \Delta\mathbf{W} \in \mathbb{R}^{m\times n}, \text{rank}(\Delta\mathbf{W}) = r\}$ (do Carmo, 2018; Vandereycken, 2014). This forms a smooth submanifold of $\mathbb{R}^{m\times n}$. This structure ensures that the updated parameter matrices $\mathbf{U}^k\mathbf{\Sigma}^k\mathbf{V}^k$ stay within the manifold, maintaining rank invariance throughout the local update process.

The tangent space $T_M$ at the point $\Delta\mathbf{W}$ on the manifold $M$ is defined as follows.

$$\begin{aligned} T_M &= \left\{ (\mathbf{U}^k\ \mathbf{U}_\perp^k) \begin{bmatrix} \mathbb{R}^{r\times r} & \mathbb{R}^{r\times(n-r)} \\ \mathbb{R}^{(m-r)\times r} & 0^{(m-r)\times(n-r)} \end{bmatrix} (\mathbf{V}^k\ \mathbf{V}_\perp^k)^T \right\} \\ &= \Big\{ \mathbf{U}^k\mathbf{G}(\mathbf{V}^k)^T + \mathbf{U}_p^k(\mathbf{V}^k)^T + \mathbf{U}^k(\mathbf{V}_p^k)^T : \mathbf{G} \in \mathbb{R}^{r\times r}, \\ &\quad \mathbf{U}_p^k \in \mathbb{R}^{m\times r}, (\mathbf{U}_p^k)^T\mathbf{U}^k = 0, \mathbf{V}_p^k \in \mathbb{R}^{n\times r}, (\mathbf{V}_p^k)^T\mathbf{V}^k = 0 \Big\} \end{aligned} \tag{13}$$

where $\mathbf{U}_\perp^k$ and $\mathbf{V}_\perp^k$ denote the orthogonal complements of $\mathbf{U}^k$ and $\mathbf{V}^k$ respectively. $\mathbf{G}, \mathbf{U}_p^k, \mathbf{V}_p^k$ represent the tangent vector at $\Delta W$. Please refer to Appendix A.5 for details of tangent space.

When the data have a manifold structure, traditional gradient descent methods in Euclidean space, such as SGD, often result in updates that stray off the manifold. Thus, we propose to project the gradient $\nabla L^k(\Delta\mathbf{W}^k)$ in Euclidean space onto the tangent space $T_M$ at the point $\Delta\mathbf{W}$ on the manifold $M$ and compute the Riemannian gradient $\Gamma L^k(\Delta\mathbf{W}^k)$. This projection can be accomplished through orthogonal projection $P_{T_M}$, ensuring that the optimization trajectory remains confined to the manifold Lee (2012) and is effectively directed towards minimizing the loss function.

$$\begin{aligned} &\Gamma L^k(\Delta\mathbf{W}^k) = (\Gamma_{\mathbf{U}^k}L^k, \Gamma_{\mathbf{\Sigma}^k}L^k, \Gamma_{\mathbf{V}^k}L^k) = P\nabla L^k \in T_M \subseteq \mathbb{R}^{m\times n} \\ &= \mathbf{U}^k((\mathbf{U}^k)^T\nabla L^k\mathbf{V}^k)(\mathbf{V}^k)^T + (\mathbf{I}_m - \mathbf{U}^k(\mathbf{U}^k)^T)\nabla L^k\mathbf{V}^k(\mathbf{V}^k)^T \\ &+ \mathbf{U}^k(\mathbf{U}^k)^T\nabla L^k(\mathbf{I}_n - (\mathbf{V}^k)(\mathbf{V}^k)^T) \end{aligned} \tag{14}$$

where $\Gamma_{\mathbf{U}^k}L^k$, $\Gamma_{\mathbf{\Sigma}^k}L^k$, and $\Gamma_{\mathbf{V}^k}L^k$ represent the Riemannian gradients with respect to $\mathbf{U}^k, \mathbf{\Sigma}^k$, and $\mathbf{V}^k$ respectively. $\mathbf{I}_m$ and $\mathbf{I}_n$ are the $m/n$-dimensional identity matrices. Please refer to Appendix A.5 for derivation details of Riemannian gradient.

Therefore, the gradients of $\mathbf{U}^k$, $\mathbf{\Sigma}^k$, and $\mathbf{V}^k$ in Riemannian space can be derived as follows.

$$\begin{aligned} &\Gamma_{\mathbf{U}^k}L^k = (\mathbf{I}_m - \mathbf{U}^k(\mathbf{U}^k)^T)\nabla_{\mathbf{U}^k}L^k, \\ &\Gamma_{\mathbf{V}^k}L^k = (\mathbf{I}_n - \mathbf{V}^k(\mathbf{V}^k)^T)\nabla_{\mathbf{V}^k}L^k, \\ &\Gamma_{\mathbf{\Sigma}^k}L^k = ((\mathbf{U}^k)^T\nabla_{\mathbf{U}^k}L^k - \nabla_U(L^k)^T\mathbf{U}^k)\mathbf{\Sigma}^k \\ &+ \mathbf{\Sigma}^k(\mathbf{V}^k\nabla_{\mathbf{V}^k}(L^k)^T - \nabla_{\mathbf{V}^k}L^k(\mathbf{V}^k)^T) + \nabla_{\mathbf{\Sigma}^k}L^k \end{aligned} \tag{15}$$

where $\nabla_{\mathbf{U}^k}L^k$, $\nabla_{\mathbf{V}^k}L^k$, and $\nabla_{\mathbf{\Sigma}^k}L^k$ denote the corresponding Euclidean gradients. They are the conventional derivatives in Euclidean space that are used to compute the gradient descent steps before projection onto the manifold.

At each step, we move along the projected gradient in the tangent space and then apply a retraction to return to the manifold. This ensures that local updates preserve the rank and remain within the fixed-rank structure. The following theorem demonstrates that the RGD optimization on the Riemannian manifold ensures the rank invariance during the local update process.

**Theorem 2.** *Let $\Delta\mathbf{W}^k$ be a point on a Riemannian manifold $M$ consisting of all matrices with a fixed rank $r$ in $\mathbb{R}^{m\times n}$. Suppose $\nabla L^k(\Delta\mathbf{W}^k)$ is the Euclidean gradient of the loss function $L^k$ at $\Delta\mathbf{W}^k$, and $\Gamma_{\mathbf{U}^k}L^k$, $\Gamma_{\mathbf{\Sigma}^k}L^k$, and $\Gamma_{\mathbf{V}^k}L^k$ represent the components of the Riemannian gradient at $\Delta\mathbf{W}^k$. The RGD optimization with a learning rate $\eta_t$ at round $t$ $(0 \le t \le C)$ ensures that the local update*

$$\begin{aligned} &\left((\mathbf{U}^k)^{(t+1)}, (\mathbf{\Sigma}^k)^{(t+1)}, (\mathbf{V}^k)^{(t+1)}\right) \\ &= f\left(-\eta_t\left(\left(\Gamma_{\mathbf{U}^k}L^k\right)^{(t)}, \left(\Gamma_{\mathbf{\Sigma}^k}L^k\right)^{(t)}, \left(\Gamma_{\mathbf{V}^k}L^k\right)^{(t)}\right)\right) \end{aligned} \tag{16}$$

*preserves the rank $r$ of $\Delta\mathbf{W}^k$, maintaining the structure within the manifold $M$, where $f$ is a retraction $f : T_M \to M$ mapping the tangent space at $\Delta\mathbf{W}^k$ to the manifold.*

*Please refer to Appendix A.5 for the derivation of Riemannian retraction function and the detailed proof of Theorem 2.*

### 4.2 Convergence Analysis

We also conduct the convergence analysis of our RAFFT algorithm based on the RGD optimization on the Riemannian manifold.

**Theorem 3** (Nonconvex)**.** *Suppose the optimization problem in Eq.(3) satisfies Assumptions 1 and 2. At each round $t$, clients $k \in \{1, \dots, K\}$ are sampled with probabilities $p_k$, and the selected clients perform gradient descent with a fixed stepsize. Let $L^{(p)}(\Delta\mathbf{W}) = \sum_{k=1}^K p_k L_k(\Delta\mathbf{W})$ be the weighted global objective with smoothness constant $c_g^{(p)} = \sum_{k=1}^K p_k c_{g,k}$, and let $\Gamma L^{(p)}(\Delta\mathbf{W})$ denote its Riemannian gradient. If $\eta_t \le 1/c_g^{(p)}$, then*

$$\begin{aligned} &\min_{0\le t\le C} \mathbb{E}\left[\|\Gamma L^{(p)}(\Delta\mathbf{W}^{(t)})\|^2\right] \le \\ &\frac{2c_g^{(p)}}{C}\left(L^{(p)}(\Delta\mathbf{W}^1) - L^{(p)}(\Delta\mathbf{W}^*)\right) + \mathcal{O}\left(\frac{\sigma^2}{K}\right), \end{aligned} \tag{17}$$

*where $\Delta\mathbf{W}^{(t)}$ is the iterate on $\mathcal{M}$ at round $t$, $\Delta\mathbf{W}^*$ is the minimizer of $L^{(p)}$, and $\sigma^2$ is a finite constant capturing the variance due to client heterogeneity.*

**Theorem 4** (Convex)**.** *Suppose Eq.(3) satisfies Assumptions 1, 2, and 3, and that each local objective $L_k$ is geodesically convex. At each round, clients are sampled with distribution $p$, giving the weighted objective $L^{(p)} = \sum_{k=1}^{K} p_k L_k$ and weighted smoothness constant $c_g^{(p)} = \sum_{k=1}^{K} p_k c_{g,k}$. Let $\Delta\mathbf{W}^* = \arg\min_{\Delta\mathbf{W}\in\mathcal{M}} L^{(p)}(\Delta\mathbf{W})$ be the global minimizer, and $d(\cdot,\cdot)$ the geodesic distance on $\mathcal{M}$. If the stepsize satisfies $\eta_t \le 1/(2c_g^{(p)})$, then*

$$\mathbb{E}\Big[L^{(p)}(\Delta\mathbf{W}^{(C)}) - L^{(p)}(\Delta\mathbf{W}^*)\Big] \le \frac{\zeta\, c_g^{(p)}\, d^2(\Delta\mathbf{W}^{(0)}, \Delta\mathbf{W}^*)}{\zeta + C - 2} + \mathcal{O}\Big(\frac{\sigma^2}{K}\Big) \tag{18}$$

*where $\Delta\mathbf{W}^{(0)}$ is the initialization, $\zeta$ is the constant from Assumption 3, and $\sigma^2$ is a variance constant due to client heterogeneity.*

Please refer to Appendix A.6 for detailed proof of Theorems 3 and 4. By assembling different pieces together, we provide the pseudo code of our RAFFT algorithm in Algorithm 1 in Appendix A.3.

## 5 EXPERIMENTAL EVALUATION

In this section, we present the experimental results over 13 baselines and 3 commonly-used tasks to demonstrate the advantages of our method. We consider an FL environment with 100 devices and a parameter server. In each epoch, we randomly sample 10 devices to perform the local update. We exploit three widely used NLP tasks including SST-2, MRPC, MPQA and QNLI (Wang et al., 2018). We evaluated fix rank method and all other methods on RoBERTa-LARGE (Liu et al., 2019b), which consists of 24 layers of transformers followed by a large language model head and 355M pretrained parameters. To demonstrate the adaptability of our method, we carried out extra experiments with two additional decoder-based models,i.e., LLaMA 3B Touvron et al. (2023a) model on MRPC, MPQA, SST-2 dataset, LLaMA2 7B model on MRPC, MPQA, SST-2 dataset and LLaMA2-13B model Touvron et al. (2023b) on QNLI dataset. At the same time, we conducted experiments on the image classification data sets CIFAR10 (Krizhevsky et al., 2010), CIFAR100 (Krizhevsky et al., 2010), and Tiny-IamgeNet Le and Yang (2015) of the ViT model. The backbones of these models are frozen for all methods. Please see Appendix A.7 for details.

**Baselines.** We take 13 existing approaches as baselines. LoRA (Hu et al., 2022) and AdaLoRA (Zhang et al., 2023b) are adapted into federated versions (**Federated_LoRA**, **FedAdaLoRA**). **Fedkseed** (Qin et al., 2024) performs full-parameter tuning with seed-based zeroth-order optimization to reduce communication. Prompt-based tuning is represented by **P-Tuning v2** (Liu et al., 2021a), **FedPrompt** (Zhao et al., 2023), **FedPepTAO** (Che et al., 2023a), **PromptFL** (Guo et al., 2024), and **PE-FL** (Zhao et al., 2024), which add lightweight prompt modules for efficient and personalized adaptation. Reparameterization-based methods include **SLoRA** (Babakniya et al., 2023), **HetLoRA** (Cho et al., 2023), **FedLoRA** (Yi et al., 2024), **FFA-LoRA** (Sun et al., 2024),**FLoRA** (Wang et al., 2024a), all of which optimize within low-rank subspaces to address client heterogeneity. Details are given in Appendix A.1.

**Variants of the RAFFT Model.** We evaluate two versions of the RAFFT model to showcase the strengths of distinct technical approaches. The first variant, which we term the RAFFT-RGD Model, solely utilizes the Riemannian gradient. This model primarily focuses on the fundamental capability to manage gradient descent within the geometric constraints of the RAFFT manifold, using FedAvg as the aggregation method. The second variant is the RAFFT-MR model, which does not use the Riemannian theory fix rank during training. This means rankings will drop during local updates.

**Evaluation metrics.** In line with protocols established in previous studies on federated learning for large language models (Babakniya et al., 2023; Cho et al., 2023; Sun et al., 2024), we employ three crucial metrics to evaluate the efficacy of parameter efficiency in fine-tuning for classification tasks: Loss, Accuracy, and Time.Loss measures the model's prediction error, providing insight into the effectiveness of the learning process. Accuracy gauges the model's performance on classifying new, unseen data, reflecting the practical applicability of the federated learning model. Time is evaluated to determine the speed of convergence and the overall computational demand, which are critical in federated settings where computational resources and time are often limited.

**Accuracy of classification with Riemannian Manifold.** Tables 1 and 2 show the classification accuracy of our method, which uses Riemannian parameter matching and a Riemannian optimizer across two datasets. For comparison, the baseline reflects the accuracy of FedPEFT. Our Non-IID dataset was partitioned using a Dirichlet distribution. Our method consistently outperforms 13 other approaches, addressing both aggregation noise and rank drift. Notably, we see accuracy improvements of up to 10.94% on MPQA for LLaMA-3B, 23.21% for LLaMA-7B, and 14.11% on SST-2 for RoBERTa. In image classification, the ViT

Table 1: Performance comparison of different methods on LLaMA 7B+MPQA.

| | $\alpha = 5$ | | | $\alpha = 3$ | | | $\alpha = 1$ | | |
|---|---|---|---|---|---|---|---|---|---|
| Method | Accuracy | Loss | Time | Accuracy | Loss | Time | Accuracy | Loss | Time |
| Federated_LoRA | 80.40 | 0.3606 | 5,712 | 70.30 | 0.8222 | 5,762 | 71.00 | 0.8047 | 5,287 |
| FedAdaLoRA | 77.75 | 0.4070 | 5,450 | 78.70 | 0.3736 | 5,464 | 77.75 | 0.4070 | 5,421 |
| P-tuning v2 | 87.25 | 0.2512 | 5,717 | 88.90 | 0.2510 | 5,820 | 87.85 | 0.2779 | 5,450 |
| FedPrompt | 87.20 | 0.2556 | 5,636 | 88.80 | 0.2632 | 5,648 | 88.30 | 0.2917 | 5,450 |
| FedPepTAO | 87.60 | 0.2460 | 5,639 | 89.65 | 0.2526 | 5,651 | 88.70 | 0.2651 | 5,442 |
| PromptFL | 87.35 | 0.2507 | 5,670 | 89.40 | 0.2507 | 5,708 | 86.55 | 0.3115 | 5,453 |
| PE_FL | 87.00 | 0.2570 | 5,682 | 88.65 | 0.2643 | 5,678 | 87.90 | 0.2954 | 5,447 |
| SLoRA | 88.75 | 0.2474 | 5,296 | 87.90 | 0.2451 | 5,318 | 86.40 | 0.2878 | 5,481 |
| HetLoRA | 83.75 | 0.2964 | 5,057 | 86.25 | 0.2611 | 5,056 | 85.95 | 0.2518 | 5,038 |
| FedLoRA | 78.10 | 0.4356 | 4,996 | 77.50 | 0.3702 | 5,033 | 76.80 | 0.4629 | 5,019 |
| FFA-LoRA | 87.05 | 0.2167 | 5,000 | 87.45 | 0.2176 | 5,318 | 86.80 | 0.2249 | 5,317 |
| Fedkseed | 87.81 | 0.2662 | 5,641 | 88.77 | 0.2698 | 5,675 | 88.74 | 0.3022 | 5,447 |
| FLoRA | 85.60 | 0.2756 | 5,306 | 88.34 | 0.2594 | 5,310 | 87.69 | 0.2656 | 5,210 |
| RAFFT | 92.00 | 0.2079 | 5,010 | 91.55 | 0.2293 | 4,980 | 90.90 | 0.1934 | 4,965 |
| RAFFT-RGD | 88.35 | 0.2365 | 4,952 | 89.10 | 0.2514 | 4,955 | 88.90 | 0.2349 | 4,961 |
| RAFFT-MR | 90.80 | 0.2602 | 5,021 | 90.60 | 0.2501 | 4,917 | 86.05 | 0.2718 | 4,886 |

Table 2: Performance comparison of different methods on ViT+CIFRA10.

| | alpha = 5 | | | alpha = 3 | | | alpha = 1 | | |
|---|---|---|---|---|---|---|---|---|---|
| Method | Accuracy | Loss | Time | Accuracy | Loss | Time | Accuracy | Loss | Time |
| Federated_LoRA | 71.90 | 0.7170 | 3,329 | 72.16 | 0.6129 | 3,395 | 67.08 | 0.6977 | 3,369 |
| FedAdaLoRA | 71.76 | 0.6936 | 3,535 | 71.35 | 0.6031 | 3,515 | 68.11 | 0.7818 | 3,529 |
| SLoRA | 71.75 | 0.6843 | 3,309 | 71.06 | 0.7023 | 3,380 | 68.14 | 0.7474 | 3,316 |
| HetLoRA | 71.76 | 0.6939 | 3,355 | 71.26 | 0.5861 | 3,331 | 65.96 | 0.6800 | 3,437 |
| FedLoRA | 71.56 | 0.7149 | 3,282 | 70.72 | 0.7149 | 3,384 | 68.19 | 0.6634 | 3,421 |
| FFA-LoRA | 71.47 | 0.7135 | 3,321 | 70.24 | 0.7369 | 3,321 | 65.76 | 0.6831 | 3,358 |
| FLoRA | 70.95 | 0.7266 | 3,401 | 71.09 | 0.6335 | 3,347 | 65.85 | 0.6890 | 3,361 |
| RAFFT | 74.54 | 0.5757 | 3,304 | 73.22 | 0.5765 | 3,281 | 70.04 | 0.6504 | 3,285 |
| RAFFT-RGD | 72.96 | 0.5945 | 3,288 | 72.52 | 0.6381 | 3,292 | 67.14 | 0.7159 | 3,299 |
| RAFFT-MR | 72.88 | 0.6070 | 3,291 | 72.02 | 0.6435 | 3,307 | 67.24 | 0.6879 | 3,311 |

model sees gains up to 16.61% on CIFAR-100. These results highlight the potential of our approach as a strong alternative to existing FedPEFT methods. For more details, see Appendix A.7.

**Ablation study.** Tables 1-2 further compare the accuracy across three datasets with two variants of our RAFFT model, which differ in their aggregation methods and optimizer updates. Our observations reveal that our method consistently achieves optimal precision and minimal error on the SST-2, MRPC, and MPQA datasets, significantly outperforming the two variants. A plausible explanation for this superiority is that our RAFFT approach performs Riemannian parameter matching, effectively addressing aggregation noise and thereby enhancing the efficacy of rank-adaptive LoRA in federated learning. Additionally, our method leverages the Riemannian Gradient Descent (RGD) technique to ensure that each iteration of federated learning by the server maintains locally updated weight matrices with a fixed optimal rank. This not only mitigates rank drift but also accelerates the aggregation process in RAFFT, enhancing the overall performance.

**Execution Time.** Tables 1-2 report the total running time for training large models across all clients for both variants of our RAFFT method and all comparison methods on three datasets. Compared to other FedPEFT methods that require operations on the full weight matrix during aggregation, our RAFFT approach achieves higher efficiency. Apart from these methods, our RAFFT method maintains similar efficiency while ensuring higher accuracy rates.

**Impact of number of client** Figure 2 (c,d) evaluates the performance effects with varying numbers of clients by changing N from 40 to 80. We observe that as N increases, the performance curve of RAFFT generally trends downward. Notably, when the number of clients reaches 80, the accuracy of RAFFT significantly decreases. A plausible explanation for this is that as the number of clients increases, the amount of data allocated to each client decreases, leading to lower quality local model updates. Additionally, the increase in the number of clients exacerbates the heterogeneity issue. Data distributions may vary significantly across different clients, resulting in substantial differences in the model parameters trained by each client. This increased training complexity ultimately affects the model's performance. As the number of clients increases, the overall training time tends to increase. This is likely due to the higher communication overhead and synchronization delays introduced when coordinating

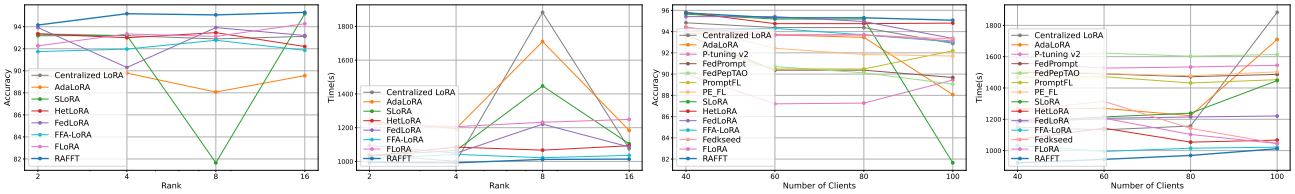


(a) Accuracy (Rank) (b) Time (Rank) (c) Accuracy (Client) (d) Time (Client)

Figure 2: Accuracy and time (s) on RoBERTa-SST2 under varying LoRA ranks and client counts.

a larger number of clients.

**Impact of initial rank** Based on Figure 2 (a,b), we evaluate the performance effect when setting the initial ranking value r to 2, 4, 8, and 16. Theoretically, the highest rank should yield the best performance. However, as ovserved in the experiments from the LoRA Hu et al. (2022) and AdaLoRA Zhang et al. (2023b) papers, there is no clear trend between performance and rank. Our results are consistent with this observation, showing that the best rank varies depending on the task. For example, rank 16 performed best for SST-2, MRPC, and MPQA, while rank 8 was optimal for CIFAR-10. Additionally, higher ranks increase training time due to greater computational complexity. When the ranking is higher, the model has more parameters to learn and optimize, which essentially requires more computing resources and time. Thus, different tasks require different ranks, and our approach is adaptive to the rank, allowing it to find the appropriate rank for each specific task.

## 6 CONCLUSIONS

In this work, we propose rank-adaptive LoRA-based federated fine-tuning algorithm for foundation models. First, we design a novel Riemannian parameter matching method with the SVD on a low-rank matrix to avoid the aggregation noise to enhance the effectiveness of FFT-FM, while further improving its efficiency. Second, we develop a Riemannian gradient descent method on Riemannian manifold to guarantee the local parameter matrices with fixed optimal rank in each iteration, to speed up the convergence.

### Acknowledgements

This research is partially sponsored by the National Science Foundation (NSF) under Grant No. OAC-2313191.

### References

Absil, P.-A., Mahony, R., and Sepulchre, R. (2008). *Optimization Algorithms on Matrix Manifolds*. Princeton University Press, Princeton, NJ.

Absil, P.-A. and Malick, J. (2012). Projection-like retractions on matrix manifolds. *SIAM Journal on Optimization*, 22(1):135–158.

Aghajanyan, A., Gupta, S., and Zettlemoyer, L. (2021). Intrinsic dimensionality explains the effectiveness of language model fine-tuning. In Zong, C., Xia, F., Li, W., and Navigli, R., editors, *Proceedings of the 59th Annual Meeting of the Association for Computational Linguistics and the 11th International Joint Conference on Natural Language Processing (Volume 1: Long Papers)*, pages 7319–7328, Online. Association for Computational Linguistics.

Atiyah, M. F. and Todd, J. A. (1960). On complex stiefel manifolds. *Mathematical Proceedings of the Cambridge Philosophical Society*, 56(4):342–353.

Babakniya, S., Elkordy, A., Ezzeldin, Y., Liu, Q., Song, K.-B., EL-Khamy, M., and Avestimehr, S. (2023). SLoRA: Federated parameter efficient fine-tuning of language models. In *International Workshop on Federated Learning in the Age of Foundation Models in Conjunction with NeurIPS 2023*.

Bai, G., Chai, Z., Ling, C., Wang, S., Lu, J., Zhang, N., Shi, T., Yu, Z., Zhu, M., Zhang, Y., Yang, C., Cheng, Y., and Zhao, L. (2024a). Beyond efficiency: A systematic survey of resource-efficient large language models.

Bai, S., Zhang, J., Li, S., Guo, S., Guo, J., Hou, J., Han, T., and Lu, X. (2024b). Diprompt: Disentangled prompt tuning for multiple latent domain generalization in federated learning. *CoRR*, abs/2403.08506.

Bao, X., Liu, L., Xiao, N., Zhou, Y., and Zhang, Q. (2015). Policy-driven autonomic configuration management for nosql. In *Proceedings of the 2015 IEEE International Conference on Cloud Computing (CLOUD'15)*, pages 245–252, New York, NY.

Boumal, N. (2023). *An Introduction to Optimization on Smooth Manifolds*. École Polytechnique Fédérale de Lausanne.

Cai, D., Wu, Y., Wang, S., Lin, F. X., and Xu, M. (2023a). Efficient federated learning for modern nlp. In *Proceedings of the 29th Annual International Conference on Mobile Computing and Networking*, ACM

MobiCom '23, New York, NY, USA. Association for Computing Machinery.

Cai, D., Wu, Y., Yuan, H., Wang, S., Lin, F. X., and Xu, M. (2023b). Towards practical few-shot federated nlp. In *Proceedings of the 3rd Workshop on Machine Learning and Systems*, EuroMLSys '23. ACM.

Chai, D., Wang, L., Zhang, J., Yang, L., Cai, S., Chen, K., and Yang, Q. (2022). Practical lossless federated singular vector decomposition over billion-scale data. In Zhang, A. and Rangwala, H., editors, *KDD '22: The 28th ACM SIGKDD Conference on Knowledge Discovery and Data Mining, Washington, DC, USA, August 14 - 18, 2022*, pages 46–55. ACM.

Chakraborty, R. and Vemuri, B. C. (2019). Statistics on the Stiefel manifold: Theory and applications. *The Annals of Statistics*, 47(1):415 – 438.

Che, T., Liu, J., Zhou, Y., Ren, J., Zhou, J., Sheng, V. S., Dai, H., and Dou, D. (2023a). Federated learning of large language models with parameter-efficient prompt tuning and adaptive optimization. In Bouamor, H., Pino, J., and Bali, K., editors, *Proceedings of the 2023 Conference on Empirical Methods in Natural Language Processing, EMNLP 2023, Singapore, December 6-10, 2023*, pages 7871–7888. Association for Computational Linguistics.

Che, T., Liu, J., Zhou, Y., Ren, J., Zhou, J., Sheng, V. S., Dai, H., and Dou, D. (2023b). Federated learning of large language models with parameter-efficient prompt tuning and adaptive optimization. In *Proceedings of the 28th Conference on Empirical Methods in Natural Language Processing (EMNLP'23)*, Singapore.

Che, T., Zhang, Z., Zhou, Y., Zhao, X., Liu, J., Jiang, Z., Yan, D., Jin, R., and Dou, D. (2022). Federated fingerprint learning with heterogeneous architectures. In *Proceedings of the 22nd IEEE International Conference on Data Mining (ICDM'22)*, pages 31–40, Orlando, FL.

Che, T., Zhou, Y., Li, T., Chang, Q., Yan, D., Zhou, H., and Jiang, Z. (2025). Fednsa: Federated noise-signature alignment for model-heterogeneous uav vehicle detection. In *Proceedings of the 2025 IEEE International Conference on Big Data (BigData'25)*, Macau, China.

Che, T., Zhou, Y., Zhang, Z., Lyu, L., Liu, J., Yan, D., Dou, D., and Huan, J. (2023c). Fast federated machine unlearning with nonlinear functional theory. In *Proceedings of the 40th International Conference on Machine Learning (ICML'23)*, pages 4241–4268, Honolulu, HI.

Chen, F., Luo, M., Dong, Z., Li, Z., and He, X. (2018). Federated meta-learning with fast convergence and efficient communication. *CoRR*, abs/1802.07876.

Chen, H., Zhang, Y., Krompass, D., Gu, J., and Tresp, V. (2024). Feddat: An approach for foundation model finetuning in multi-modal heterogeneous federated learning. In Wooldridge, M. J., Dy, J. G., and Natarajan, S., editors, *Thirty-Eighth AAAI Conference on Artificial Intelligence, AAAI 2024, Thirty-Sixth Conference on Innovative Applications of Artificial Intelligence, IAAI 2024, Fourteenth Symposium on Educational Advances in Artificial Intelligence, EAAI 2014, February 20-27, 2024, Vancouver, Canada*, pages 11285–11293. AAAI Press.

Chen, Z., Ta, X., Zhou, Z., and Zhou, Y. (2023). A channel aggregation based dynamic pruning method in federated learning. In *Proceedings of the 24th IEEE Global Communications Conference (GLOBECOM'23)*, Kuala Lumpur, Malaysia.

Cheng, Q., Yan, D., Wu, T., Yuan, L., Cheng, J., Huang, Z., and Zhou, Y. (2025). Efficient enumeration of large maximal k-plexes. In *Proceedings 28th International Conference on Extending Database Technology (EDBT'25)*, pages 53–65, Barcelona, Spain.

Cho, Y. J., Liu, L., Xu, Z., Fahrezi, A., Barnes, M., and Joshi, G. (2023). Heterogeneous loRA for federated fine-tuning of on-device foundation models. In *International Workshop on Federated Learning in the Age of Foundation Models in Conjunction with NeurIPS 2023*.

Chua, T. J., Yu, W., Zhao, J., and Lam, K. (2023). Fedpeat: Convergence of federated learning, parameter-efficient fine tuning, and emulator assisted tuning for artificial intelligence foundation models with mobile edge computing. *CoRR*, abs/2310.17491.

Collins, L., Wu, S., Oh, S., and Sim, K. C. (2023). Profit: Benchmarking personalization and robustness trade-off in federated prompt tuning. *CoRR*, abs/2310.04627.

Deng, W., Thrampoulidis, C., and Li, X. (2024). Unlocking the potential of prompt-tuning in bridging generalized and personalized federated learning.

Devlin, J., Chang, M.-W., Lee, K., and Toutanova, K. (2019). BERT: Pre-training of deep bidirectional transformers for language understanding. In Burstein, J., Doran, C., and Solorio, T., editors, *Proceedings of the 2019 Conference of the North American Chapter of the Association for Computational Linguistics: Human Language Technologies, Volume 1 (Long and Short Papers)*, pages 4171–4186, Minneapolis, Minnesota. Association for Computational Linguistics.

Ding, N., Lv, X., Wang, Q., Chen, Y., Zhou, B., Liu, Z., and Sun, M. (2023). Sparse low-rank adaptation

of pre-trained language models. In *Conference on Empirical Methods in Natural Language Processing*.

do Carmo, M. P. (2018). *Introduction to Riemannian Manifolds*, volume 176. Springer.

Dolan, W. B. and Brockett, C. (2005). Automatically constructing a corpus of sentential paraphrases. In *Proceedings of the Third International Workshop on Paraphrasing (IWP2005)*.

Dong, Y., Yan, D., Almudaifer, A. I., Yan, S., Jiang, Z., and Zhou, Y. (2020). Belt: A pipeline for stock price prediction using news. In *Proceedings of the 2020 IEEE International Conference on Big Data (BigData'20)*, pages 1137–1146, Atlanta, GA.

Edalati, A., Tahaei, M. S., Kobyzev, I., Nia, V. P., Clark, J. J., and Rezagholizadeh, M. (2022). Krona: Parameter efficient tuning with kronecker adapter. *CoRR*, abs/2212.10650.

Falini, A. (2022). A review on the selection criteria for the truncated svd in data science applications. *Journal of Computational Mathematics and Data Science*, 5:100064.

Fang, Z., Lin, Z., Chen, Z., Chen, X., Gao, Y., and Fang, Y. (2024). Automated federated pipeline for parameter-efficient fine-tuning of large language models.

Feng, C.-M., Li, B., Xu, X., Liu, Y., Fu, H., and Zuo, W. (2023). Learning federated visual prompt in null space for mri reconstruction. In *2023 IEEE/CVF Conference on Computer Vision and Pattern Recognition (CVPR)*, pages 8064–8073.

Golub, G., Hoffman, A., and Stewart, G. (1987). A generalization of the eckart-young-mirsky matrix approximation theorem. *Linear Algebra and its Applications*, 88-89:317–327.

Golub, G. H. and Van Loan, C. F. (2013). *Matrix Computations - 4th Edition*. Johns Hopkins University Press, Philadelphia, PA.

Goswami, S., Pokhrel, A., Lee, K., Liu, L., Zhang, Q., and Zhou, Y. (2020). Graphmap: Scalable iterative graph processing using nosql. *The Journal of Supercomputing (TJSC)*, 76(9):6619–6647.

Guimu Guo, Da Yan, L. Y. J. K. C. L. Z. J. and Zhou, Y. (2022). Maximal directed quasi-clique mining. In *Proceedings of the 38th IEEE International Conference on Data Engineering (ICDE'22)*, pages 1900–1913, Kuala Lumpur, Malaysia.

Guo, P., Zeng, S., Wang, Y., Fan, H., Wang, F., and Qu, L. (2025). Selective aggregation for low-rank adaptation in federated learning.

Guo, T., Guo, S., Wang, J., Tang, X., and Xu, W. (2024). Promptfl: Let federated participants cooperatively learn prompts instead of models - federated learning in age of foundation model. *IEEE Trans. Mob. Comput.*, 23(5):5179–5194.

He, J., Zhou, C., Ma, X., Berg-Kirkpatrick, T., and Neubig, G. (2022). Towards a unified view of parameter-efficient transfer learning. In *The Tenth International Conference on Learning Representations, ICLR 2022, Virtual Event, April 25-29, 2022*. OpenReview.net.

Hong, J., Zhu, Z., Lyu, L., Zhou, Y., Boddeti, V. N., and Zhou, J. (2023). International workshop on federated learning for distributed data mining. In *Proceedings of the 29th ACM SIGKDD Conference on Knowledge Discovery and Data Mining (KDD'23)*, pages 5861–5862, Long Beach, CA.

Horn, R. A. and Johnson, C. R. (2012). *Matrix Analysis*. Cambridge University Press, second edition.

Houlsby, N., Giurgiu, A., Jastrzebski, S., Morrone, B., de Laroussilhe, Q., Gesmundo, A., Attariyan, M., and Gelly, S. (2019). Parameter-efficient transfer learning for NLP. In Chaudhuri, K. and Salakhutdinov, R., editors, *Proceedings of the 36th International Conference on Machine Learning, ICML 2019, 9-15 June 2019, Long Beach, California, USA*, volume 97 of *Proceedings of Machine Learning Research*, pages 2790–2799. PMLR.

Hsieh, K., Phanishayee, A., Mutlu, O., and Gibbons, P. B. (2020). The non-iid data quagmire of decentralized machine learning. In *Proceedings of the 37th International Conference on Machine Learning, ICML 2020, 13-18 July 2020, Virtual Event*, pages 4387–4398.

Hu, E. J., Shen, Y., Wallis, P., Allen-Zhu, Z., Li, Y., Wang, S., Wang, L., and Chen, W. (2022). Lora: Low-rank adaptation of large language models. In *The Tenth International Conference on Learning Representations, ICLR 2022, Virtual Event, April 25-29, 2022*. OpenReview.net.

Hu, Y., Xie, Y., Wang, T., Chen, M., and Pan, Z. (2023). Structure-aware low-rank adaptation for parameter-efficient fine-tuning. *Mathematics*.

Jia, J., Li, K., Malek, M., Malik, K., Mahadeokar, J., Kalinli, O., and Seide, F. (2023). Joint federated learning and personalization for on-device asr. In *2023 IEEE Automatic Speech Recognition and Understanding Workshop (ASRU)*, pages 1–8.

Jia, J., Liu, J., Huo, C., Shen, Y., Zhou, Y., Dai, H., and Dou, D. (2025). Efficient federated learning with timely update dissemination. *Knowledge and Information Systems (KAIS)*, 67:10691–10725.

Jiang, J., Liu, X., and Fan, C. (2023). Low-parameter federated learning with large language models. *CoRR*, abs/2307.13896.

Jiang, Y., Perng, C.-S., Sailer, A., Silva-Lepe, I., Zhou, Y., and Li, T. (2016). Csm: A cloud service marketplace for complex service acquisition. *ACM Transactions on Intelligent Systems and Technology (TIST)*, 8(1):1–25.

Jin, J., Ren, J., Zhou, Y., Lv, L., Liu, J., and Dou, D. (2022a). Accelerated federated learning with decoupled adaptive optimization. In *Proceedings of the 39th International Conference on Machine Learning (ICML'22)*, pages 10298–10322, Baltimore, MD.

Jin, J., Zhang, Z., Zhou, Y., and Wu, L. (2022b). Input-agnostic certified group fairness via gaussian parameter smoothing. In *Proceedings of the 39th International Conference on Machine Learning (ICML'22)*, pages 10340–10361, Baltimore, MD.

Kendall, W. S., Barden, D., Carne, T. K., and Le, H. (2003). *Statistics on Special Manifolds*, volume 174. Springer-Verlag.

Khalid, U., Iqbal, H., Vahidian, S., Hua, J., and Chen, C. (2023). CEFHRI: A communication efficient federated learning framework for recognizing industrial human-robot interaction. In *IROS*, pages 10141–10148.

Khalil, J., Yan, D., Yuan, L., Han, J., Adhikari, S., Long, C., and Zhou, Y. (2024). Fsm-explorer: An interactive tool for frequent subgraph pattern mining from a big graph. In *Proceedings of the 40th IEEE International Conference on Data Engineering (ICDE'24)*, pages 5405–5408, Utrecht, Netherlands.

Khodak, M., Balcan, M., and Talwalkar, A. S. (2019). Adaptive gradient-based meta-learning methods. In *Advances in Neural Information Processing Systems 32: Annual Conference on Neural Information Processing Systems 2019, NeurIPS 2019, December 8-14, 2019, Vancouver, BC, Canada*, pages 5915–5926.

Kim, Y., Kim, J., Mok, W.-L., Park, J.-H., and Lee, S. (2023). Client-customized adaptation for parameter-efficient federated learning. In Rogers, A., Boyd-Graber, J., and Okazaki, N., editors, *Findings of the Association for Computational Linguistics: ACL 2023*, pages 1159–1172, Toronto, Canada. Association for Computational Linguistics.

Koo, J., Jang, M., and Ok, J. (2024). Towards robust and efficient federated low-rank adaptation with heterogeneous clients.

Krizhevsky, A., Nair, V., and Hinton, G. (2010). Cifar-10 (canadian institute for advanced research). `https://www.cs.toronto.edu/~kriz/cifar.html`.

Le, Y. and Yang, X. (2015). Tiny imagenet visual recognition challenge. `https://www.kaggle.com/c/tiny-imagenet`.

Lee, J. M. (2012). *Introduction to Smooth Manifolds*. Springer, 2 edition. New edition extensively revised and clarified, with topics substantially rearranged. Introduces the rank theorem and the fundamental theorem on flows earlier. Added topics include Sard's theorem, transversality, infinitesimal Lie group actions, first-order partial differential equations, degree theory for smooth maps between compact manifolds, and an introduction to contact structures. Supplementary material available at sn.pub/extras.

Lee, K., Liu, L., Ganti, R. L., Srivatsa, M., Zhang, Q., Zhou, Y., and Wang, Q. (2019). Lightwieight indexing and querying services for big spatial data. *IEEE Transactions on Services Computing (TSC)*, 12(3):343–355.

Lee, K., Liu, L., Schwan, K., Pu, C., Zhang, Q., Zhou, Y., Yigitoglu, E., and Yuan, P. (2015). Scaling iterative graph computations with graphmap. In *Proceedings of the 27th IEEE international conference for High Performance Computing, Networking, Storage and Analysis (SC'15)*, pages 57:1–57:12, Austin, TX.

Lee, K., Liu, L., Tang, Y., Zhang, Q., and Zhou, Y. (2013). Efficient and customizable data partitioning framework for distributed big rdf data processing in the cloud. In *Proceedings of the 2013 IEEE International Conference on Cloud Computing (CLOUD'13)*, pages 327–334, Santa Clara, CA.

Lester, B., Al-Rfou, R., and Constant, N. (2021). The power of scale for parameter-efficient prompt tuning. In Moens, M., Huang, X., Specia, L., and Yih, S. W., editors, *Proceedings of the 2021 Conference on Empirical Methods in Natural Language Processing, EMNLP 2021, Virtual Event / Punta Cana, Dominican Republic, 7-11 November, 2021*, pages 3045–3059. Association for Computational Linguistics.

Li, D., Zhu, Y., Gong, X., Mao, S., and Zhou, Y. (2024). Anarchic federated bilevel optimization. In *Proceedings of the 22nd International Symposium on Modeling and Optimization in Mobile, Ad Hoc, and Wireless Networks (WiOpt'24)*, pages 353–360, Seoul, Republic of Korea.

Li, G., Wu, W., Sun, Y., Shen, L., Wu, B., and Tao, D. (2023). Visual prompt based personalized federated learning. *CoRR*, abs/2303.08678.

Li, X. L. and Liang, P. (2021). Prefix-tuning: Optimizing continuous prompts for generation. In Zong, C., Xia, F., Li, W., and Navigli, R., editors, *Proceedings of the 59th Annual Meeting of the Association for Computational Linguistics and the 11th International Joint Conference on Natural Language Processing, ACL/IJCNLP 2021, (Volume 1: Long Papers), Virtual Event, August 1-6, 2021*, pages 4582–4597. Association for Computational Linguistics.

Liao, B., Meng, Y., and Monz, C. (2023). Parameter-efficient fine-tuning without introducing new latency. In Rogers, A., Boyd-Graber, J. L., and Okazaki, N., editors, *Proceedings of the 61st Annual Meeting of the Association for Computational Linguistics (Volume 1: Long Papers), ACL 2023, Toronto, Canada, July 9-14, 2023*, pages 4242–4260. Association for Computational Linguistics.

Lin, Z., Madotto, A., and Fung, P. (2020). Exploring versatile generative language model via parameter-efficient transfer learning. In Cohn, T., He, Y., and Liu, Y., editors, *Findings of the Association for Computational Linguistics: EMNLP 2020, Online Event, 16-20 November 2020*, volume EMNLP 2020 of *Findings of ACL*, pages 441–459. Association for Computational Linguistics.

Lin, Z., Sun, Y., Shi, Y., Wang, X., Huang, L., Shen, L., and Tao, D. (2023). Efficient federated prompt tuning for black-box large pre-trained models. *CoRR*, abs/2310.03123.

Liu, B., Ding, Z., Zhang, Y., She, H., and Du, Y. P. (2023a). Low-rank tensor subspace decomposition with weighted group sparsity for the acceleration of non-cartesian dynamic mri. *IEEE Transactions on Biomedical Engineering*, 70(2):681–693.

Liu, B., Zhang, Z., He, P., Wang, Z., Xiao, Y., Ye, R., Zhou, Y., Ku, W., and Hu, B. (2024a). A survey of lottery ticket hypothesis. *CoRR*, abs/2403.04861.

Liu, J., Che, T., Zhou, Y., Jin, R., Dai, H., Dou, D., and Valduriez, P. (2024b). Aedfl: Efficient asynchronous decentralized federated learning with heterogeneous devices. In *Proceedings of the 24th SlAM International Conference on Data Mining (SDM'24)*, pages 833–841, Houston, TX.

Liu, J., Huang, J., Zhou, Y., Li, X., Ji, S., Xiong, H., and Dou, D. (2022a). From distributed machine learning to federated learning: A survey. *Knowledge and Information Systems (KAIS)*, 64(4):885–917.

Liu, J., Jia, J., Che, T., Huo, C., Ren, J., Zhou, Y., Dai, H., and Dou, D. (2024c). Fedasmu: Efficient asynchronous federated learning with dynamic staleness-aware model update. In *Proceedings of the 38th AAAI Conference on Artificial Intelligence (AAAI'24)*, pages 13900–13908, Vancouver, Canada.

Liu, J., Jia, J., Ma, B., Zhou, C., Zhou, J., Zhou, Y., Dai, H., and Dou, D. (2023b). Multi-job intelligent scheduling with cross-device federated learning. *IEEE Transactions on Parallel and Distributed Systems (TPDS)*, 34(2):535–551.

Liu, J., Jia, J., Zhang, H., Yun, Y., Wang, L., Zhou, Y., Dai, H., and Dou, D. (2024d). Efficient federated learning using dynamic update and adaptive pruning with momentum on shared server data. *ACM Transactions on Intelligent Systems and Technology (TIST)*, 15(6):122:1–122:28.

Liu, J., Ma, B., Yu, Q., Jin, R., Zhou, J., Zhou, Y., Dai, H., Wang, H., Dou, D., and Valduriez, P. (2025). Efficient federated learning with heterogeneous data and adaptive dropout. *ACM Transactions on Knowledge Discovery from Data (TKDD)*, 19(8):146:1–146:31.

Liu, J., Ren, J., Jin, R., Zhang, Z., Zhou, Y., Valduriez, P., and Dou, D. (2024e). Fisher information-based efficient curriculum federated learning with large language models. In *Proceedings of the 29th Conference on Empirical Methods in Natural Language Processing (EMNLP'24)*, pages 10497–10523, Miami, FL.

Liu, L., Zhang, J., Song, S., and Letaief, K. B. (2019a). Edge-assisted hierarchical federated learning with non-iid data. *CoRR*, abs/1905.06641.

Liu, X., Ji, K., Fu, Y., Du, Z., Yang, Z., and Tang, J. (2021a). P-tuning v2: Prompt tuning can be comparable to fine-tuning universally across scales and tasks. *CoRR*, abs/2110.07602.

Liu, X., Ji, K., Fu, Y., Tam, W., Du, Z., Yang, Z., and Tang, J. (2022b). P-tuning: Prompt tuning can be comparable to fine-tuning across scales and tasks. In Muresan, S., Nakov, P., and Villavicencio, A., editors, *Proceedings of the 60th Annual Meeting of the Association for Computational Linguistics (Volume 2: Short Papers)*, pages 61–68, Dublin, Ireland. Association for Computational Linguistics.

Liu, X., Ratnarajah, T., Sellathurai, M., and Eldar, Y. C. (2024f). Adaptive model pruning and personalization for federated learning over wireless networks.

Liu, X., Zheng, Y., Du, Z., Ding, M., Qian, Y., Yang, Z., and Tang, J. (2021b). GPT understands, too. *CoRR*, abs/2103.10385.

Liu, X., Zhu, R., Zha, D., Gao, J., Zhong, S., and Qiu, M. (2023c). Differentially private low-rank adaptation of large language model using federated learning. *CoRR*, abs/2312.17493.

Liu, Y., Bi, X., Li, L., Chen, S., Yang, W., and Sun, X. (2023d). Communication efficient federated learning for multilingual neural machine translation with adapter. In Rogers, A., Boyd-Graber, J., and Okazaki, N., editors, *Findings of the Association for Computational Linguistics: ACL 2023*, pages 5315–5328, Toronto, Canada. Association for Computational Linguistics.

Liu, Y., Ott, M., Goyal, N., Du, J., Joshi, M., Chen, D., Levy, O., Lewis, M., Zettlemoyer, L., and Stoyanov, V. (2019b). Roberta: A robustly optimized BERT pretraining approach. *CoRR*, abs/1907.11692.

Liu, Y., Zhang, K., Li, Y., Yan, Z., Gao, C., Chen, R., Yuan, Z., Huang, Y., Sun, H., Gao, J., He, L., and Sun, L. (2024g). Sora: A review on background, technology, limitations, and opportunities of large vision models. *CoRR*, abs/2402.17177.

Liu, Z., Lyn, J., Zhu, W., Tian, X., and Graham, Y. (2024h). Alora: Allocating low-rank adaptation for fine-tuning large language models. *CoRR*, abs/2403.16187.

Lu, W., Hu, X., Wang, J., and Xie, X. (2023). Fedclip: Fast generalization and personalization for CLIP in federated learning. *IEEE Data Eng. Bull.*, 46(1):52–66.

McMahan, B., Moore, E., Ramage, D., Hampson, S., and y Arcas, B. A. (2017). Communication-efficient learning of deep networks from decentralized data. In Singh, A. and Zhu, X. J., editors, *Proceedings of the 20th International Conference on Artificial Intelligence and Statistics, AISTATS 2017, 20-22 April 2017, Fort Lauderdale, FL, USA*, volume 54 of *Proceedings of Machine Learning Research*, pages 1273–1282. PMLR.

Nguyen, N.-H., Nguyen, T.-A., Nguyen, T., Hoang, V. T., Le, D. D., and Wong, K.-S. (2024). Towards efficient communication and secure federated recommendation system via low-rank training. In *Proceedings of the ACM Web Conference 2024*, WWW '24, page 3940–3951, New York, NY, USA. Association for Computing Machinery.

Niu, Y., Prakash, S., Kundu, S., Lee, S., and Avestimehr, S. (2023). Overcoming resource constraints in federated learning: Large models can be trained with only weak clients. *Transaction on Machine Learning Research (TMLR)*.

Palanisamy, B., Liu, L., Zhou, Y., and Wang, Q. (2018). Privacy-preserving publishing of multilevel utility-controlled graph datasets. *ACM Transactions on Internet Technology (TOIT)*, 18(2):24:1–24:21.

Pfeiffer, J., Kamath, A., Rücklé, A., Cho, K., and Gurevych, I. (2021). Adapterfusion: Non-destructive task composition for transfer learning. In Merlo, P., Tiedemann, J., and Tsarfaty, R., editors, *Proceedings of the 16th Conference of the European Chapter of the Association for Computational Linguistics: Main Volume, EACL 2021, Online, April 19 - 23, 2021*, pages 487–503. Association for Computational Linguistics.

Qin, Z., Chen, D., Qian, B., Ding, B., Li, Y., and Deng, S. (2024). Federated full-parameter tuning of billion-sized language models with communication cost under 18 kilobytes.

Qiu, C., Li, X., Mummadi, C. K., Ganesh, M. R., Li, Z., Peng, L., and Lin, W.-Y. (2024). Federated text-driven prompt generation for vision-language models. In *The Twelfth International Conference on Learning Representations*.

Qu, W., Yan, D., Guo, G., Wang, X., Zou, L., and Zhou, Y. (2020). Parallel mining of frequent subtree patterns. In *Software Foundations for Data Interoperability and Large Scale Graph Data Analytics - 4th International Workshop, SFDI 2020, and 2nd International Workshop, LSGDA 2020, held in Conjunction with VLDB 2020*, pages 18–32, Tokyo, Japan.

Radford, A., Wu, J., Child, R., Luan, D., Amodei, D., and Sutskever, I. (2019). Language models are unsupervised multitask learners.

Rajabzadeh, H., Valipour, M., Zhu, T., Tahaei, M. S., Kwon, H. J., Ghodsi, A., Chen, B., and Rezagholizadeh, M. (2024). Qdylora: Quantized dynamic low-rank adaptation for efficient large language model tuning. *CoRR*, abs/2402.10462.

Ren, J., Zhang, Z., Jin, J., Zhao, X., Wu, S., Zhou, Y., Shen, Y., Che, T., Jin, R., and Dou, D. (2021). Integrated defense for resilient graph matching. In *Proceedings of the 38th International Conference on Machine Learning (ICML'21)*, pages 8982–8997, Virtual Event.

Ren, J., Zhou, Y., Jin, J., Lyu, L., and Yan, D. (2023). Dimension-independent certified neural network watermarks via mollifier smoothing. In *Proceedings of the 40th International Conference on Machine Learning (ICML'23)*, pages 28976–29008, Honolulu, HI.

Rücklé, A., Geigle, G., Glockner, M., Beck, T., Pfeiffer, J., Reimers, N., and Gurevych, I. (2021). Adapterdrop: On the efficiency of adapters in transformers. In Moens, M., Huang, X., Specia, L., and Yih, S. W., editors, *Proceedings of the 2021 Conference on Empirical Methods in Natural Language Processing, EMNLP 2021, Virtual Event / Punta Cana, Dominican Republic, 7-11 November, 2021*, pages 7930–7946. Association for Computational Linguistics.

Sattler, F., Wiedemann, S., Müller, K., and Samek, W. (2019). Robust and communication-efficient federated learning from non-iid data. *CoRR*, abs/1903.02891.

Schneider, A. (2015). Investigating traces of matrix products. Ms thesis, University of Minnesota Duluth, Duluth, Minnesota. Submitted in partial fulfillment of the requirements for the degree of MS Applied and Computational Mathematics.

Shysheya, A., Bronskill, J., Patacchiola, M., Nowozin, S., and Turner, R. E. (2023). Fit: Parameter efficient few-shot transfer learning for personalized and federated image classification. In *The Eleventh*

*International Conference on Learning Representations, ICLR 2023, Kigali, Rwanda, May 1-5, 2023*. OpenReview.net.

Singhal, R., Ponkshe, K., and Vepakomma, P. (2025). Fedex-lora: Exact aggregation for federated and efficient fine-tuning of foundation models.

Smith, V., Chiang, C., Sanjabi, M., and Talwalkar, A. S. (2017). Federated multi-task learning. In *Advances in Neural Information Processing Systems 30: Annual Conference on Neural Information Processing Systems 2017, December 4-9, 2017, Long Beach, CA, USA*, pages 4424–4434.

Socher, R., Perelygin, A., Wu, J., Chuang, J., Manning, C. D., Ng, A., and Potts, C. (2013). Recursive deep models for semantic compositionality over a sentiment treebank. In Yarowsky, D., Baldwin, T., Korhonen, A., Livescu, K., and Bethard, S., editors, *Proceedings of the 2013 Conference on Empirical Methods in Natural Language Processing*, pages 1631–1642, Seattle, Washington, USA. Association for Computational Linguistics.

Su, S., Li, B., and Xue, X. (2023). Fedra: A random allocation strategy for federated tuning to unleash the power of heterogeneous clients. *CoRR*, abs/2311.11227.

Su, Z., Liu, L., Li, M., Fan, X., and Zhou, Y. (2013). Servicetrust: Trust management in service provision networks. In *Proceedings of the 10th IEEE International Conference on Services Computing (SCC'13)*, pages 272–279, Santa Clara, CA.

Su, Z., Liu, L., Li, M., Fan, X., and Zhou, Y. (2015). Reliable and resilient trust management in distributed service provision networks. *ACM Transactions on the Web (TWEB)*, 9(3):1–37.

Sun, G., Mendieta, M., Luo, J., Wu, S., and Chen, C. (2023a). Fedperfix: Towards partial model personalization of vision transformers in federated learning. In *IEEE/CVF International Conference on Computer Vision, ICCV 2023, Paris, France, October 1-6, 2023*, pages 4965–4975. IEEE.

Sun, J., Xu, Z., Yin, H., Yang, D., Xu, D., Chen, Y., and Roth, H. R. (2023b). Fedbpt: Efficient federated black-box prompt tuning for large language models. *CoRR*, abs/2310.01467.

Sun, Y., Li, Z., Li, Y., and Ding, B. (2024). Improving loRA in privacy-preserving federated learning. In *The Twelfth International Conference on Learning Representations*.

Tobaben, M., Shysheya, A., Bronskill, J., Paverd, A., Tople, S., Béguelin, S. Z., Turner, R. E., and Honkela, A. (2023). On the efficacy of differentially private few-shot image classification. *CoRR*, abs/2302.01190.

Touvron, H., Lavril, T., Izacard, G., Martinet, X., Lachaux, M., Lacroix, T., Rozière, B., Goyal, N., Hambro, E., Azhar, F., Rodriguez, A., Joulin, A., Grave, E., and Lample, G. (2023a). Llama: Open and efficient foundation language models. *CoRR*, abs/2302.13971.

Touvron, H., Martin, L., Stone, K., Albert, P., Almahairi, A., Babaei, Y., Bashlykov, N., Batra, S., Bhargava, P., Bhosale, S., Bikel, D., Blecher, L., Ferrer, C. C., Chen, M., Cucurull, G., Esiobu, D., Fernandes, J., Fu, J., Fu, W., Fuller, B., Gao, C., Goswami, V., Goyal, N., Hartshorn, A., Hosseini, S., Hou, R., Inan, H., Kardas, M., Kerkez, V., Khabsa, M., Kloumann, I., Korenev, A., Koura, P. S., Lachaux, M.-A., Lavril, T., Lee, J., Liskovich, D., Lu, Y., Mao, Y., Martinet, X., Mihaylov, T., Mishra, P., Molybog, I., Nie, Y., Poulton, A., Reizenstein, J., Rungta, R., Saladi, K., Schelten, A., Silva, R., Smith, E. M., Subramanian, R., Tan, X. E., Tang, B., Taylor, R., Williams, A., Kuan, J. X., Xu, P., Yan, Z., Zarov, I., Zhang, Y., Fan, A., Kambadur, M., Narang, S., Rodriguez, A., Stojnic, R., Edunov, S., and Scialom, T. (2023b). Llama 2: Open foundation and fine-tuned chat models.

Trefethen, L. N. and Bau, D. (1997). *Numerical Linear Algebra*. SIAM.

Tribes, C., Benarroch-Lelong, S., Lu, P., and Kobyzev, I. (2023). Hyperparameter optimization for large language model instruction-tuning. *CoRR*, abs/2312.00949.

Valipour, M., Rezagholizadeh, M., Kobyzev, I., and Ghodsi, A. (2023). Dylora: Parameter-efficient tuning of pre-trained models using dynamic search-free low-rank adaptation. In Vlachos, A. and Augenstein, I., editors, *Proceedings of the 17th Conference of the European Chapter of the Association for Computational Linguistics, EACL 2023, Dubrovnik, Croatia, May 2-6, 2023*, pages 3266–3279. Association for Computational Linguistics.

Vandereycken, B. (2014). Fixed-rank matrix factorizations and riemannian low-rank optimization. *Computational Statistics*, 29:591–621.

Wang, A., Singh, A., Michael, J., Hill, F., Levy, O., and Bowman, S. (2018). GLUE: A multi-task benchmark and analysis platform for natural language understanding. In Linzen, T., Chrupała, G., and Alishahi, A., editors, *Proceedings of the 2018 EMNLP Workshop BlackboxNLP: Analyzing and Interpreting Neural Networks for NLP*, pages 353–355, Brussels, Belgium. Association for Computational Linguistics.

Wang, J., Wu, Z., Zhang, Y., Yuan, X., Lin, T., and Tao, Z. (2023). Cooperative hardware-prompt learning for snapshot compressive imaging. *CoRR*, abs/2306.01176.

Wang, Z., Shen, Z., He, Y., Sun, G., Wang, H., Lyu, L., and Li, A. (2024a). Flora: Federated fine-tuning large language models with heterogeneous low-rank adaptations.

Wang, Z., Shen, Z., He, Y., Sun, G., Wang, H., Lyu, L., and Li, A. (2024b). FLoRA: Federated fine-tuning large language models with heterogeneous low-rank adaptations. In *The Thirty-eighth Annual Conference on Neural Information Processing Systems*.

Wiebe, J., Wilson, T., and Cardie, C. (2005). Annotating expressions of opinions and emotions in language. *Lang. Resour. Evaluation*, 39(2-3):165–210.

Wu, C., Wu, F., Liu, R., Lyu, L., Huang, Y., and Xie, X. (2021). Fedkd: Communication efficient federated learning via knowledge distillation. *CoRR*, abs/2108.13323.

Wu, C., Wu, F., Lyu, L., et al. (2022). Communication-efficient federated learning via knowledge distillation. *Nature Communications*, 13:2032.

Wu, P., Li, K., Wang, T., and Wang, F. (2023). Fedms: Federated learning with mixture of sparsely activated foundations models. *CoRR*, abs/2312.15926.

Xu, J., Saravanan, K., van Dalen, R. C., Mehmood, H., Tuckey, D., and Ozay, M. (2024). Dp-dylora: Fine-tuning transformer-based models on-device under differentially private federated learning using dynamic low-rank adaptation.

Xu, M., Song, C., Tian, Y., Agrawal, N., Granqvist, F., van Dalen, R. C., Zhang, X., Argueta, A., Han, S., Deng, Y., Liu, L., Walia, A., and Jin, A. (2023). Training large-vocabulary neural language models by private federated learning for resource-constrained devices. In *IEEE International Conference on Acoustics, Speech and Signal Processing ICASSP 2023, Rhodes Island, Greece, June 4-10, 2023*, pages 1–5. IEEE.

Yan, D., Qu, W., Guo, G., Wang, X., and Zhou, Y. (2022a). Prefixfpm: A parallel framework for general-purpose mining of frequent and closed patterns. *The VLDB Journal (VLDBJ)*, 31(2):253–286.

Yan, D., Zhou, Y., and Guo, G. (2022b). Think-like-a-task programming model. In Albert Zomaya, J. T. and Sakr, S., editors, *Encyclopedia of Big Data Technologies*. Springer.

Yan, D., Zhou, Y., Guo, G., and Liu, H. (2022c). Parallel graph processing. In Albert Zomaya, J. T. and Sakr, S., editors, *Encyclopedia of Big Data Technologies*. Springer.

Yan, J., Liu, J., Wang, S., Xu, H., Liu, H., and Zhou, J. (2023). Heroes: Lightweight federated learning with neural composition and adaptive local update in heterogeneous edge networks. *CoRR*, abs/2312.01617.

Yang, Y., Long, G., Shen, T., Jiang, J., and Blumenstein, M. (2024). Dual-personalizing adapter for federated foundation models. *CoRR*, abs/2403.19211.

Yi, L., Yu, H., Wang, G., Liu, X., and Li, X. (2024). pfedlora: Model-heterogeneous personalized federated learning with lora tuning.

Yin, X., Yan, D., Almudaifer, A., Yan, S., and Zhou, Y. (2021). Forecasting stock prices using stock correlation graph: A graph convolutional network approach. In *Proceedings of the 34th International Joint Conference on Neural Networks (IJCNN'21)*, pages 1–8, Shenzhen, China.

Yu, S., Muñoz, J. P., and Jannesari, A. (2023). Federated foundation models: Privacy-preserving and collaborative learning for large models. *CoRR*, abs/2305.11414.

Yuan, L., Ahmad, A., Yan, D., Han, J., Adhikari, S., Yu, X., and Zhou, Y. (2024a). G2-aimd: A memory-efficient subgraph-centric framework for efficient subgraph search on gpus. In *Proceedings of the 40th IEEE International Conference on Data Engineering (ICDE'24)*, pages 3164–3177, Utrecht, Netherlands.

Yuan, L., Yan, D., Ahmad, A., Han, J., Adhikari, S., and Zhou, Y. (2025a). Out-of-core parallel spatial join outperforming in-memory systems: A BFS-DFS hybrid approach. In *Proceedings of the 34th ACM Symposium on High-Performance Parallel and Distributed Computing (HPDC'25)*, pages 23:1–23:14, Notre Dame, IN.

Yuan, L., Yan, D., Han, J., Ahmad, A., Zhou, Y., and Jiang, Z. (2024b). Faster depth-first subgraph matching on gpus. In *Proceedings of the 40th IEEE International Conference on Data Engineering (ICDE'24)*, pages 3151–3163, Utrecht, Netherlands.

Yuan, L., Yan, D., Tao, D., Han, J., Adhikari, S., Long, C., and Zhou, Y. (2025b). T-fsm: A scalable distributed task-based system for frequent subgraph pattern mining from a big graph. *ACM Transactions on Database Systems (TODS)*.

Zhang, F., Li, L., Chen, J., Jiang, Z., Wang, B., and Qian, Y. (2023a). Increlora: Incremental parameter allocation method for parameter-efficient fine-tuning. *CoRR*, abs/2308.12043.

Zhang, H., Liu, J., Jia, J., Zhou, Y., Dai, H., and Dou, D. (2022). Fedduap: Federated learning with dynamic update and adaptive pruning using shared data on the server. In *Proceedings of the 31st International Joint Conference on Artificial Intelligence (IJCAI'22)*, pages 2776–2782, Messe Wien, Vienna, Austria.

Zhang, H., Reddi, S. J., and Sra, S. (2017). Riemannian svrg: Fast stochastic optimization on riemannian manifolds.

Zhang, H. and Sra, S. (2016). First-order methods for geodesically convex optimization.

Zhang, J., Hu, J., So, A. M.-C., and Johansson, M. (2024a). Nonconvex federated learning on compact smooth submanifolds with heterogeneous data. In *The Thirty-eighth Annual Conference on Neural Information Processing Systems*.

Zhang, Q., Chen, M., Bukharin, A., He, P., Cheng, Y., Chen, W., and Zhao, T. (2023b). Adaptive budget allocation for parameter-efficient fine-tuning. In *The Eleventh International Conference on Learning Representations, ICLR 2023, Kigali, Rwanda, May 1-5, 2023*. OpenReview.net.

Zhang, Q., Liu, L., Lee, K., Zhou, Y., Singh, A., Mandagere, N., Gopisetty, S., and Alatorre, G. (2014). Improving hadoop service provisioning in a geographically distributed cloud. In *Proceedings of the 2014 IEEE International Conference on Cloud Computing (CLOUD'14)*, pages 432–439, Anchorage, AK.

Zhang, Q., Liu, L., Ren, Y., Lee, K., Tang, Y., Zhao, X., and Zhou, Y. (2013). Residency aware inter-vm communication in virtualized cloud: Performance measurement and analysis. In *Proceedings of the 2013 IEEE International Conference on Cloud Computing (CLOUD'13)*, pages 204–211, Santa Clara, CA.

Zhang, Z., Jin, J., Zhang, Z., Zhou, Y., Zhao, X., Ren, J., Liu, J., Wu, L., Jin, R., and Dou, D. (2021a). Validating the lottery ticket hypothesis with inertial manifold theory. In *Advances in Neural Information Processing Systems 34: Annual Conference on Neural Information Processing Systems 2021 (NeurIPS'21)*, pages 30196–30210, Virtual.

Zhang, Z., Yang, Y., Dai, Y., Wang, Q., Yu, Y., Qu, L., and Xu, Z. (2023c). FedPETuning: When federated learning meets the parameter-efficient tuning methods of pre-trained language models. In Rogers, A., Boyd-Graber, J., and Okazaki, N., editors, *Findings of the Association for Computational Linguistics: ACL 2023*, pages 9963–9977, Toronto, Canada. Association for Computational Linguistics.

Zhang, Z., Zhang, J., Huang, J., Qu, L., Zhang, H., and Xu, Z. (2024b). Fedpit: Towards privacy-preserving and few-shot federated instruction tuning. *CoRR*, abs/2403.06131.

Zhang, Z., Zhang, Z., Zhou, Y., Wu, L., Wu, S., Han, X., Dou, D., Che, T., and Yan, D. (2021b). Adversarial attack against cross-lingual knowledge graph alignment. In *Proceedings of the 26th Conference on Empirical Methods in Natural Language Processing (EMNLP'21)*, pages 5320–5337, Virtual Event / Punta Cana, Dominican Republic.

Zhao, H., Du, W., Li, F., Li, P., and Liu, G. (2023). Fedprompt: Communication-efficient and privacy-preserving prompt tuning in federated learning. In *ICASSP 2023 - 2023 IEEE International Conference on Acoustics, Speech and Signal Processing (ICASSP)*, pages 1–5.

Zhao, W., Chen, Y., Lee, R., Qiu, X., Gao, Y., Fan, H., and Lane, N. D. (2024). Breaking physical and linguistic borders: Multilingual federated prompt tuning for low-resource languages. In *The Twelfth International Conference on Learning Representations*.

Zhao, X., Zhang, Z., Zhang, Z., Wu, L., Jin, J., Zhou, Y., Jin, R., Dou, D., and Yan, D. (2021). Expressive 1-lipschitz neural networks for robust multiple graph learning against adversarial attacks. In *Proceedings of the 38th International Conference on Machine Learning (ICML'21)*, pages 12719–12735, Virtual Event.

Zhou, C., Liu, J., Jia, J., Zhou, J., Zhou, Y., Dai, H., and Dou, D. (2022a). Efficient device scheduling with multi-job federated learning. In *Proceedings of the 36th AAAI Conference on Artificial Intelligence (AAAI'22)*, pages 9971–9979, Vancouver, Canada.

Zhou, P., Hu, M., Xie, X., Huang, Y., Chen, K., and Chen, M. (2024a). MIP: clip-based image reconstruction from PEFT gradients. *CoRR*, abs/2403.07901.

Zhou, Y., Amimeur, A., Jiang, C., Dou, D., Jin, R., and Wang, P. (2018a). Density-aware local siamese autoencoder network embedding with autoencoder graph clustering. In *Proceedings of the 2018 IEEE International Conference on Big Data (BigData'18)*, pages 1162–1167, Seattle, WA.

Zhou, Y. and Liu, L. (2015). Social influence based clustering and optimization over heterogeneous information networks. *ACM Transactions on Knowledge Discovery from Data (TKDD)*, 10(1):1–53.

Zhou, Y., Liu, L., and Buttler, D. (2015a). Integrating vertex-centric clustering with edge-centric clustering for meta path graph analysis. In *Proceedings of the 21st ACM SIGKDD Conference on Knowledge Discovery and Data Mining (KDD'15)*, pages 1563–1572, Sydney, Australia.

Zhou, Y., Liu, L., Lee, K., Pu, C., and Zhang, Q. (2015b). Fast iterative graph computation with resource aware graph parallel abstractions. In *Proceedings of the 24th ACM Symposium on High-Performance Parallel and Distributed Computing (HPDC'15)*, pages 179–190, Portland, OR.

Zhou, Y., Liu, L., Lee, K., and Zhang, Q. (2015c). Graphtwist: Fast iterative graph computation with two-tier optimizations. *Proceedings of the VLDB Endowment (PVLDB)*, 8(11):1262–1273.

Zhou, Y., Liu, L., Seshadri, S., and Chiu, L. (2016). Analyzing enterprise storage workloads with graph modeling and clustering. *IEEE Journal on Selected Areas in Communications (JSAC)*, 34(3):551–574.

Zhou, Y., Ren, J., Jin, R., Zhang, Z., Zheng, J., Jiang, Z., Yan, D., and Dou, D. (2022b). Unsupervised adversarial network alignment with reinforcement learning. *ACM Transactions on Knowledge Discovery from Data (TKDD)*, 16(3):50:1–50:29.

Zhou, Y., Wu, S., Jiang, C., Zhang, Z., Dou, D., Jin, R., and Wang, P. (2018b). Density-adaptive local edge representation learning with generative adversarial network multi-label edge classification. In *Proceedings of the 18th IEEE International Conference on Data Mining (ICDM'18)*, pages 1464–1469, Singapore.

Zhou, Y., Zhang, Z., Wu, S., Sheng, V., Han, X., Zhang, Z., and Jin, R. (2021). Robust network alignment via attack signal scaling and adversarial perturbation elimination. In *Proceedings of the 30th Web Conference (WWW'21)*, pages 3884–3895, Virtual Event / Ljubljana, Slovenia.

Zhou, Y., Zhang, Z., Zhang, Z., Lyu, L., and Ku, W.-S. (2024b). Effective federated graph matching. In *Proceedings of the 41st International Conference on Machine Learning (ICML'24)*, Vienna, Austria.

Zhou, Z., Zhou, Y., Zhang, Z., Lyu, L., Yan, D., Jin, R., and Dou, D. (2025). Flexible, efficient, and stable adversarial attacks on machine unlearning. In *Proceedings of the 42nd International Conference on Machine Learning (ICML'25)*, Vancouver, Canada.

## Checklist

1. For all models and algorithms presented, check if you include:
   (a) A clear description of the mathematical setting, assumptions, algorithm, and/or model. Yes
   (b) An analysis of the properties and complexity (time, space, sample size) of any algorithm. Yes
   (c) (Optional) Anonymized source code, with specification of all dependencies, including external libraries. Yes Justification: We promise to release our open-source codes on GitHub and maintain a project website with detailed documentation for long-term access by other researchers and end-users after the paper is accepted.

2. For any theoretical claim, check if you include:
   (a) Statements of the full set of assumptions of all theoretical results. Yes
   (b) Complete proofs of all theoretical results. Yes
   (c) Clear explanations of any assumptions. Yes

3. For all figures and tables that present empirical results, check if you include:
   (a) The code, data, and instructions needed to reproduce the main experimental results (either in the supplemental material or as a URL). Yes
   (b) All the training details (e.g., data splits, hyperparameters, how they were chosen). Yes
   (c) A clear definition of the specific measure or statistics and error bars (e.g., with respect to the random seed after running experiments multiple times). Yes
   (d) A description of the computing infrastructure used. (e.g., type of GPUs, internal cluster, or cloud provider). Yes

4. If you are using existing assets (e.g., code, data, models) or curating/releasing new assets, check if you include:
   (a) Citations of the creator If your work uses existing assets. Yes
   (b) The license information of the assets, if applicable. Yes
   (c) New assets either in the supplemental material or as a URL, if applicable. Not Applicable
   (d) Information about consent from data providers/curators. Yes
   (e) Discussion of sensible content if applicable, e.g., personally identifiable information or offensive content. Not Applicable

5. If you used crowdsourcing or conducted research with human subjects, check if you include:
   (a) The full text of instructions given to participants and screenshots. Not Applicable
   (b) Descriptions of potential participant risks, with links to Institutional Review Board (IRB) approvals if applicable. Not Applicable
   (c) The estimated hourly wage paid to participants and the total amount spent on participant compensation. Not Applicable

# A Appendix

## A.1 Related Work

**Parameter Efficient Fine Tuning (PEFT).** As the scale of large language models (LLMs) continues to grow, the cost associated with the standard full fine-tuning paradigm has become extremely high. To address this issue, parameter-efficient fine-tuning (PEFT) methods Houlsby et al. (2019) have been proposed. These methods introduce a minimal set of additional trainable parameters to enhance model performance while keeping the majority of the pre-trained parameters frozen. Generally, PEFT approaches can be classified into two main categories based on how they manipulate model parameters. The first category, additive PEFT, involves the incorporation of new trainable modules or parameters to adjust the model architecture, minimizing the parameter count for downstream tasks. This includes Adapter Tuning (Houlsby et al., 2019), where small, trainable adapter modules are inserted within the model architecture to allow for task-specific adaptation without altering the original model weights, and methods such as prefix-tuning (Devlin et al., 2019), P-tuning (Liu et al., 2022b), P-tuning v2 (Liu et al., 2021a), and prompt tuning (Lester et al., 2021), which append learnable vectors at the beginning of input sequences. The second category involves reparameterized PEFT techniques that build low-rank representations of original model parameters, incorporating additional trainable parameters during training. This category includes Low-Rank Decomposition, techniques like LoRA Hu et al. (2022) and KronA (Edalati et al., 2022), which decompose original model parameters into low-rank and residual matrices, and LoRA derivatives such as AdaLoRA Zhang et al. (2023b) and SoRA (Liu et al., 2024g), which dynamically select the rank of LoRA to construct adaptable low-rank representations. Collectively, these methods represent the cutting-edge in efficient model training techniques, enabling the deployment of large language models in resource-constrained environments without sacrificing performance.

**Additive PEFT Methods in Federated Learning.** Parallel, distributed, and federated learning, which are specifically designed to minimize computational demands and associated communication overheads, have been extensively studied in recent years (Zhang et al., 2013; Lee et al., 2013; Su et al., 2013; Zhang et al., 2014; Su et al., 2015; Zhou et al., 2015b; Bao et al., 2015; Zhou et al., 2015c; Lee et al., 2015; Zhou et al., 2015a; Zhou and Liu, 2015; Jiang et al., 2016; Zhou et al., 2016, 2018b,a; Palanisamy et al., 2018; Lee et al., 2019; Qu et al., 2020; Dong et al., 2020; Goswami et al., 2020; Zhang et al., 2021a; Zhao et al., 2021; Zhou et al., 2021; Ren et al., 2021; Zhang et al., 2021b; Yin et al., 2021; Zhou et al., 2022a; Guimu Guo and Zhou, 2022; Jin et al., 2022a; Zhang et al., 2022; Che et al., 2022; Yan et al., 2022a; Liu et al., 2022a; Yan et al., 2022b,c; Zhou et al., 2022b; Jin et al., 2022b; Che et al., 2023c; Hong et al., 2023; Chen et al., 2023; Che et al., 2023b; Liu et al., 2023b; Ren et al., 2023; Liu et al., 2024c,b; Yuan et al., 2024b,a; Khalil et al., 2024; Zhou et al., 2024b; Li et al., 2024; Liu et al., 2024e,d,a; Cheng et al., 2025; Yuan et al., 2025a; Jia et al., 2025; Liu et al., 2025; Che et al., 2025; Yuan et al., 2025a,b; Zhou et al., 2025). The additive PEFT methods in federated learning integrate lightweight trainable blocks into the frozen foundational models (FMs) and fine-tune additional parameters for localized model adaptation in the federated setting. These approaches not only enhance computational and communication efficiency but also allow for the customization of heterogeneous models based on specific local data characteristics or user preferences. Recent work has introduced FedCLIP, a method that leverages lightweight adapters to enhance CLIP's performance in federated settings, significantly reducing computational and communication costs while ensuring fast generalization and personalization (Lu et al., 2023). Similarly, FedDAT has been developed to fine-tune foundation models in a multi-modal, heterogeneous federated learning environment, utilizing Dual-Adapter Teachers to efficiently handle data heterogeneity and improve knowledge transfer (Chen et al., 2024). The Client-Customized Adaptation approach further tailors federated learning to address client heterogeneity through hypernetworks that generate client-specific adapters, enhancing both the efficiency and efficacy of pre-trained model adaptation (Kim et al., 2023). In addressing the challenges of multilingual neural machine translation, a communication-efficient framework has been proposed that minimizes the need for heavy data transmission by transferring only lightweight adapters, thus maintaining performance despite substantial discrepancies in data distribution (Liu et al., 2023d). A practical approach toward federated learning in NLP, AdaFL1, identifies and configures adapter modules to optimize training efficiency and model performance across various NLP tasks (Cai et al., 2023a). Joint efforts in federated learning and personalization for on-device ASR have shown that integrating personalized adapters with federated training substantially reduces word error rates, demonstrating the effectiveness of combined federated learning and personalization strategies (Jia et al., 2023). Furthermore, the FedPETuning framework explores parameter-efficient tuning methods within federated learning, offering insights into privacy protection, performance efficiency, and resource constraints

(Zhang et al., 2023c). Research into image reconstruction from PEFT gradients within federated learning frameworks reveals potential security vulnerabilities, suggesting that even lightweight adapter gradients can be exploited to reconstruct training data (Zhou et al., 2024a). The novel concept of Dual-Personalizing Adapter for Federated Foundation Models introduces test-time personalization to address distribution shifts effectively, enhancing both global and local adaptation (Yang et al., 2024). FedPEAT combines emulator-assisted tuning with parameter-efficient fine-tuning within a federated context to tackle the challenges of deploying large foundation models efficiently (Chua et al., 2023). Adaptive model pruning within federated learning frameworks demonstrates a significant reduction in computation and communication latency, enabling efficient learning even over wireless networks (Liu et al., 2024f). The development of a communication-efficient federated learning framework for industrial human-robot interaction addresses data privacy and heterogeneity while reducing communication costs (Khalid et al., 2023). Moreover, new approaches in parameter-efficient fine-tuning aim to reduce latency and storage requirements without compromising the model's performance, indicating a shift towards more sustainable and efficient federated learning methodologies (Liao et al., 2023; Tobaben et al., 2023; Cai et al., 2023a; Shysheya et al., 2023). The other is promt tuning. prompt tuning incorporates trainable task-specific continuous cue vectors at the input layer (Liu et al., 2022b). PromptFL Guo et al. (2024) ships an off-the-shelf CLIP, to distributed clients who would cooperatively train shared soft prompts based on very few local data. FedPerfix Sun et al. (2023a) use a local adapter to generate prefixes and aggregate raw self-attention layers.Efforts to mitigate communication overhead in deploying large pre-trained models across decentralized networks have introduced techniques like model split aggregation, which significantly reduce the parameter transmission cost while maintaining robust defenses against adversarial attacks (Zhao et al., 2023). Other studies have emphasized the reduction of communication costs by employing compact, federated visual prompts specifically in contexts like medical imaging, where data heterogeneity often leads to catastrophic forgetting (Feng et al., 2023; Li et al., 2023). The PromptFL framework exemplifies another novel approach, shifting from traditional model training to prompt-based federated learning, leveraging foundational models to improve local training efficiency on limited data (Guo et al., 2024). Concurrently, text-driven prompt generation methods have been developed to adapt vision-language models to federated settings, demonstrating superior generalization capabilities across seen and unseen classes (Qiu et al., 2024). Multilingual and domain-specific adaptations further extend the applicability of prompt tuning in federated learning, offering significant improvements in data efficiency and robustness across various languages, especially in low-resource scenarios (Zhao et al., 2024; Bai et al., 2024b; Deng et al., 2024). Meanwhile, research on personalization and robustness trade-offs in federated systems has explored the implications of localized fine-tuning on model performance, revealing that strategic prompt tuning can significantly enhance both the personalization and robustness of federated models under diverse conditions (Collins et al., 2023; Lin et al., 2023). Innovative methods such as Federated Black-Box Prompt Tuning have also been proposed to address privacy concerns associated with large pre-trained models, emphasizing parameter-efficient strategies that reduce memory and communication requirements without compromising the model effectiveness (Lin et al., 2023; Sun et al., 2023b). The exploration of federated prompt tuning continues to evolve, tackling not only linguistic and domain-specific challenges but also aiming at enhancing the deployment efficiency and personalization of large-scale models across heterogeneous environments (Wang et al., 2023; Yu et al., 2023; Cai et al., 2023b; Che et al., 2023a).

**Reparametrization-based PEFT Methods in Federated Learning.** The hypothesis behind this class of methods is that fine-tuning adaptions can be reparameterized into optimization within low-rank subspaces (Aghajanyan et al., 2021). Low-Rank Adaptation (LoRA) (Hu et al., 2022), as a popular PEFT method from the area of LLMs, reduces the number of trainable parameters for downstream tasks by representing the weight updates with two smaller matrices (called update matrices) through low-rank decomposition (Liu et al., 2023a). For instance, FedIT Zhang et al. (2024b) leverages LoRA to improve the response quality of LLMs by utilizing diverse instructions from different clients. Noticeably, LoRA and its variants have also exhibited considerable potential in addressing the challenges inherent in data heterogeneity among clients in FL. Researchers have developed Heterogeneous LoRA, which introduces a novel approach by employing low-rank approximations with heterogeneous ranks across clients to balance overfitting risks and convergence speed, significantly enhancing federated fine-tuning efficiency and efficacy (Cho et al., 2023). Similarly, the SLoRA method tackles the challenges posed by high data heterogeneity in federated environments by employing a data-driven initialization technique that effectively bridges the performance gap between traditional fine-tuning and parameter-efficient methods (Babakniya et al., 2023). The application of LoRA in privacy-preserving federated settings has also been refined through Federated Freeze A LoRA (FFA-LoRA), which optimizes the stability and efficiency by adjusting the update mechanisms for low-rank matrices (Sun et al., 2024).FedRA introduces a random allocation strategy

that leverages heterogeneous client capabilities to optimize federated tuning, highlighting an approach that can dynamically adapt to varying client resources without requiring each to support the full model (Su et al., 2023). The pFedLoRA framework emerges as a solution to model-heterogeneous personalized federated learning by using homogeneous small adapters for efficient knowledge exchange across diverse federated clients, proving to significantly outperform existing methods in terms of computational and communication overheads (Yi et al., 2024). Moreover, the DP-LoRA algorithm has been tailored for differentially private federated learning, enabling secure, efficient large language model fine-tuning across sensitive domains by incorporating a Gaussian noise mechanism for privacy preservation (Liu et al., 2023c). In scenarios with severe resource constraints, Low-Parameter Federated Learning (LP-FL) combines few-shot prompt learning and LoRA techniques to mitigate the high costs associated with large language models, demonstrating robust performance even in limited data environments (Jiang et al., 2023). The automated FedPipe system has also been developed to enhance the parameter-efficient fine-tuning of large language models, employing low-rank adapters and a novel parameter quantization strategy to optimize both training efficiency and memory usage (Fang et al., 2024). Lastly, FedMS introduces a novel two-stage federated learning algorithm that integrates a mixture of sparsely activated foundation models to cater to personalized needs, employing a unique activation strategy to manage computational demands effectively (Wu et al., 2023). Heroes presents a lightweight federated learning framework employing a novel neural composition and adaptive local update mechanism, tailored for heterogeneous edge networks. This method significantly reduces traffic consumption and enhances the speed of federated learning by adaptively configuring neural components and update frequencies according to the capabilities and resources of participating clients (Yan et al., 2023). Meanwhile, efforts to facilitate large-vocabulary neural language model training in resource-constrained environments incorporate Differential Privacy and Partial Embedding Updates. This approach, combined with Low-Rank Adaptation and Noise Contrastive Estimation, allows for effective language model training on compute-constrained devices while ensuring privacy and reducing memory demands (Xu et al., 2023).

**Rank-Adaptive Low-Rank Adaption for FFT-FM.** This category of algorithms aim to dynamically allocate the rank among low-rank parameter matrices based on their importance score. DyLoRA Valipour et al. (2023) addresses these issues by introducing dynamic, search-free rank adjustment during training, allowing for flexible adaptation across a range of ranks with minimal retraining and significantly accelerates training times across various tasks without substantial sacrifices in performance. QDyLoRA Rajabzadeh et al. (2024) evolves this concept into quantized settings, facilitating dynamic rank adjustments within a single training session on constrained hardware, thus maintaining competitive performance while optimizing hardware utilization efficiently. DP-DyLoRA Xu et al. (2024) integrates dynamic low-rank adaptation with differential privacy under federated learning settings to enhance privacy while mitigating typical performance degradation associated with such measures, making it feasible to deploy large models in privacy-sensitive environments. Structure-Aware Low-Rank Adaptation (SaLoRA) Hu et al. (2023) fine-tunes LLMs by adapting the rank of updates based on the inherent structural properties of the model's layers, optimizing the allocation of trainable parameters to reflect varying importance across different model components. Sparse Low-rank Adaptation (SoRA) Ding et al. (2023) introduces an innovative method to dynamically adjust the intrinsic rank during the adaptation process using a gating mechanism that optimizes parameter sparsity, effectively balancing the trade-off between parameter efficiency and computational overhead. Hyperparameter Optimization for Large Language Model Instruction-Tuning Tribes et al. (2023)challenges optimizing LoRA's parameters through advanced blackbox optimization techniques to enhance the model's alignment with human-like processing abilities. ALoRA Liu et al. (2024h) pushes boundaries by dynamically allocating ranks during the fine-tuning process based on evaluated importance of different model components, thus allowing for more targeted and efficient adaptation tailored to specific downstream tasks. Lastly, IncreLoRA Zhang et al. (2023a) proposes an incremental parameter allocation method that adaptively adjusts ranks based on real-time assessments of module importance during training, showing great potential particularly in resource-constrained environments by optimizing parameter efficiency and model performance. Several pioneer rank-adaptive LoRA algorithms for FFT-FM iteratively aggregate local full parameter metrics into a global one and perform the SVD on the latter to find the optimal rank (Chai et al., 2022; Wu et al., 2021; Niu et al., 2023).

To our best knowledge, the common characteristics of the above rank-adaptive low-rank adaption methods is to (1) either fail to transplanting from the centralized setting to the federated environment (SVD-based rank-adaptive LoRA methods Zhang et al. (2023b); Ding et al. (2023); Zhang et al. (2023a)) due to the aggregation noise (Sun et al., 2024). (2) or raise extremely expensive cost in centralize learning and federated learning (rank sampling-based algorithms Valipour et al. (2023); Rajabzadeh et al. (2024); Xu et al. (2024) due to multi-time model fine-tuning at different ranks and federated rank-adaptive LoRA algorithms Chai et al. (2022); Wu et al.

(2021); Niu et al. (2023) with iterative SVD on large-scale full parameter metrics). This work is the first to offer a rank-adaptive low-rank adaptation solution for FFT-FM with Riemannian manifold theory, by eliminating the aggregation noise and the multi-time model FT, and reducing the SVD of large-scale full parameter matrix to the SVD of a low-rank matrix with low dimensions, for further enhancing both effectiveness and efficiency of FFT-FM.

### A.2 Aggregation Noise and Rank-drift Issue Definition

**Aggregation Noise:** The aggregation noise is due to the aggregation of low-rank matrices in the FFT-FM. Here, we introduce an illustrative example with two clients to better understand the aggregation noise.

Concretely, if the clients locally fine-tune on full parameters and the server aggregates with FedAvg, the new global model parameters can be expressed as follows.

$$\mathbf{W} = \mathbf{W}^0 + \frac{1}{2}(\Delta\mathbf{W}^1 + \Delta\mathbf{W}^2) \tag{19}$$

In our work, the clients locally fine-tune on both low-rank parameter matrices $\mathbf{U}^k$ and $\mathbf{V}^k$ and diagonal matrix $\mathbf{\Sigma}^k$ to determine the rank. The server uses FedAvg to aggregate the low-rank matrices and diagonal matrix.

$$\Delta\mathbf{W}^k = \mathbf{U}^k\mathbf{\Sigma}^k\mathbf{V}^k, \quad k \in 1, 2 \tag{20}$$

The expected global model parameter updates $\Delta\mathbf{W}$ can be expressed as follows.

$$\Delta\mathbf{W} = \frac{1}{2}(\Delta\mathbf{W}^1 + \Delta\mathbf{W}^2) = \frac{1}{2}(\mathbf{U}^1\mathbf{\Sigma}^1\mathbf{V}^1 + \mathbf{U}^2\mathbf{\Sigma}^2\mathbf{V}^2) \tag{21}$$

After using FedAvg to aggregate the local matrices $\mathbf{U}^k, \mathbf{\Sigma}^k, \mathbf{V}^k$, the server produces

$$\begin{aligned}
\Delta\tilde{\mathbf{W}} &= \frac{1}{2}\left(\mathbf{U}^1 + \mathbf{U}^2\right) \times \frac{1}{2}\left(\mathbf{\Sigma}^1 + \mathbf{\Sigma}^2\right) \times \frac{1}{2}\left(\mathbf{V}^1 + \mathbf{V}^2\right) \\
&= \frac{1}{2}(\mathbf{U}^1\mathbf{\Sigma}^1\mathbf{V}^1 + \mathbf{U}^2\mathbf{\Sigma}^2\mathbf{V}^2) \underline{- \frac{3}{8}\mathbf{U}^1\mathbf{\Sigma}^1\mathbf{V}^1 - \frac{3}{8}\mathbf{U}^2\mathbf{\Sigma}^2\mathbf{V}^2 + \frac{1}{8}\mathbf{U}^1\mathbf{\Sigma}^1\mathbf{V}^2 + \frac{1}{8}\mathbf{U}^1\mathbf{\Sigma}^2\mathbf{V}^1} \\
&+ \underline{\frac{1}{8}\mathbf{U}^1\mathbf{\Sigma}^2\mathbf{V}^2 + \frac{1}{8}\mathbf{U}^2\mathbf{\Sigma}^1\mathbf{V}^1 + \frac{1}{8}\mathbf{U}^2\mathbf{\Sigma}^1\mathbf{V}^2 + \frac{1}{8}\mathbf{U}^2\mathbf{\Sigma}^2\mathbf{V}^1} \\
&= \Delta\mathbf{W} \underline{- \frac{3}{8}\mathbf{U}^1\mathbf{\Sigma}^1\mathbf{V}^1 - \frac{3}{8}\mathbf{U}^2\mathbf{\Sigma}^2\mathbf{V}^2 + \frac{1}{8}\mathbf{U}^1\mathbf{\Sigma}^1\mathbf{V}^2 + \frac{1}{8}\mathbf{U}^1\mathbf{\Sigma}^2\mathbf{V}^1} \\
&+ \underline{\frac{1}{8}\mathbf{U}^1\mathbf{\Sigma}^2\mathbf{V}^2 + \frac{1}{8}\mathbf{U}^2\mathbf{\Sigma}^1\mathbf{V}^1 + \frac{1}{8}\mathbf{U}^2\mathbf{\Sigma}^1\mathbf{V}^2 + \frac{1}{8}\mathbf{U}^2\mathbf{\Sigma}^2\mathbf{V}^1}
\end{aligned} \tag{22}$$

where the underlined terms denote the difference between $\Delta\tilde{\mathbf{W}}$ and $\Delta\mathbf{W}$.

It is obvious that $\Delta\tilde{\mathbf{W}} \neq \Delta\mathbf{W}$ when $\mathbf{U}^1 \neq \mathbf{U}^2$, $\mathbf{\Sigma}^1 \neq \mathbf{\Sigma}^2$, and $\mathbf{V}^1 \neq \mathbf{V}^2$ due to the data heterogeneity property of federated learning. Therefore, the aggregation noise is raised.

$$\underbrace{\tilde{\mathbf{W}} = \mathbf{W}^0 + \Delta\tilde{\mathbf{W}}}_{\text{Parameter aggregation with SVD-based rank-adaptive LoRA + FedAvg}} \neq \underbrace{\mathbf{W}^0 + \Delta\mathbf{W} = \mathbf{W}}_{\text{Ideal parameter aggregation with FedAvg on full parameter matrices}} \tag{23}$$

The difference between $\Delta\tilde{\mathbf{W}}$ and $\Delta\mathbf{W}$ is mainly due to the noise introduced by the cross-products of LoRA modules from different clients. This difference may become more significant when (1) the number of local update steps between aggregations is large and (2) the local datasets are different across clients.

In the (Sun et al., 2024) paper, when the clients locally fine-tune on low-rank parameters based on LoRA and the server uses FedAvg to aggregate the low-rank matrices, the global model parameters can be expressed as follows.

$$\underbrace{\tilde{\mathbf{W}} = \mathbf{W}^0 + \frac{1}{2}(\mathbf{B}^1 + \mathbf{B}^2) \times \frac{1}{2}(\mathbf{A}^1 + \mathbf{A}^2)}_{\text{Parameter aggregation with LoRA + FedAvg}} \neq \underbrace{\mathbf{W}^0 + \frac{1}{2}(\mathbf{B}^1\mathbf{A}^1 + \mathbf{B}^2\mathbf{A}^2) = \mathbf{W}_0 + \frac{1}{2}(\Delta\mathbf{W}^1 + \Delta\mathbf{W}^2) = \mathbf{W}}_{\text{Ideal parameter aggregation with FedAvg on full parameter matrices}} \tag{24}$$

When the clients use LoRA locally, we have $\Delta\mathbf{W}^k = \mathbf{B}^k\mathbf{A}^k$ on client $k$. The data heterogeneity is a common challenging problem in the federated learning. The collected data on different clients are Non-Independent Identically Distributed (NonIID). Thus, the parameters of local models trained on the non-IID data are quite different from each other, i.e., $\mathbf{B}^1 \neq \mathbf{B}^2$ and $\mathbf{A}^1 \neq \mathbf{A}^2$. This leads to the aggregation noise in the (Sun et al., 2024) paper, i.e., the difference between $\mathbf{W}$ and $\tilde{\mathbf{W}}$ is not equal to 0. In order to address the aggregation noise, the (Sun et al., 2024) paper keeps both $\mathbf{W}^0$ and $\mathbf{A}^0$ frozen and makes only $\mathbf{B}$ trainable.

$$\underbrace{\tilde{\mathbf{W}} = \mathbf{W}^0 + \frac{1}{2}(\mathbf{B}^1 + \mathbf{B}^2) \times \mathbf{A}^0}_{\text{Parameter aggregation with LoRA + FedAvg}} = \underbrace{\mathbf{W}^0 + \frac{1}{2}(\mathbf{B}^1\mathbf{A}^0 + \mathbf{B}^2\mathbf{A}^0) = \mathbf{W}_0 + \frac{1}{2}(\Delta\mathbf{W}^1 + \Delta\mathbf{W}^2) = \mathbf{W}}_{\text{Ideal parameter aggregation with FedAvg on full parameter matrices}} \tag{25}$$

The magic of the (Sun et al., 2024) paper to handle the aggregation noise is to have only one parameter matrix ($\mathbf{B}$) trainable while freezing other parameter matrices. However, this approach cannot be directly utilized to conduct the client-drift issue in our work. Our work has three trainable parameter matrices $\mathbf{U}^k$, $\mathbf{V}^k$, and $\mathbf{\Sigma}^k$. If updating only the diagonal matrix $\mathbf{\Sigma}^k$ and freezing the parameter matrices $\mathbf{U}^k$ and $\mathbf{V}^k$, then the algorithm fails to update the parameter matrices, resulting in poor model performance. If updating either $\mathbf{U}^k$ or $\mathbf{V}^k$ and freezing $\mathbf{\Sigma}^k$, then the rank cannot be optimized, leading to high computational cost (by higher rank) or poor model performance (by lower rank).

Thus, We propose a Riemannian parameter matching method to match the local parameter matrices $\mathbf{U}^k$ and $\mathbf{V}^k$ on other clients with pivots $\mathbf{U}^1$ and $\mathbf{V}^1$ on client 1, in terms of their lengths and directions, i.e. $\tilde{\mathbf{U}}^k = \mathbf{U}^k\mathbf{R}^k \approx \mathbf{U}^1$ and $\tilde{\mathbf{V}}^k = \mathbf{S}^k\mathbf{V}^k \approx \mathbf{V}^1$. To maintain the consistency between low-rank parameter metrics before and after the Riemannian parameter matching, i.e., $\mathbf{U}^2\mathbf{\Sigma}^2\mathbf{V}^2 = \tilde{\mathbf{U}}^2\tilde{\mathbf{\Sigma}}^2\tilde{\mathbf{V}}^2 \approx \mathbf{U}^1\tilde{\mathbf{\Sigma}}^2\mathbf{V}^1$, for ensuring the effectiveness of FFT-FM with rank-adaptive LoRA, we derive a modified diagonal matrix $\tilde{\mathbf{\Sigma}}^k$ for the other clients by performing the SVD on low-dimensional $r \times r$ matrices $(\mathbf{U}^1)^T\mathbf{U}^k$ and $(\mathbf{V}^1)^T\mathbf{V}^k$. Thus, the aggregation noise is resolved.

$$\begin{aligned}\Delta\tilde{\mathbf{W}} &= \frac{1}{2}\left(\mathbf{U}^1 + \tilde{\mathbf{U}^2}\right) \times \frac{1}{2}\left(\mathbf{\Sigma}^1 + \tilde{\mathbf{\Sigma}}^2\right) \times \frac{1}{2}\left(\mathbf{V}^1 + \tilde{\mathbf{V}^K}\right) \\ &\approx \mathbf{U}^1 \times \frac{1}{2}\left(\mathbf{\Sigma}^1 + \tilde{\mathbf{\Sigma}}^2\right) \times \mathbf{V}^1 = \frac{1}{2}\left(\mathbf{U}^1\mathbf{\Sigma}^1\mathbf{V}^1 + \mathbf{U}^2\mathbf{\Sigma}^2\mathbf{V}^2\right) = \Delta\mathbf{W}\end{aligned} \tag{26}$$

Based on the global diagonal matrix $\frac{1}{2}\left(\mathbf{\Sigma}^1 + \tilde{\mathbf{\Sigma}}^2\right)$, it is easy to find the optimal rank of the global parameter matrix, with aggregation on only the local low-rank matrices $\mathbf{U}^k, \tilde{\mathbf{\Sigma}}^k$, and $\mathbf{V}^k$.

**Rank-drift issue:** The data heterogeneity is a common challenging problem in the federated learning. The collected data on different clients are Non-Independent Identically Distributed (Non-IID). Thus, the parameters of local models trained on the non-IID data are quite different from each other as well as the parameters of global model. Each local model may oscillate back and forth in different training rounds, leading to unstable and slow convergence and causing suboptimal model performance.

At the same time, due to the heterogeneity of local models, the optimal ranks of local models are quite different from each other as well as the one of global model, raising the rank-drift issue. Similarly, the oscillation of the optimal rank of each local model can slow down the model convergence and degrade the model performance. For example, given two clients 1 and 2, in round 1, the local model on client 1/2 has the optimal rank 5/20. The server aggregates local models from clients to generate a global model based on FedAvg. The global model by model aggregation has the optimal rank 12. In round 2, after the global model are sent back to the clients, the clients begin the training with the global model with the optimal rank 12. Thus, the optimal rank of local models oscillate between 5/20 and 12. The rank oscillation may repeat in each training round, slowing down the model convergence.

The following table 3 presents a case study regarding the rank-drift in federated learning. In round 1, the optimal rank of the global model is 16. In round 2, the optimal rank is changed to 11. In subsequent rounds, the optimal

rank continue to oscillate back and forth. The ranks of local models fluctuate around values such as 9.75, 10.17, and 10.53, while the rank of global modelgradually decreases and stabilizes at 8. These results confirm that rank-drift introduces instability into the training process, slowing convergence and degrading performance, which emphasizes the importance of our Riemannian gradient descent optimization approach to stabilize ranks and ensure efficient training.

Table 3: Client and Server Ranks for LLaMA 7B + MPQA across 25 Rounds

| **Round (1-25)** | **Client Rank** | **Server Rank** |
|---|---|---|
| 1 | 16.000000 | 16 |
| 2 | 9.206250 | 11 |
| 3 | 9.153125 | 10 |
| 4 | 9.750000 | 10 |
| 5 | 10.165625 | 9 |
| 6 | 10.004688 | 9 |
| 7 | 9.881250 | 9 |
| 8 | 9.951563 | 9 |
| 9 | 10.168750 | 9 |
| 10 | 10.392188 | 8 |
| 11 | 10.467188 | 8 |
| 12 | 10.526563 | 8 |
| 13 | 10.506250 | 8 |
| 14 | 10.518750 | 8 |
| 15 | 10.507813 | 8 |
| 16 | 10.454688 | 8 |
| 17 | 10.393750 | 8 |
| 18 | 10.295313 | 8 |
| 19 | 10.212500 | 8 |
| 20 | 10.175000 | 8 |
| 21 | 10.110938 | 8 |
| 22 | 10.029688 | 8 |
| 23 | 9.981250 | 8 |
| 24 | 9.932813 | 8 |
| 25 | 9.903125 | 8 |

### A.3 Algorithm

**Algorithm 1** Federated Learning with Optimal Rank Selection and Alignment

**Input:** Client datasets $\{\mathcal{D}_k\}_{k=1}^{K}$, Threshold $\alpha$, The number of local epoch $E$, The number of global round $R$
**Output:** Optimally ranked updated matrices $U_R, S_R, V_R$
**function** SERVER INITIALIZATION
    Initialize $S$ as zero matrix
    Initialize $U, V$ with random Gaussian values
**end function**
**function** CLIENT UPDATE (K,U,S,V) // RUN ON CLIENT K
    **for** each local epoch i from 1 to E **do**
        batches $\leftarrow$ ($\mathcal{D}_k$ spilt into batches of size)
        **for** batch b in batches **do**
            computes the Riemannian gradient $P\nabla L^k$ based on Eq.(15)
            $(\mathbf{U}^k L^k, \mathbf{\Sigma}^k L^k, \mathbf{V}^k L^k)$
            computes $(\mathbf{U}^k)^{(t+1)}, (\mathbf{\Sigma}^k)^{(t+1)}, (\mathbf{V}^k)^{(t+1)}$ based on Eq.(16)
            $\left((\mathbf{U}^k)^{(t+1)}, (\mathbf{\Sigma}^k)^{(t+1)}, (\mathbf{V}^k)^{(t+1)}\right) = f\left(-\eta_t\left(\left(\Gamma_{\mathbf{U}^k} L^k\right)^{(t)}, \left(\Gamma_{\mathbf{\Sigma}^k} L^k\right)^{(t)}, \left(\Gamma_{\mathbf{V}^k} L^k\right)^{(t)}\right)\right)$
        **end for**
    **end for**
    return $(\mathbf{U}^k)^{(t+1)}, (\mathbf{\Sigma}^k)^{(t+1)}, (\mathbf{V}^k)^{(t+1)}$ to the server
**end function**
**function** SERVER ALIGNMENT AND AGGREGATION
    **for** each round t from 1 to C **do**
        **for** each client k in K clients **do**
            $(\mathbf{U}^k)^{(t+1)}, (\mathbf{\Sigma}^k)^{(t+1)}, (\mathbf{V}^k)^{(t+1)} \leftarrow$ Client Update (k,$(\mathbf{U}^k)^{(t)}, (\mathbf{\Sigma}^k)^{(t)}, (\mathbf{V}^k)^{(t)}$)
        **end for**
        Compute alignment matrix $\mathbf{S}^k, \mathbf{R}^k$ using $(\mathbf{U}^1)^{(t+1)}, (\mathbf{V}^1)^{(t+1)}$ as reference based on Eq.(7)
        **for** $k = 1$ to $K$ **do**
            Align $(\mathbf{U}^k)^{(t+1)}$ to $(\mathbf{U}^1)^{(t+1)}$: $(\tilde{\mathbf{U}}^k)^{(t+1)} = (\mathbf{U}^k)^{(t+1)}\mathbf{R}^k$
            Align $(\mathbf{V}^k)^{(t+1)}$ to $(\mathbf{V}^1)^{(t+1)}$: $(\tilde{\mathbf{V}}^k)^{(t+1)} = \mathbf{S}^k(\mathbf{V}^k)^{(t+1)}$
        **end for**
        Update $(\mathbf{\Sigma}^k)^{(t+1)}$ based on Eq.(9)
        Aggregate updates:
        $\tilde{\mathbf{U}}' = \sum_{k=1}^{K} \frac{n_k}{n} \tilde{\mathbf{U}}^k$
        $\tilde{\mathbf{\Sigma}}' = \sum_{k=1}^{K} \frac{n_k}{n} \tilde{\mathbf{\Sigma}}^k$
        $\tilde{\mathbf{V}}' = \sum_{k=1}^{K} \frac{n_k}{n} \tilde{\mathbf{V}}^k$
        Determine rank $r$ based on Eq.(11):
        $\Theta(r) = \frac{\sum_{i=1}^{r} \tilde{\mathbf{\Sigma}}'_{ii}}{\sum_{i=1}^{r_{max}} \tilde{\mathbf{\Sigma}}'_{ii}} \geq \varphi$
        Update $\tilde{\mathbf{\Sigma}}'$ to only include top $r$ singular values
        Update $\tilde{\mathbf{U}}', \tilde{\mathbf{V}}'$ accordingly
    **end for**
**end function**

In order to solve the aggregation noise and rank-drift issues and significantly improves the computational cost, we exploit a Riemannian manifold based method as detailed in Algorithm 1. Within each round, every client performs local updates(algorithm 1). The updates are based on the Riemannian gradient and the retraction function (algorithm 1,algorithm 1). After the updates, each client sends the updated parameters back to the server(algorithm 1). The server then performs Riemannian parameter matching between the U and V matrices of all clients and those of the first client to achieve alignment in both length and direction.(algorithm 1-algorithm 1) The singular value matrix is updated according to Formula6, and the aggregated U, V and Σ matrices from all clients are combined.(algorithm 1-algorithm 1) The rank for the next round of training is selected through Formula 11, and the model parameter matrix is updated accordingly.(algorithm 1-algorithm 1)

### A.4 Approximation Matrix Upper Bound

Lemmas 1-3 are the preliminary steps of proof of Theorem 1. Lemmas 1-3 and Theorem 1 together derive the upper bound on the Frobenius norm error for off-diagonal elements after an orthogonal transformation in Eq.(10).

Lemma 1 demonstrates the Frobenius norm of a matrix orthogonally invariant. It is used to conduct the approximation error analysis in Eq.(29).

**Lemma 1** (Orthogonal Matrix and Frobenius Norm Preservation)**.** *Let $U \in \mathbb{R}^{n\times n}$ be an orthogonal matrix, i.e., $U^\top U = I$. For any $A \in \mathbb{R}^{n\times m}$, the Frobenius norm $\|A\|_F$ satisfies:*

$$\|U^\top A\|_F = \|A\|_F. \tag{27}$$

*Please refer to Golub and Van Loan (2013) for the detailed proof.*

Lemma 2 is the extension of the Cauchy-Schwarz inequality on matrices. It is utilized to derive an upper bound of Eq.(30) and further the bounded error of matrix approximation.

**Lemma 2** (Cauchy-Schwarz Inequality for Frobenius Norm)**.** *For any $A, B \in \mathbb{R}^{n\times m}$, the Frobenius norms $\|A\|_F$ and $\|B\|_F$ satisfy:*

$$|tr(A^\top B)| \leq \|A\|_F \|B\|_F. \tag{28}$$

*where $tr(\cdot)$ is the trace of a matrix.*

*Please refer to Horn and Johnson (2012) for the detailed proof.*

Lemma 3 validates how the condition number of $S^k$ governs the amplification of off-diagonal errors during inversion, thereby quantifying the impact on the approximation error. It is employed to obtain the total approximation error bound in Eq. (33) in Theorem 1.

**Lemma 3** (Condition Number and Off-Diagonal Error Amplification)**.** *Let $S \in \mathbb{R}^{n\times n}$ be a symmetric positive definite matrix with condition number $\kappa(S) = \lambda_{\max}(S)/\lambda_{\min}(S)$. Then the Frobenius norm of the off-diagonal part of the inverse matrix is bounded by:*

$$\|S^{-1}_{\textit{off-diagonal}}\|_F \leq \kappa(S)\|S_{\textit{off-diagonal}}\|_F. \tag{29}$$

*where $S^{-1}$ is the inverse of the matrix $S$.*

*Please refer to Trefethen and Bau (1997) for the detailed proof.*

The following theorems provide upper bounds on the Frobenius norm error for off-diagonal elements after an orthogonal transformation.

**Theorem 1.** *We assume that the Frobenius norm of $\mathbf{R}^k$ is bounded by a constant $H$, and its eigenvalues lie within the interval $[\lambda_{R_{\min}}, \lambda_{R_{\max}}]$. Similarly, the Frobenius norm of $\mathbf{S}^k$ is bounded by a constant $N$, with eigenvalues in the range $[\lambda_{S_{\min}}, \lambda_{S_{\max}}]$. Additionally, the matrix $\Delta W$ has rank $r$. Given these conditions, the total approximation error bound in Equation 10 is derived as follows*

$$\begin{aligned}
&\|\mathbf{U}^1 \times \frac{1}{K}\left(\mathbf{\Sigma}^1 + \sum_{k=2}^{K}\tilde{\mathbf{\Sigma}}^k\right) \times \mathbf{V}^1 - \frac{1}{K}\left(\sum_{k=1}^{K}\mathbf{U}^k\mathbf{\Sigma}^k\mathbf{V}^k\right)\|_F^2 \\
&= \sum_{k=2}^{K}\left(2r(1-H-N) + (1+(\frac{\lambda_{R_{\max}}}{\lambda_{R_{\min}}})^2)H^2 + (1+(\frac{\lambda_{S_{\max}}}{\lambda_{S_{\min}}})^2)N^2\right)
\end{aligned} \tag{30}$$

*Proof.* From Equation 10, we observe that the total approximation error consists of three components: the approximation error from the matrices $\mathbf{U^k R^k}$, the approximation error from $\mathbf{V^k S^k}$, and the approximation error due to the diagonal optimal solution of the $\tilde{\mathbf{\Sigma}}^k$ matrix. We calculate the error between the two components by

computing the square of the Frobenius norm between them. These components can be expressed as follows:

$$\begin{aligned}&\|\mathbf{U}^1 \times \frac{1}{K}\left(\mathbf{\Sigma}^1 + \sum_{k=2}^{K}\tilde{\mathbf{\Sigma}}^k\right) \times \mathbf{V}^1 - \frac{1}{K}\left(\sum_{k=1}^{K}\mathbf{U}^k\mathbf{\Sigma}^k\mathbf{V}^k\right)\| \\ &= \sum_{k=2}^{K}(\|\mathbf{U}^1 - \mathbf{U}^k\mathbf{R}^k\|_F^2 + \|\mathbf{V}^1 - \mathbf{S}^k\mathbf{V}^k\|_F^2 \\ &+ \|(\mathbf{R_{ii}}^k)^{-1}\mathbf{\Sigma_{ii}}^k(\mathbf{S_{ii}}^k)^{-1} - (\mathbf{R}^k)^{-1}\mathbf{\Sigma}^k(\mathbf{S}^k)^{-1}\|_F^2)\end{aligned} \tag{31}$$

The approximation error analysis for both $\mathbf{U^kR^k}$ and $\mathbf{V^kS^k}$ is similar. Therefore, we focus on $\mathbf{U^kR^k}$ as an example. By expanding the Frobenius norm of the difference, we obtain the following expression:

$$\|\mathbf{U}^1 - \mathbf{U}^k\mathbf{R}^k\|_F^2 = \mathrm{tr}\left((\mathbf{U}^1)^T\mathbf{U}^1\right) - 2\mathrm{tr}\left((\mathbf{U}^1)^T\mathbf{U}^k\mathbf{R}^k\right) + \mathrm{tr}\left((\mathbf{R}^k)^T(\mathbf{U}^k)^T\mathbf{U}^k\mathbf{R}^k\right) \tag{32}$$

For the first term, since $\mathbf{U}^1$ is an orthogonal matrix, we have $(\mathbf{U}^1)^T\mathbf{U}^1 = I$, and thus $\mathrm{tr}(I) = r$. Similarly, since $U^k$ is an orthogonal matrix, the third term can be simplified as $tr(\mathbf{R}^k)^T\mathbf{R}^k)) = \|\mathbf{R}^k\|_F^2 \leq H^2$ For the second term, as shown in Equation (15), we have $-2\mathrm{tr}(\mathbf{P}^k\mathbf{\Lambda}^k(\mathbf{Q}^k)^T\mathbf{R}^k)$. Using the Cauchy-Schwarz inequality, we can further bound this term as follows:

$$\mathrm{tr}(\mathbf{\Lambda}^k(\mathbf{Q}^k)^T\mathbf{R}^k\mathbf{P}^k) \leq \|\mathbf{\Lambda}^k\|_F \cdot \|(\mathbf{Q}^k)^T\mathbf{R}^k\mathbf{P}^k\|_F \leq rH \tag{33}$$

Then we get approximation error between $\mathbf{U^kR^k}$ and $\mathbf{U}^1$

$$\|\mathbf{U}^1 - \mathbf{U}^k\mathbf{R}^k\|_F^2 = r - 2rH + H^2 \tag{34}$$

Similarly, the approximation error between $\mathbf{V^kS^k}$ and $\mathbf{V}^1$ be bounded as follows

$$\|\mathbf{V}^1 - \mathbf{S}^k\mathbf{V}^k\|_F^2 = r - 2rN + N^2 \tag{35}$$

The error between the optimal diagonal solution and the original complete matrix primarily arises from the off-diagonal elements. Since $\mathbf{\Sigma}^k$ is a diagonal matrix, the off-diagonal error is determined solely by the off-diagonal components of $\mathbf{R}^k$ and $\mathbf{S}^k$. Then we have

$$\begin{aligned}&\|(\mathbf{R_{ii}}^k)^{-1}\mathbf{\Sigma_{ii}}^k(\mathbf{S_{ii}}^k)^{-1} - (\mathbf{R}^k)^{-1}\mathbf{\Sigma}^k(\mathbf{S}^k)^{-1}\|_F^2 \\ &= \sum_{i\neq j}((\mathbf{R}^k)_{ij}^{-1}(\mathbf{S}^k)_{ji}^{-1})^2 \leq \|(\mathbf{R}^k)_{ij}^{-1}\|_F^2\|(\mathbf{S}^k)_{ji}^{-1}\|_F^2\end{aligned} \tag{36}$$

Based on the condition number of the matrix, we know that the norm of the off-diagonal part of the inverse matrix can be amplified by at most $\kappa$ times the norm of the off-diagonal part of the original matrix. Since $\mathbf{R}^k$ and $\mathbf{S}^k$ are symmetric positive definite matrices, the condition number is determined by the ratio of the largest to smallest eigenvalues, then we get

$$\|(\mathbf{R_{ii}}^k)^{-1}\mathbf{\Sigma_{ii}}^k(\mathbf{S_{ii}}^k)^{-1} - (\mathbf{R}^k)^{-1}\mathbf{\Sigma}^k(\mathbf{S}^k)^{-1}\|_F^2 \leq (\frac{\lambda_{R_{\max}}}{\lambda_{R_{\min}}})^2H^2 + (\frac{\lambda_{S_{\max}}}{\lambda_{S_{\min}}})^2N^2 \tag{37}$$

□

Theorem 1 obtains the upper bound on the Frobenius norm error for off-diagonal elements after an orthogonal transformation in Eq.(10). Eq.(10) consists of three terms: the aligned parameter matrices $\mathbf{U}^k\mathbf{R}^k$ and $\mathbf{V}^k\mathbf{S}^k$ for client $k$ and the modified version $\tilde{\mathbf{\Sigma}}^k$ of diagonal matrix $\mathbf{\Sigma}^k$. The approximation error in Eq.(12) in Theorem 1 is raised by all the above three terms together. Eq.(28) leverages Lemma 1 to separate three components from the left side in Eq.(12). Eqs.(29)-(32) utilize Lemma 2 to estimate the error bounds led by $\mathbf{U}^k\mathbf{R}^k$ and $\mathbf{V}^k\mathbf{S}^k$. Eq.(A.4) employs Lemma 3 to derive the amplification of off-diagonal errors by $\|\tilde{\mathbf{\Sigma}}^k - \mathbf{\Sigma}^k\|_F$.

### A.5 Riemann Gradient and Retraction

Lemmas 4-8 are the preliminary steps of proof of Theorem 2. Lemmas 4-8 and Theorem 2 together demonstrates that the Riemannian gradient descent (RGD) optimization on the Riemannian manifold ensures the rank invariance during the local update process.

Lemma 4 analyzes the correlation between a submatrix $\mathbf{w}_{11}$ of a matrix $\mathbf{W}$ and other submatrices of $\mathbf{W}$, which is essential for constructing the local defining function for the smooth manifold $M_r$. Therefore, it underpins the theoretical foundation of the matrix decomposition in Eq.(39).

**Lemma 4** (Partitioning and Submatrix Inversion)**.** *Let $W \in \mathbb{R}^{m\times n}$ with rank $r$. If $w_{11} \in \mathbb{R}^{r\times r}$ is an invertible submatrix of $W$, then $W$ can be partitioned as:*

$$W = \begin{bmatrix} w_{11} & w_{12} \\ w_{21} & w_{22} \end{bmatrix} \tag{38}$$

*where $w_{12}$, $w_{21}$, and $w_{22}$ are submatrices. The submatrix $X \in \mathbb{R}^{r\times(n-r)}$ satisfies:*

$$X = w_{11}^{-1} w_{12}, \quad w_{22} = w_{21}X = w_{21}w_{11}^{-1}w_{12} \tag{39}$$

*Please refer to Boumal (2023) for detailed proof.*

Lemma 5 ensures that the tangent space $T_M$ is well-defined and $M_r$ is an embedded submanifold of $\mathbb{R}^{m\times n}$, and thus introduces Definition 1.

**Lemma 5** (Differentiability of Local Defining Function)**.** *Let $h : \mathbb{R}^{(m-r)\times(n-r)} \to \mathbb{R}^{m\times n}$ be defined as:*

$$h(Y) = Y_{22} - Y_{21}Y_{11}^{-1}Y_{12} \tag{40}$$

*where $Y_{ij}$ are submatrices of $Y$. Then $h$ is smooth and has an inverse mapping $h^{-1}$ such that $ker(Dh(Y))$ is a linear subspace that spans $\mathbb{R}^{m\times n}$.*

*Please refer to Boumal (2023) for detailed proof.*

Lemma 6 characterizes the dynamics of the corresponding smooth curves $\mathbf{U}(t)$ and $\mathbf{V}(t)$ of any vectors within $T_{\mathbf{U}}St(m,r)$ and $T_{\mathbf{V}}St(n,r)$ respectively, when they evolve smoothly on their respective manifolds.

**Lemma 6** (Tangent Space on the Stiefel Manifold)**.** *Let $\mathbf{U}^k \in \mathbb{R}^{m\times r}$ and $\mathbf{V}^k \in \mathbb{R}^{n\times r}$ lie on the Stiefel manifolds $St(m,r)$ and $St(n,r)$, respectively. For any $\Omega \in Skew(r)$ and $B \in \mathbb{R}^{(m-n)\times r}$, the tangent space velocities $\mathbf{U}^{k\prime}(0)$ and $\mathbf{V}^{k\prime}(0)$ are given by:*

$$\mathbf{U}^{k\prime}(0) = \mathbf{U}^k\Omega + \mathbf{U}_\perp^k B, \quad \mathbf{V}^{k\prime}(0) = \mathbf{V}^k\Omega' + \mathbf{V}_\perp^k C \tag{41}$$

*where $\mathbf{U}_\perp^k$ and $\mathbf{V}_\perp^k$ are orthogonal complements.*

*Please refer to Absil et al. (2008) for detailed proof.*

Lemma 7 decomposes $Z^k$ into components within the tangent space, ensuring the projection results in a matrix that respects the manifold structure of a manifold $M_r$. It is utilized to compute the gradients in our proposed Riemannian gradient descent algorithm.

**Lemma 7** (Orthogonal Projection onto Tangent Space)**.** *Let $\Delta W^k = U^k\Sigma^k(V^k)^\top$ represent a point on $M_r$. The orthogonal projection of a matrix $Z^k \in \mathbb{R}^{m\times n}$ onto the tangent space $T_{M_r}$ at $\Delta W^k$ is given by:*

$$Proj_{\Delta W^k}(Z^k) = U^kG(V^k)^\top + U_\perp^k(V_\perp^k)^\top + U^k(V_\perp^k)^\top \tag{42}$$

*where $G$ is a general matrix related to the variation of $U^k$ and $V^k$ along their tangent directions, $U_\perp^k$ and $V_\perp^k$ denote the components of $Z^k$ orthogonal to $U^k$ and $V^k$, respectively.*

*Please refer to Absil et al. (2008) for detailed proof.*

Lemma 8 provides the theoretical foundation for projecting the updated matrix back onto the manifold after applying a gradient step in Eq.(61). The Eckart-Young-Mirsky theorem ensures that the retraction operation preserves the rank structure.

**Lemma 8** (Retraction for Fixed-Rank Matrices)**.** *Let $H \in \mathbb{R}^{m\times n}$ represent the perturbation in the ambient space. The retraction function $f$ maps the tangent space $T_M$ to the manifold $M$ by minimizing the Frobenius norm distance:*

$$f(H) = \arg\min_{\Delta W \in M} \|\Delta W^k + H - \Delta W\|_F^2 \tag{43}$$

*Under the constraint of fixed rank $r$, the retraction is given by the truncated singular value decomposition of $\Delta W^k + H$.*

*Please refer to Golub and Van Loan (2013) for detailed proof.*

We define the set of weight parameter matrices of size $m \times n$ with rank $r$ as:

$$M_r = \{\Delta \mathbf{W}^k \in \mathbb{R}^{m\times n} : \operatorname{rank}(\Delta \mathbf{W}^k) = r\} \tag{44}$$

which is an embedded submanifold of $\mathbb{R}^{m\times n}$. For any $\Delta \mathbf{W}^k \in \mathbb{R}_r^{m\times n}$, we define a continuous, smooth, local defining function. Given that the rank of $\Delta \mathbf{W}^k$ is $r$, it contains an invertible submatrix of size $r \times r$. Consequently, $\Delta \mathbf{W}^k$ can be partitioned as:

$$\Delta \mathbf{W}^k = \begin{bmatrix} \mathbb{R}^{r\times r} & \mathbb{R}^{r\times(n-r)} \\ \mathbb{R}^{(m-r)\times r} & \mathbb{R}^{(m-r)\times(n-r)} \end{bmatrix} \tag{45}$$

We assume that $w_{11} \in \mathbb{R}^{r\times r}$ is an invertible matrix, $w_{12} \in \mathbb{R}^{r\times(n-r)}$, $w_{21} \in \mathbb{R}^{(m-r)\times r}$, $w_{22} \in \mathbb{R}^{(m-r)\times(n-r)}$ Given a matrix $w \in \mathbb{R}^{m\times n}$ with rank $r$, its last $n-r$ columns are linear combinations of the first $r$ columns. This implies the existence of a matrix $X \in \mathbb{R}^{r\times(n-r)}$ such that:

$$\begin{bmatrix} w_{12} \\ w_{22} \end{bmatrix} = \begin{bmatrix} w_{11} \\ w_{21} \end{bmatrix} X \tag{46}$$

Here, $w_{11}$ is an invertible $r \times r$ matrix, and $w_{12}$, $w_{21}$, $w_{22}$ are submatrices of $X$ partitioned accordingly.

From this relationship, it follows that:

$$X = w_{11}^{-1} w_{12} \tag{47}$$

and consequently,

$$w_{22} = w_{21} X = w_{21} w_{11}^{-1} w_{12} \tag{48}$$

This decomposition shows that under the assumption of $w_{11}$ being invertible, the described relationship between the blocks of $w$ is both necessary and sufficient for $w$ to maintain a rank of $r$. Consider $U$ to be a subset of $\mathbb{R}^{m\times n}$ where the upper-left $r \times r$ submatrix is invertible. This subset $U$, being an open set in $\mathbb{R}^{m\times n}$, serves as the domain for the candidate local defining function $h$ given by:

$$h : U \to \mathbb{R}^{(m-r)\times(n-r)}, \quad Y = \begin{bmatrix} Y_{11} & Y_{12} \\ Y_{21} & Y_{22} \end{bmatrix} \mapsto Y_{22} - Y_{21} Y_{11}^{-1} Y_{12} \tag{49}$$

This mapping $h$ is smooth within $U$ and has the inverse mapping $h^{-1}(0) = \mathbb{R}^{m\times n} \cap U$, indicating that the pre-image of zero under $h$ intersects with $U$. Moreover, the differential of $h$ at any matrix $Y$ in $U$, for $V \in \mathbb{R}^{m\times n}$, is:

$$Dh(Y)[V] = V_{22} - V_{21} Y_{11}^{-1} Y_{12} + Y_{21} Y_{11}^{-1} V_{11} Y_{11}^{-1} Y_{12} - Y_{21} Y_{11}^{-1} V_{12} \tag{50}$$

utilizing the identity for differentiating a matrix inverse:

$$D(M \mapsto M^{-1})(M)[H] = -M^{-1} H M^{-1} \tag{51}$$

Please refer to the book Boumal (2023) for detailed proof.
The codomain of $Dh(Y)$ spans $\mathbb{R}^{(m-r)\times(n-r)}$, meaning any matrix in this space can be achieved by choosing an appropriate $V$. Setting $V_{11}, V_{12}, V_{21}$ to zero simplifies $Dh(Y)[V]$ to $V_{22}$, showing that $Dh(Y)$ is surjective. Thus, $h$ serves as a local defining function for the smooth submanifold around $w$ in $\mathbb{R}^{m\times n}$. If the top-left submatrix of size $r \times r$ is non-invertible, another local defining function can be constructed similarly for different submatrix choices.
These local defining functions collectively establish that $\mathbb{R}_r^{m\times n}$ is an embedded submanifold of $\mathbb{R}^{m\times n}$, endowed with dimension:

$$\dim \mathbb{R}_r^{m\times n} = \dim \mathbb{R}^{m\times n} - \dim \mathbb{R}^{(m-r)\times(n-r)} = mn - (m-r)(n-r) = r(m+n-r) \tag{52}$$

**Definition 1** (Tangent Spaces and Embedded Submanifolds)**.** *Boumal (2023) Let $M$ be a subset of $\mathcal{E}$ and $w \in M$. The tangent space at $w$, denoted $T_wM$, consists of velocity vectors at $w$ of all smooth curves $c : I \to M$ that pass through $w$ at $t = 0$, where $I$ is an open interval containing $t = 0$. Formally,*

$$T_wM = \{c'(0) \mid c : I \to M \text{ is smooth and } c(0) = w\} \tag{53}$$

*For an embedded submanifold $M$ of $\mathcal{E}$, $T_wM$ coincides with the subspace defined by $\ker Dh(w)$ if $M$ is not open within $\mathcal{E}$, otherwise $T_wM = \mathcal{E}$. This structure highlights that $T_wM$ not only captures the linear approximation to $M$ at $w$ but also conforms to the embedding properties of submanifolds within $\mathcal{E}$.*

We recognize that each tangent space possesses a dimension as delineated in equation 52, it is sufficient to exhibit a linear subspace of that dimension which is included in the tangent space. Returning to the 13 of the tangent space , we undertake the explicit construction of smooth curves on $\mathbb{R}_r^{m\times n}$. We have $\Delta\mathbf{W}^k = \mathbf{U}^k\mathbf{\Sigma}^k(\mathbf{V}^k)^T$, define $U(t)$ as a smooth trajectory within $St(m, r)$ initiating at $U(0) = \mathbf{U}^k$, and similarly for $V(t)$ within $St(n, r)$ starting from $V(0) = \mathbf{V}^k$. Additionally, let $S(t)$ describe a trajectory within the invertible $r \times r$ matrices, forming an open submanifold, starting from $S(0) = \mathbf{\Sigma}^k$. Consequently, the curve $c(t) = U(t)S(t)V(t)^T$ forms a smooth trajectory in $\mathbb{R}_r^{m\times n}$ with $c(0) = \Delta\mathbf{W}^k$, where its initial velocity $c'(0)$ represents a tangent vector at $w$:

$$c'(0) = U'(0)\mathbf{\Sigma}^k(\mathbf{V}^k)^T + \mathbf{U}^kS'(0)(\mathbf{V}^k)^T + \mathbf{U}^k\mathbf{\Sigma}^kV'(0)^T \in T_w\mathbb{R}_r^{m\times n} \tag{54}$$

Given that $U(t)$ traverses smoothly through $\mathbf{U}^k$ on $St(m, r)$, the velocity $U'(0)$ lies within its tangent space at $\mathbf{U}^k$. For any vector within $T_USt(m, r)$, a corresponding smooth curve $U(t)$ can exhibit such velocity at $t = 0$. Referencing the specified relationship for the tangent space at $\Delta\mathbf{W}^k$ in the Stiefel manifold Absil and Malick (2012) $T_{\Delta\mathbf{W}^k}St(n, p) = \{\Delta\mathbf{W}^k\Omega + \Delta\mathbf{W}_\perp^kB : \Omega \in \text{Skew}(p), B \in \mathbb{R}^{(n-p)\times p}\}$, it implies for any $\Omega \in \text{Skew}(p)$ and $B \in \mathbb{R}^{(n-p)\times p}$ that:

$$U'(0) = \mathbf{U}^k\Omega + \mathbf{U}_\perp^kB \tag{55}$$

where $\mathbf{U}_\perp^k$ ensures orthogonality with $\mathbf{U}^k$. Likewise, for any $\Omega' \in \text{Skew}(r)$ and $C \in \mathbb{R}^{(n-r)\times r}$, the expression for $V'(0)$ becomes:

$$V'(0) = \mathbf{V}^k\Omega' + \mathbf{V}_\perp^kC \tag{56}$$

with $\mathbf{V}_\perp^k$ maintaining orthogonality with $\mathbf{V}^k$. As $S(t)$ evolves smoothly within its manifold, the derivative $S'(0)$ can adopt any matrix configuration within $\mathbb{R}^{r\times r}$. with $\mathbf{V}_\perp^k$ such that $\mathbf{V}^k\mathbf{V}_\perp^k$ is orthogonal. Since $S(t)$ is a smooth curve on an open submanifold of $\mathbb{R}^{r\times r}$, we can choose $S'(0)$ to be any matrix $A \in \mathbb{R}^{r\times r}$. Finally, incorporating the relationships with $\mathbf{U}_\perp^k$ and $\mathbf{V}_\perp^k$, we observe that $U'(0)$ can be represented as $\mathbf{U}^k\Omega + \mathbf{U}_\perp^kB$ and $V'(0)$ as $\mathbf{V}^k\Omega' + \mathbf{V}_\perp^kC$, with $\Omega, \Omega' \in \text{Skew}(r)$ and $B, C \in \mathbb{R}^{(m-r)\times r}$. These adjustments ensure the continuation of $U(t)$ and $V(t)$ as smooth curves, affirming the orthogonality of $\mathbf{U}^k$ and $\mathbf{V}^k$ to their respective complements. Overall, this analysis demonstrates that the following velocities are within the tangent space of $\mathbb{R}_r^{m\times n}$ at $w$:

$$\begin{aligned} c'(0) &= (\mathbf{U}^k\Omega_2 + \mathbf{U}_\perp^kB)\mathbf{\Sigma}^k(\mathbf{V}^k)^T + \mathbf{U}^k\mathbf{\Sigma}^k((\mathbf{V}^k)\Omega_2' + \mathbf{V}_\perp^kC)^T \\ &= \mathbf{U}^k(\Omega_2 + A - \mathbf{\Sigma}^k\Omega_2')(\mathbf{V}^k)^T + \mathbf{U}_\perp^kB(\mathbf{V}^k)^T + \mathbf{U}^k(\mathbf{V}_\perp^kC)^T \end{aligned} \tag{57}$$

with $A = \mathbf{\Sigma}^k\Omega_2 - \Omega_2\mathbf{\Sigma}^k$, where $\Omega_2, \Omega_2' \in \text{Skew}(r)$, $B \in \mathbb{R}^{(m-r)\times r}$, and $C \in \mathbb{R}^{(n-r)\times r}$ are arbitrary matrices. Since $\mathbf{\Sigma}^k$ is invertible, it follows that any matrix of the form

$$\mathbf{U}^kM(\mathbf{V}^k)^T + \mathbf{U}_p^k(\mathbf{V}^k)^T + \mathbf{U}^k(\mathbf{V}_p^k)^T \tag{58}$$

with $M \in \mathbb{R}^{r\times r}$, $\mathbf{U}_p^k \in \mathbb{R}^{m\times r}$, $\mathbf{V}_p^k \in \mathbb{R}^{n\times r}$ such that $(\mathbf{U}^k)^T\mathbf{U}_p^k = (\mathbf{V}^k)^T\mathbf{V}_p^k = 0$ is tangent at $\Delta\mathbf{W}^k$. The conditions on $\mathbf{U}_p^k$ and $\mathbf{V}_p^k$ impose $2r^2$ linear constraints, thereby defining a linear subspace of $T_w\mathbb{R}_r^{m\times n}$ with dimension

$$r^2 + mr + nr - 2r^2 = r(m + n - r) \tag{59}$$

Then the singular value decomposition $(\mathbf{U}^k, \mathbf{\Sigma}^k, \mathbf{V}^k)$ of the matrix $\Delta\mathbf{W}^k$, the tangent space $T_{M_r}$ at the point $\Delta\mathbf{W}^k$ on the manifold $M_r$ can be represented as:

$$\begin{aligned} T_M &= \left\{ (\mathbf{U}^k\ \mathbf{U}_\perp^k) \begin{bmatrix} \mathbb{R}^{r\times r} & \mathbb{R}^{r\times(n-r)} \\ \mathbb{R}^{(m-r)\times r} & 0^{(m-r)\times(n-r)} \end{bmatrix} (\mathbf{V}^k\ \mathbf{V}_\perp^k)^T \right\} \\ &= \big\{ \mathbf{U}^k\mathbf{G}(\mathbf{V}^k)^T + \mathbf{U}_p^k(\mathbf{V}^k)^T + \mathbf{U}^k(\mathbf{V}_p^k)^T \\ &\quad : \mathbf{G} \in \mathbb{R}^{r\times r}, \mathbf{U}_p^k \in \mathbb{R}^{m\times r}, (\mathbf{U}_p^k)^T\mathbf{U}^k = 0, \mathbf{V}_p^k \in \mathbb{R}^{n\times r}, (\mathbf{V}_p^k)^T\mathbf{V}^k = 0 \quad \big\} \end{aligned} \tag{60}$$

With $\mathbb{R}_r^{m\times n}$ still endowed with the standard inner product, we now consider the orthogonal projectors of $\mathbb{R}_r^{m\times n}$. From equation 13, the normal space at $\Delta\mathbf{W}^k = \mathbf{U}^k\mathbf{\Sigma}^k(\mathbf{V}^k)^T$ is defined as:

$$\mathbf{N}^k = \{\mathbf{U}^k\mathbf{\Sigma}^k(\mathbf{V}^k)^T : \Delta\mathbf{W}^k \in \mathbb{R}^{(m-r)\times(n-r)}\} \tag{61}$$

The orthogonal projection of a matrix $\mathbf{Z}^k \in \mathbb{R}^{m\times n}$ onto the tangent space $T_{\Delta\mathbf{W}^k}\mathbb{R}_r^{m\times n}$ can be expressed as:

$$\mathbf{Z}^k - \text{Proj}_{\Delta\mathbf{W}^k}(\mathbf{Z}^k) = \mathbf{U}^k\Delta\mathbf{W}_\perp^k(\mathbf{V}^k)^T \tag{62}$$

for some orthogonal complement $\Delta\mathbf{W}_\perp^k$, and subsequently,

$$\text{Proj}_{\Delta\mathbf{W}^k}(\mathbf{Z}^k) = \mathbf{U}^k\mathbf{G}(\mathbf{V}^k)^T + \mathbf{U}_\perp^k(\mathbf{V}_p^k)^T + \mathbf{U}^k(\mathbf{V}_p^k)^T \tag{63}$$

for matrices $\mathbf{G}$, $\mathbf{U}_p^k$, $\mathbf{V}_p^k$ such that $(\mathbf{U}^k)^T\mathbf{U}_p^k = (\mathbf{V}^k)^T\mathbf{V}_p^k = 0$. These matrices satisfy:

$$\mathbf{Z}^k = \mathbf{U}^k\mathbf{G}(\mathbf{V}^k)^T + \mathbf{U}_p^k(\mathbf{V}^k)^T + \mathbf{U}^k(\mathbf{V}_p^k)^T + \mathbf{U}_\perp^k\Delta\mathbf{W}_\perp^k(\mathbf{V}^k)_\perp^T \tag{64}$$

Define the projectors $P_U^k = \mathbf{U}^k(\mathbf{U}^k)^T$, $P_V^k = \mathbf{V}^k(\mathbf{V}^k)^T$, and their complements $P_{U_\perp}^k = I_m - P_U^k$, $P_{V_\perp}^k = I_n - P_V^k$. Then, we derive:

$$P_U^kP_V^k\mathbf{Z}^k = \mathbf{U}^k\mathbf{G}(\mathbf{V}^k)^T, \quad P_{U_\perp}^kP_V^k\mathbf{Z}^k = U_p^k(\mathbf{V}^k)^T, \quad \text{and} \quad P_U^kP_{V_\perp}^k\mathbf{Z}^k = \mathbf{U}^k(\mathbf{V}_p^k)^T \tag{65}$$

This leads to a reformulated projection:

$$\text{Proj}_{\Delta\mathbf{W}^k}(\mathbf{Z}^k) = P_U^k\mathbf{Z}^kP_V^k + P_{U_\perp}^k\mathbf{Z}^kP_V^k + P_U\mathbf{Z}^kP_{V_\perp}^k \tag{66}$$

yielding the complete orthogonal projection:

$$\text{Proj}_w(\mathbf{Z}^k) = \mathbf{U}^k((\mathbf{U}^k)^T\mathbf{Z}^k\mathbf{V}^k)(\mathbf{V}^k)^T + (I_m - \mathbf{U}^k(\mathbf{U}^k)^T)\mathbf{Z}^k\mathbf{V}^k(\mathbf{V}^k)^T + \mathbf{U}^k(\mathbf{U}^k)^T\mathbf{Z}^k(I_n - \mathbf{V}^k(\mathbf{V}^k)^T) \tag{67}$$

Here, $M = (\mathbf{U}^k)^T\mathbf{Z}^k\mathbf{V}^k$, $U_p^k = \mathbf{Z}^k\mathbf{V}^k - \mathbf{U}^kM$, and $V_p^k = (\mathbf{Z}^k)^T\mathbf{U}^k - \mathbf{V}^kM^T$, indicating that these components form a tangent vector at $w$ represented by the variation $\mathbf{Z}^k$.

Therefore, the gradient of $(\mathbf{U}^k, \mathbf{\Sigma}^k, \mathbf{V}^k)$ in Riemannian space can be expressed as:

$$\begin{aligned}
&\Gamma_{\mathbf{U}^k}L^k = (\mathbf{I}_m - \mathbf{U}^k(\mathbf{U}^k)^T)\nabla_{\mathbf{U}^k}L^k, \qquad \Gamma_{\mathbf{V}^k}L^k = (\mathbf{I}_n - \mathbf{V}^k(\mathbf{V}^k)^T)\nabla_{\mathbf{V}^k}L^k, \\
&\Gamma_{\mathbf{\Sigma}^k}L^k = ((\mathbf{U}^k)^T\nabla_{\mathbf{U}^k}L^k - \nabla_U(L^k)^T\mathbf{U}^k)\mathbf{\Sigma}^k + \mathbf{\Sigma}^k(\mathbf{V}^k\nabla_{\mathbf{V}^k}(L^k)^T - \nabla_{\mathbf{V}^k}L^k(\mathbf{V}^k)^T) + \nabla_{\mathbf{\Sigma}^k}L^k
\end{aligned} \tag{68}$$

According to the theorem2, we can ensure that the rank remains unchanged during the local training process.

**Theorem 2.** *Let $\Delta\mathbf{W}^k$ be a point on a Riemannian manifold $M$ consisting of all matrices with a fixed rank $r$ in $\mathbb{R}^{m\times n}$. Suppose $\nabla L^k(\Delta\mathbf{W}^k)$ is the Euclidean gradient of the loss function $L^k$ at $\Delta\mathbf{W}^k$, and $\Gamma_{\mathbf{U}^k}L^k$, $\Gamma_{\mathbf{\Sigma}^k}L^k$, and $\Gamma_{\mathbf{V}^k}L^k$ represent the components of the Riemannian gradient at $\Delta\mathbf{W}^k$. The RGD optimization with a learning rate $\eta_t$ at round $t$ ensures that the local update*

$$\left((\mathbf{U}^k)^{(t+1)}, (\mathbf{\Sigma}^k)^{(t+1)}, (\mathbf{V}^k)^{(t+1)}\right) = f\left(-\eta_t\left(\left(\Gamma_{\mathbf{U}^k}L^k\right)^{(t)}, \left(\Gamma_{\mathbf{\Sigma}^k}L^k\right)^{(t)}, \left(\Gamma_{\mathbf{V}^k}L^k\right)^{(t)}\right)\right) \tag{69}$$

*preserves the rank $r$ of $\Delta\mathbf{W}^k$, maintaining the structure within the manifold $M$, where $f$ is a retraction $f : T_M \to M$ mapping the tangent space at $\Delta\mathbf{W}^k$ to the manifold.*

*Proof.* To construct a retraction $f$ for updating within a Riemannian manifold, we utilize metric projection. This method involves making a step in the ambient space, denoted by $H$, and then projecting back to the manifold to minimize the distance in the Frobenius norm, ensuring that the updated matrix retains the same rank as the original. The retraction function is formulated as:

$$f(H) = \arg\min_{\Delta\mathbf{W}^k \in \mathbb{R}_{m\times n}^r} \|\Delta\mathbf{W}^k + H - \Delta\mathbf{W}^k\|_F^2 \tag{70}$$

According to the Eckart-Young-Mirsky theorem Golub et al. (1987), the optimal solution to this optimization problem, under the constraint of rank $r$, is achieved by the truncated singular value decomposition of $\Delta\mathbf{W}^k + H$. According to quation 13, the $\Delta\mathbf{W}^k + H$ can be represented as:

$$\begin{aligned}
\Delta\mathbf{W}^k + H &= (\mathbf{U}^k)^{(t)}((\mathbf{\Sigma}^k)^{(t)} + (-\eta_t\left(\Gamma_{\mathbf{\Sigma}^k}L^k\right)^{(t)}))((\mathbf{V}^k)^{(t)})^T + U_p((\mathbf{V}^k)^{(t)})^T + (\mathbf{U}^k)^{(t)}V_p^T \\
&= \begin{bmatrix}(\mathbf{U}^k)^{(t)} & U_p\end{bmatrix}\begin{bmatrix}((\mathbf{\Sigma}^k)^{(t)} + (-\eta_t\left(\Gamma_{\mathbf{\Sigma}^k}L^k\right)^{(t)})) & I_r \\ I_r & 0\end{bmatrix}\begin{bmatrix}(\mathbf{V}^k)^{(t)} & V_p\end{bmatrix}^T.
\end{aligned} \tag{71}$$

Where $I_r$ is the $r$-dimensional identity matrix. QR factorizations of the augmented matrices $(\mathbf{U}^k)^{(t)}$ and $U_p$, as well as $(\mathbf{V}^k)^{(t)}$ and $V_p$, are given by:

$$Q_U R_U = [(\mathbf{U}^k)^{(t)}\ U_p], \quad Q_V R_V = [(\mathbf{V}^k)^{(t)}\ V_p] \tag{72}$$

Here, $Q_U$ and $Q_V$ represent the orthogonal matrices resulting from the QR factorizations of the left and right matrices, ensuring that columns are orthonormal. $R_U$ and $R_V$ are upper triangular matrices which correspond to the R components in the QR factorization process.

Employing the QR factorizations, the perturbed matrix $W + H$ is expressed as:

$$\Delta\mathbf{W}^k + H = Q_U R_U \begin{bmatrix} ((\mathbf{\Sigma}^k)^{(t)} + (-\eta_t \left(\Gamma_{\mathbf{\Sigma}^k} L^k\right)^{(t)})) & I_r \\ I_r & 0 \end{bmatrix} R_V^T Q_V^T. \tag{73}$$

By performing singular value decomposition on the middle part, we obtain $\tilde{U}\tilde{\Sigma}\tilde{V}^T$, where $\tilde{U}$, $\tilde{V}$, and $\tilde{\Sigma}$ represent the orthogonal matrices and diagonal matrix of singular values, respectively.

The retraction $f(H)$ of the perturbation $H$ at the point $\Delta\mathbf{W}^k$ on the manifold is given by:

$$f(H) = (Q_U\tilde{U})\tilde{\Sigma}(Q_V\tilde{V})^T \tag{74}$$

This expression concludes that the triplet $(Q_U\tilde{U}, \tilde{\Sigma}, Q_V\tilde{V})$ represents the retracted point on the rank-$r$ manifold $\mathbb{R}_r^{m\times n}$. The final outcome of our optimization process on the manifold, representing the updated components for the next iteration, is:

$$\left((\mathbf{U}^k)^{(t+1)}, (\mathbf{\Sigma}^k)^{(t+1)}, (\mathbf{V}^k)^{(t+1)}\right) = (Q_U\tilde{U}, \tilde{\Sigma}, Q_V\tilde{V}) \tag{75}$$

□

### A.6 Convergence on Riemannian manifold

**Definition 2** (L-smoothness on manifolds)**.** *A function $L$ is said to be Lipschitz smooth on a manifold $\mathcal{M}$ if there exists a constant $c \geq 0$ such that the following inequality holds:*

$$\|grad\, L(y) - P_{y\to x} grad\, L(x)\| \leq c d(x, y), \tag{76}$$

*where $P_{y\to x}$ is the parallel transport operator along the geodesic connecting $y$ and $x$, and $d(x, y)$ is the geodesic distance between $x$ and $y$.*

*For a complete Riemannian manifold, the following inequality holds:*

$$L(y) \leq L(x) + \langle g_x, Exp_x^{-1}(y)\rangle_x + \frac{L_g}{2} d^2(x, y), \quad \forall x, y \in \mathcal{M} \tag{77}$$

*Please refer to the paper Zhang and Sra (2016) for detailed proof.*

**Definition 3** (Geodesic convexity)**.** *A function $L \in C^1(\mathcal{M})$ is said to be geodesically convex if for all $x, y \in \mathcal{M}$, there exists a geodesic $\gamma$ such that $\gamma(0) = x$, $\gamma(1) = y$, and:*

$$f(\gamma(t)) \leq (1 - t)L(x) + tL(y), \quad \forall t \in [0, 1] \tag{78}$$

*Or equivalently,*

$$L(y) \geq L(x) + \langle grad\, L(x), Exp_x^{-1}(y)\rangle_x \tag{79}$$

*Please refer to the paper Zhang and Sra (2016) for detailed proof.*

**Assumption 1.** *For all client $k$, we assume that the function $L_i$ is geodesically $c_L$-Lipschitz continuous. Therefore, the function $l$ is also geodesically $c_L$-Lipschitz continuous.*

**Assumption 2.** *For all client $k$, we assume that the function $L_i$ is geodesically $c_g$-smooth, which implies that the function $L$ is geodesically $c_g$-smooth.*

**Assumption 3.** *We assume that the manifold under consideration is complete and that there exists a compact subset $\mathcal{W} \subset \mathcal{M}$ with diameter bounded by $M$, such that all the iterates of Algorithm 1 and the optimal points lie within $\mathcal{W}$. The sectional curvature of $\mathcal{W}$ is bounded within the interval $[\kappa_{\min}, \kappa_{\max}]$. Furthermore, we define the following key geometric constant that captures the impact of the manifold's curvature (Zhang et al., 2017)*

$$\zeta = \begin{cases} \frac{\sqrt{|\kappa_{\min}|}M}{\tanh\left(\sqrt{|\kappa_{\min}|}M\right)} & \text{if } \kappa_{\min} < 0, \\ 1 & \text{if } \kappa_{\min} \geq 0. \end{cases} \tag{80}$$

**Theorem 3** (Nonconvex)**.** *Suppose the optimization problem in Eq.(3) satisfies Assumptions 1 and 2. At each round $t$, clients $k \in \{1, \ldots, K\}$ are sampled with probabilities $p_k$, and the selected clients perform gradient descent with a fixed stepsize. Let $L^{(p)}(\Delta\mathbf{W}) = \sum_{k=1}^{K} p_k L_k(\Delta\mathbf{W})$ be the weighted global objective with smoothness constant $c_g^{(p)} = \sum_{k=1}^{K} p_k c_{g,k}$, and let $\Gamma L^{(p)}(\Delta\mathbf{W})$ denote its Riemannian gradient. If $\eta_t \leq 1/c_g^{(p)}$, then*

$$\min_{0\leq t\leq C} \mathbb{E}\left[\|\Gamma L^{(p)}(\Delta\mathbf{W}^{(t)})\|^2\right] \leq \frac{2c_g^{(p)}}{C}\left(L^{(p)}(\Delta\mathbf{W}^1) - L^{(p)}(\Delta\mathbf{W}^*)\right) + \mathcal{O}\left(\tfrac{\sigma^2}{K}\right), \tag{81}$$

*where $\Delta\mathbf{W}^{(t)}$ is the iterate on $\mathcal{M}$ at round $t$, $\Delta\mathbf{W}^*$ is the minimizer of $L^{(p)}$, and $\sigma^2$ is a finite constant capturing the variance due to client heterogeneity.*

*Proof.* According to Equation10, our aggregation method is equivalent to the aggregation of the matrix $\Delta\mathbf{W}$. However, in Euclidean space, it is challenging to accurately measure the distance between two points before and after the update. Therefore, following the approach from [12, 13], we project $\Delta\mathbf{W}$ back to the tangent space using the inverse retraction for aggregation. To measure the distance between the updated point $x_{t+1}$ and the previous point $x_t$, we use the following distance formula

$$d(x_{t+1}, x_t) = \left\|\mathrm{f}_{x_t}^{-1}(x_{t+1})\right\| = \left\|\frac{1}{k}\sum_{i\in S_t} \mathrm{f}_{x_t}^{-1}(x^{(i)})\right\| \tag{82}$$

According to the update rule of formula 16 we have:

$$\begin{aligned} (\Delta\mathbf{W}^k)^{(t+1)} &= \left((\mathbf{U}^k)^{(t+1)}, (\mathbf{\Sigma}^k)^{(t+1)}, (\mathbf{V}^k)^{(t+1)}\right) \\ &= f\left(-\eta_t\left(\left(\Gamma_{\mathbf{U}^k}L^k\right)^{(t)}, \left(\Gamma_{\mathbf{\Sigma}^k}L^k\right)^{(t)}, \left(\Gamma_{\mathbf{V}^k}L^k\right)^{(t)}\right)\right) \\ f^{-1}_{(\Delta\mathbf{W}^k)^{(t)}}\left((\Delta\mathbf{W}^k)^{(t+1)}\right) &= \left(-\eta_t\left(\left(\Gamma_{\mathbf{U}^k}L^k\right)^{(t)}, \left(\Gamma_{\mathbf{\Sigma}^k}L^k\right), \left(\Gamma_{\mathbf{V}^k}L^k\right)^{(t)}\right)\right) \end{aligned} \tag{83}$$

Using Lipschitz smooth ($c_g$-smooth) of $\mathbf{L_i}$ based on Definition 2, we have

$$\begin{aligned} L((\Delta\mathbf{W}^k)^{(t+1)}) - L((\Delta\mathbf{W}^k)^{(t)}) &\leq \left\langle f^{-1}_{(\Delta\mathbf{W}^k)^{(t)}}\left((\Delta\mathbf{W}^k)^{(t+1)}\right), \left(\left(\Gamma_{\mathbf{U}^k}L^k\right)^{(t)}, \left(\Gamma_{\mathbf{\Sigma}^k}L^k\right), \left(\Gamma_{\mathbf{V}^k}L^k\right)^{(t)}\right)\right\rangle \\ &\quad + \frac{c_g}{2}d^2((\Delta\mathbf{W}^k)^{(t+1)}, (\Delta\mathbf{W}^k)^{(t)}) \\ &= \left\langle \frac{1}{K}\sum_{k=1}^{K} f^{-1}_{(\Delta\mathbf{W}^k)^{(t)}}\left((\Delta\mathbf{W}^k)^{(t+1)}\right), \left(\left(\Gamma_{\mathbf{U}^k}L^k\right)^{(t)}, \left(\Gamma_{\mathbf{\Sigma}^k}L^k\right), \left(\Gamma_{\mathbf{V}^k}L^k\right)^{(t)}\right)\right\rangle \\ &\quad + \frac{c_g}{2}\left\|\frac{1}{k}\sum_{k=1}^{K} f^{-1}_{(\Delta\mathbf{W}^k)^{(t)}}\left((\Delta\mathbf{W}^k)^{(t+1)}\right)\right\|^2 \\ &= -\eta_t\| \left(\left(\Gamma_{\mathbf{U}^k}L^k\right)^{(t)}, \left(\Gamma_{\mathbf{\Sigma}^k}L^k\right)^{(t)}, \left(\Gamma_{\mathbf{V}^k}L^k\right)^{(t)}\right)\|^2 \\ &\quad + \frac{\eta_t^2 c_g}{2}\| \left(\left(\Gamma_{\mathbf{U}^k}L^k\right)^{(t)}, \left(\Gamma_{\mathbf{\Sigma}^k}L^k\right)^{(t)}, \left(\Gamma_{\mathbf{V}^k}L^k\right)^{(t)}\right)\|^2 \end{aligned} \tag{84}$$

Then we have

$$\begin{aligned} \mathbb{E}\left[L((\Delta\mathbf{W}^k)^{(t+1)}) - L((\Delta\mathbf{W}^k)^{(t)})\right] &\leq -\eta_t\mathbb{E}\left[\| \left(\left(\Gamma_{\mathbf{U}^k}L^k\right)^{(t)}, \left(\Gamma_{\mathbf{\Sigma}^k}L^k\right)^{(t)}, \left(\Gamma_{\mathbf{V}^k}L^k\right)^{(t)}\right)\|^2\right] \\ &\quad + \mathbb{E}\left[\frac{\eta_t^2 c_g}{2}\| \left(\left(\Gamma_{\mathbf{U}^k}L^k\right)^{(t)}, \left(\Gamma_{\mathbf{\Sigma}^k}L^k\right)^{(t)}, \left(\Gamma_{\mathbf{V}^k}L^k\right)^{(t)}\right)\|^2\right] \end{aligned} \tag{85}$$

By taking $\eta_t \leq \frac{1}{c_g}$, then we have

$$\begin{aligned}\mathbb{E}\left[L((\Delta\mathbf{W}^k)^{(t+1)}) - L((\Delta\mathbf{W}^k)^{(t)})\right] &\leq -\frac{1}{c_g}\mathbb{E}\left[\| \left(\left(\Gamma_{\mathbf{U}^k}L^k\right)^{(t)}, \left(\Gamma_{\mathbf{\Sigma}^k}L^k\right)^{(t)}, \left(\Gamma_{\mathbf{V}^k}L^k\right)^{(t)}\right) \|^2\right] \\ &+ \mathbb{E}\left[\frac{(\frac{1}{c_g})^2 c_g}{2}\| \left(\left(\Gamma_{\mathbf{U}^k}L^k\right)^{(t)}, \left(\Gamma_{\mathbf{\Sigma}^k}L^k\right)^{(t)}, \left(\Gamma_{\mathbf{V}^k}L^k\right)^{(t)}\right) \|^2\right] \\ &= -\frac{1}{2c_g}\| \left(\left(\Gamma_{\mathbf{U}^k}L^k\right)^{(t)}, \left(\Gamma_{\mathbf{\Sigma}^k}L^k\right)^{(t)}, \left(\Gamma_{\mathbf{V}^k}L^k\right)^{(t)}\right) \|^2\end{aligned} \tag{86}$$

Summing this inequality over t from 1 to C, we have

$$\begin{aligned}\frac{1}{2c_g}\sum_{t=1}^{C}\| \left(\left(\Gamma_{\mathbf{U}^k}L^k\right)^{(t)}, \left(\Gamma_{\mathbf{\Sigma}^k}L^k\right)^{(t)}, \left(\Gamma_{\mathbf{V}^k}L^k\right)^{(t)}\right) \|^2 &\leq L((\Delta\mathbf{W})^1) - L((\Delta\mathbf{W})^R) \\ &\leq L((\Delta\mathbf{W})^1) - L((\Delta\mathbf{W}^*))\end{aligned} \tag{87}$$

□

**Lemma 9** ( Zhang and Sra (2016)[Corollary 8]). *For any Riemannian manifold $\mathcal{M}$ where the sectional curvature is lower bounded by $\kappa_{\min}$ and any point $x, x^{(t)} \in \mathcal{M}$, the update $x^{(t+1)} = Exp_{x^{(t)}}(-\alpha g^{(t)})$ with $g^{(t)} \in T_{x^{(t)}}\mathcal{M}$ satisfies*

$$\left\langle -g^{(t)}, Exp^{-1}_{x^{(t)}}(x)\right\rangle \leq \frac{1}{2\alpha}\left(dist^2(x, x^{(t)}) - dist^2(x, x^{(t+1)})\right) + \frac{\zeta(\kappa_{\min}, dist(x, x^{(t)}))\alpha}{2}\|g^{(t)}\|^2, \tag{88}$$

*Where $Exp_{x^{(t)}}(x)$ is the exponentail map that projects a tangent vctor $x$ onto the manifold, $Exp^{-1}_{x^{(t)}}(x)$ is the inverse exponential map that maps a point $x$ back to the tangent space, $\alpha$ is the learning rate controlling the magnitude of the update, $dist(x, x^{(t+1)})$ denotes the geodesic distance between points $x$ and $x^{(t+1)}$ on the manifold, and $\zeta(\kappa, c) = \frac{\sqrt{|\kappa|}c}{\tanh\left(\sqrt{|\kappa|}c\right)}$ is the curvature adjustment for distance.*

**Theorem 4** (Convex). *Suppose Eq.(3) satisfies Assumptions 1, 2, and 3, and that each local objective $L_k$ is geodesically convex. At each round, clients are sampled with distribution $p$, giving the weighted objective $L^{(p)} = \sum_{k=1}^{K} p_k L_k$ and weighted smoothness constant $c_g^{(p)} = \sum_{k=1}^{K} p_k c_{g,k}$. Let $\Delta\mathbf{W}^* = \arg\min_{\Delta\mathbf{W}\in\mathcal{M}} L^{(p)}(\Delta\mathbf{W})$ be the global minimizer, and $d(\cdot,\cdot)$ the geodesic distance on $\mathcal{M}$. If the stepsize satisfies $\eta_t \leq 1/(2c_g^{(p)})$, then*

$$\mathbb{E}\Big[L^{(p)}(\Delta\mathbf{W}^{(C)}) - L^{(p)}(\Delta\mathbf{W}^*)\Big] \leq \frac{\zeta\, c_g^{(p)}\, d^2(\Delta\mathbf{W}^{(0)}, \Delta\mathbf{W}^*)}{\zeta + C - 2} + \mathcal{O}\Big(\frac{\sigma^2}{K}\Big) \tag{89}$$

*where $\Delta\mathbf{W}^{(0)}$ is the initialization, $\zeta$ is the constant from Assumption 3, and $\sigma^2$ is a variance constant due to client heterogeneity.*

*Proof.* From Lemma 9 we have

$$\begin{aligned}\left\langle \frac{1}{K}\sum_{k=1}^{K} f^{-1}_{(\Delta\mathbf{W})^t}\left((\Delta\mathbf{W}^k)\right), f^{-1}_{(\Delta\mathbf{W})^t}\left((\Delta\mathbf{W})\right)\right\rangle &\leq \frac{1}{2}\left(d^2(\Delta\mathbf{W})^t, \Delta\mathbf{W})) - d^2(\Delta\mathbf{W})^{(t+1)}, \Delta\mathbf{W}))\right) \\ &+ \frac{\zeta}{2}\left\|\frac{1}{k}\sum_{k=1}^{K} f^{-1}_{(\Delta\mathbf{W})^t}\left((\Delta\mathbf{W}^k)\right)\right\|^2\end{aligned} \tag{90}$$

According to the formula 84 we get

$$\begin{aligned}&-\eta_t\left\langle\left(\frac{1}{K}\sum_{k=1}^{K}\left(\left(\Gamma_{\mathbf{U}^k}L^k\right)^{(t)}, \left(\Gamma_{\mathbf{\Sigma}^k}L^k\right)^{(t)}, \left(\Gamma_{\mathbf{V}^k}L^k\right)^{(t)}\right)\right), f^{-1}_{(\Delta\mathbf{W})^t}\left((\Delta\mathbf{W})\right)\right\rangle \\ &\leq \frac{1}{2}\left(d^2(\Delta\mathbf{W})^t, \Delta\mathbf{W})) - d^2(\Delta\mathbf{W})^{(t+1)}, \Delta\mathbf{W}))\right) + \frac{\zeta}{2}\left\|\frac{1}{k}\sum_{k=1}^{K} f^{-1}_{(\Delta\mathbf{W})^t}\left((\Delta\mathbf{W}^k)\right)\right\|^2\end{aligned} \tag{91}$$

Based on the geodesic convexity of $L_i$ and inequality 91, we define $\Delta_t = L(\Delta\mathbf{W})^t) - L(\Delta\mathbf{W}^*)$ and $\Delta_t^k = L_k(\Delta\mathbf{W})^t) - L_k(\Delta\mathbf{W}^*)$, and we have:

$$\Delta_t^k \leq -\langle \left( \left(\Gamma_{\mathbf{U}^k} L^k\right)^{(t)}, \left(\Gamma_{\mathbf{\Sigma}^k} L^k\right)^{(t)}, \left(\Gamma_{\mathbf{V}^k} L^k\right)^{(t)} \right), f^{-1}_{(\Delta\mathbf{W})^t}(\Delta\mathbf{W}^*) \rangle. \tag{92}$$

Summing this inequality over $k = 1, \ldots, K$, we get:

$$\begin{aligned}
\Delta_t &\leq -\frac{1}{n} \left\langle \left( \frac{1}{K} \sum_{k=1}^{K} \left( \left(\Gamma_{\mathbf{U}^k} L^k\right)^{(t)}, \left(\Gamma_{\mathbf{\Sigma}^k} L^k\right)^{(t)}, \left(\Gamma_{\mathbf{V}^k} L^k\right)^{(t)} \right) \right), f^{-1}_{(\Delta\mathbf{W})^t}(\Delta\mathbf{W}^*) \right\rangle \\
&\leq \frac{1}{2\eta} \left( d^2((\Delta\mathbf{W})^t, \Delta\mathbf{W}^*)) - d^2((\Delta\mathbf{W})^{(t+1)}, \Delta\mathbf{W}^*)) \right) + \frac{\zeta}{2\eta} \left\| \frac{1}{k} \sum_{k=1}^{K} f^{-1}_{(\Delta\mathbf{W})^t} \left( (\Delta\mathbf{W}^k) \right) \right\|^2 \\
&\leq \frac{1}{2\eta} \left( d^2((\Delta\mathbf{W})^t, \Delta\mathbf{W}^*)) - d^2((\Delta\mathbf{W})^{(t+1)}, \Delta\mathbf{W}^*)) \right) + \frac{\zeta\eta}{2n} \| \left( \left(\Gamma_{\mathbf{U}^k} L^k\right)^{(t)}, \left(\Gamma_{\mathbf{\Sigma}^k} L^k\right)^{(t)}, \left(\Gamma_{\mathbf{V}^k} L^k\right)^{(t)} \right) \|^2.
\end{aligned} \tag{93}$$

From Inequality84 we have

$$\Delta_{(t+1)} - \Delta_t \leq (-\eta + \frac{\eta^2 c_g}{2}) \| \left( \left(\Gamma_{\mathbf{U}^k} L^k\right)^{(t)}, \left(\Gamma_{\mathbf{\Sigma}^k} L^k\right)^{(t)}, \left(\Gamma_{\mathbf{V}^k} L^k\right)^{(t)} \right) \|^2 \tag{94}$$

we multiply 94 by $\zeta$ and add it into 93, then we get:

$$\begin{aligned}
\zeta\Delta_{(t+1)} - (\zeta - 1)\Delta_t \leq \zeta \left( \frac{\eta}{2n} - \eta + \frac{\eta^2 c_g}{2} \right) \| \left( \left(\Gamma_{\mathbf{U}^k} L^k\right)^{(t)}, \left(\Gamma_{\mathbf{\Sigma}^k} L^k\right)^{(t)}, \left(\Gamma_{\mathbf{V}^k} L^k\right)^{(t)} \right) \|^2 \\
+ \frac{1}{2\eta} \left( d^2((\Delta\mathbf{W})^t, \Delta\mathbf{W}^*)) - d^2((\Delta\mathbf{W})^{(t+1)}, \Delta\mathbf{W}^*)) \right)
\end{aligned} \tag{95}$$

We take $\eta \leq \frac{1}{2c_g}$ and $\left( \frac{\eta}{2n} - \eta + \frac{\eta^2 c_g}{2} \right) \leq 0$, thus

$$\zeta\Delta_{(t+1)} - (\zeta - 1)\Delta_t \leq \frac{1}{2\eta} \left( d^2((\Delta\mathbf{W})^t, \Delta\mathbf{W}^*)) - d^2((\Delta\mathbf{W})^{(t+1)}, \Delta\mathbf{W}^*)) \right) \tag{96}$$

Summing this up over t from 0 to C-1 we get

$$\zeta\Delta_C + \sum_{t=0}^{C-1} \Delta_t \leq (\zeta - 1)\Delta_1 + \frac{d^2(\Delta\mathbf{W}, \Delta\mathbf{W}^*)}{2\eta} \leq \frac{\zeta d^2(\Delta\mathbf{W}, \Delta\mathbf{W}^*)}{2\eta} \tag{97}$$

Where the last inequality follows from $\eta \leq \frac{1}{2c_g}$ and $\Delta^0 \leq c_g dist(\Delta\mathbf{W}, \Delta\mathbf{W}^*)$. Taking expectation for 94 then we get

$$(\zeta + C - 2)\mathbb{E}[\Delta_C] \leq \frac{\zeta d^2(\Delta\mathbf{W}, \Delta\mathbf{W}^*)}{2\eta} \leq \zeta c_g d^2(\Delta\mathbf{W}, \Delta\mathbf{W}^*) \tag{98}$$

thus

$$\Delta_C \leq \frac{\zeta c_g d^2(\Delta\mathbf{W}, \Delta\mathbf{W}^*)}{(\zeta + C - 2)} = \frac{\zeta c_g d^2(\Delta(\mathbf{U_0}, \mathbf{\Sigma_0}, \mathbf{V_0}), \Delta(\mathbf{U}^*, \mathbf{\Sigma}^*, \mathbf{V}^*))}{(\zeta + C - 2)} \tag{99}$$

□

We further analyze the theoretical convergence rates of different methods under the nonconvex optimization setting. Our method RAFFT achieves an $\mathcal{O}(1/C)$ convergence rate with a constant depending on the manifold geometry and the distance between low-rank factors.

In comparison, the Riemannian baseline NFLHD Zhang et al. (2024a) satisfies a sublinear convergence bound:

$$\frac{1}{R} \sum_{r=1}^{R} \mathbb{E} \left\| \mathcal{G}_{\mathcal{P}_\mathcal{M}}(x^r) \right\|^2 \leq \frac{8\Omega^1}{\sqrt{n\tau R}} + \frac{64\sigma^2}{n\tau b} \tag{100}$$

where $\Omega^1$ measures the initial optimization gap, $\sigma^2$ captures gradient variance, and $\tau$ is the number of local steps. While the method considers the Riemannian structure, the convergence is sublinear and sensitive to both local batch size and client participation rate. Moreover, the constants in the bound (e.g., curvature, diameter, Lipschitz smoothness) scale poorly with dimensionality. In high-dimensional settings, these constants typically grow with the ambient dimension $d$ and the rank $r$, which can substantially slow down convergence and reduce its practicality in real-world large-scale systems.

Additionally, the Euclidean-space baseline FLoRA Wang et al. (2024b) guarantees an $\mathcal{O}(1/T)$ convergence rate:

$$\delta^{(T)} = \mathbb{E}[F(\mathbf{w}^{(T-1)} + \mathcal{B}^{(T)}(\mathcal{A}^{(T)}))] - F^* \leq \frac{2k}{\gamma + T}\left(\frac{M}{\mu} + 2L\|\mathbf{W}^{(1)} - \mathbf{W}^*\|^2\right) \tag{101}$$

where $M = \sum_{k=1}^{K} p_k^2 \sigma_k^2 + 6L\Gamma + 8(E-1)^2 G^2$ includes the effects of stochastic gradient variance, aggregation noise, and batch inconsistency. While the bound has a clean form, the constant is large and less stable in heterogeneous settings. In addition, FLoRA applies LoRA updates in the full parameter space. If one wishes to dynamically adjust the rank during training, it requires computing the full SVD of the weight matrix, which becomes prohibitively expensive in large-scale models.

In contrast, RAFFT maintains a low-rank representation throughout training and supports dynamic rank adjustment without reconstructing or decomposing the full matrix, which significantly improves efficiency and scalability.

### A.7 Experimental Details

**Environment.** The experiments were conducted on a compute server running on Red Hat Enterprise Linux 7.2 with 2 CPUs of Intel Xeon E5-2650 v4 (at 2.66 GHz) and 8 GPUs of NVIDIA GeForce GTX 2080 Ti (with 11 GB of GDDR6 on a 352-bit memory bus and memory bandwidth in the neighborhood of 620GB/s) and 4 GPUs of NVIDIA H100 (each with 80GB of HBM2e memory on a 5120-bit memory bus, offering a memory bandwidth of approximately 3TB/s),256GB of RAM, and 1TB of HDD. Overall, the experiments took about 10 days in a shared resource setting. We expect that a consumer-grade single-GPU machine could complete the full set of experiments in around 21-23 days, if its full resources were dedicated. The codes were implemented in Python 3.7.10 and PyTorch 1.9.0. Since the datasets used are all public datasets and our methodologies and the hyperparameter settings are explicitly described in section 5 and A.7, our codes and experiments can be easily reproduced on top of a GPU server. We promise to release our open source codes on GitHub and maintain a project website with detailed documentation for long-term access by other researchers and end-users after the paper is accepted.

**Training.** We study text classification model on three standard text datasets: SST-2 Socher et al. (2013),MRPC Dolan and Brockett (2005), MPQA (Wiebe et al., 2005) and QNLI (Wang et al., 2018). The above three text datasets are all public datasets, which allow researchers to use non-commercial research and educational purposes. We use 7606 examples as training data and 1000 examples as test data for MPQA. We use 3668 examples as training data and 408 as test data for MRPC. We use 20000 examples as training data and 872 examples as test data for SST-2. We use 104743 examples as training data and 5463 examples as test data for QNLI. We train LLaMA-3B,LLaMA2-7B and Roberta on this three dataset for text classification, LLaMA2-13B on QNLI. We also train a ViT on CIFAR-10, CIFAR-100 and Tiny-imagnet for image classification. The neural networks are trained with Kaiming initialization using RGD for 50 epochs with an initial learning rate of 4e-4 and batch size 8. In addition, we run each experiment for 3 trials for obtaining more stable results.

**Implementation.** For 11 state-of-the-art federated large language models of LoRA Hu et al. (2022), AdaLoRA Zhang et al. (2023b), P-Tuningv2 Liu et al. (2021a), FedPrompt Zhao et al. (2023), FedPepTAO Che et al. (2023a), PromptFL Guo et al. (2024),PE-FL Zhao et al. (2024), SLoRA Babakniya et al. (2023), Het-LoRA Cho et al. (2023), FedLoRA Yi et al. (2024)and FFA-LoRA Sun et al. (2024), we utilized the same model architecture as the official open-source implementation and default parameter settings provided by the original authors for FedPEFT in all experiments. All hyperparameters are standard values from reference codes or prior works. We validate the performance of different FedPEFT methods with a range of rank $\in \{2, 4, 8, 16\}$. All models were trained for 10, 25 and 50 epochs, with a batch size of 8, and a learning rate of 4e-4. We use the Dirichlet distribution with concentration parameters $\alpha \in \{1, 3, 5\}$ to partition the data into non-IID splits. Each

device is then assigned a certain number of samples based on the corresponding Dirichlet distribution. The above open-source codes from the GitHub are licensed under the MIT License, which only requires preservation of copyright and license notices and includes the permissions of commercial use, modification, distribution, and private use.

For our RAFFT model, we performed hyperparameter selection by performing a parameter rank $r \in \{2, 4, 8, 16\}$, Dirichlet alpha $\alpha \in \{1, 3, 5\}$, training epochs of the FedPEFT model $\in \{10, 25, 50, 100\}$, select rank and learning rate$\in \{1e^{-4}, 3e^{-4}, 4e^{-4}, 5e^{-5}\}$. We select the best parameters over 50 epochs of training and evaluate the model at test time.

**Hyperparameter settings.** Unless otherwise explicitly stated, we used the following default parameter settings in the experiments. As shown in Table 38

Table 4: Model parameters and settings

| **Parameter** | **Value** |
|---|---|
| Training data on SST-2 | 20,000 |
| Test data ratio on SST-2 | 872 |
| Training data on MRPC | 3,668 |
| Test data on MRPC | 408 |
| Training data on MPQA | 7,606 |
| Test data on MPQA | 1,000 |
| Training data on CIFRA10 | 50,000 |
| Test data on CIFRA10 | 10,000 |
| Training data on CIFRA100 | 5,000 |
| Test data on CIFRA100 | 1,000 |
| Training data on Tiny-ImageNet | 100,000 |
| Test data on Tiny-ImageNet | 10,000 |
| Select rank threshold $\alpha$ | 0.9 |
| Training epochs of the FedPEFT model | 50 |
| Batch size for training the model | 8 |
| Learning rate | 4e-4 |

### A.8 AdditionalExperiments

In this section, we present additional experimental results beyond those described in Section 3 to demonstrate the advantages of our proposed method. We considered a Federated Learning (FL) environment with 100 devices and a parameter server, randomly sampling 10 devices in each epoch to perform local updates. We utilized three widely-used NLP tasks, including SST-2 Socher et al. (2013), MRPC Dolan and Brockett (2005), and MPQA (Wiebe et al., 2005). Evaluations were conducted on the RoBERTa-LARGE Liu et al. (2019b) model for the MRPC and SST-2 datasets, the LLaMA 3B Touvron et al. (2023a) model for the MRPC and SST-2 datasets, and the LLaMA 7B Radford et al. (2019) model for the MRPC and SST-2 datasets. Additionally, we experimented with the ViT model on image classification datasets CIFAR-10 and CIFAR-100. For all methods, the backbone models remained frozen. These comprehensive evaluations across multiple models and datasets illustrate the robustness and effectiveness of our fixed rank approach compared to 11 baseline methods across three common tasks.

Table 5: Performance comparison of different methods on Roberta+MPQA.

| | alpha = 5 | | | alpha = 3 | | | alpha = 1 | | |
|---|---|---|---|---|---|---|---|---|---|
| Method | Accuracy | Loss | Time | Accuracy | Loss | Time | Accuracy | Loss | Time |
| Federated_LoRA | 89.65 | 0.2510 | 1,442 | 89.85 | 0.2857 | 1,419 | 86.25 | 0.3776 | 1,433 |
| FedAdaLoRA | 85.85 | 0.4134 | 1,774 | 82.00 | 2.2912 | 1,748 | 81.95 | 2.3407 | 1,763 |
| P-tuning v2 | 87.45 | 0.3563 | 1,581 | 86.80 | 0.3256 | 1,614 | 86.50 | 0.3509 | 1,623 |
| FedPrompt | 86.00 | 0.5352 | 1,463 | 85.45 | 0.4666 | 1,479 | 84.80 | 0.4345 | 1,537 |
| FedPepTAO | 89.20 | 0.2854 | 1,608 | 89.05 | 0.2545 | 1,565 | 88.45 | 0.2749 | 1,592 |
| PromptFL | 85.75 | 0.5358 | 1,696 | 83.75 | 0.4847 | 1,516 | 83.35 | 0.4236 | 1,498 |
| PE_FL | 85.50 | 0.5331 | 1,663 | 85.25 | 0.4669 | 1,568 | 83.35 | 0.4274 | 1,505 |
| SLoRA | 90.05 | 0.2545 | 1,473 | 89.75 | 0.2546 | 1,446 | 86.70 | 0.2579 | 1,488 |
| HetLoRA | 87.70 | 0.3377 | 1,207 | 87.15 | 0.3159 | 1,212 | 87.25 | 0.3227 | 1,239 |
| FedLoRA | 89.95 | 0.2473 | 1,416 | 89.95 | 0.2416 | 1,517 | 89.60 | 0.2492 | 1,399 |
| FFA-LoRA | 87.50 | 0.3580 | 1,193 | 86.95 | 0.3386 | 1,168 | 87.30 | 0.3443 | 1,166 |
| Fedkseed | 81.90 | 0.6226 | 1,193 | 82.35 | 0.5921 | 1,186 | 82.75 | 0.5833 | 1,176 |
| FLoRA | 82.25 | 0.5549 | 1,216 | 83.35 | 0.5286 | 1,213 | 84.25 | 0.5227 | 1,154 |
| RAFFT | 91.45 | 0.1692 | 905 | 91.60 | 0.1701 | 902 | 91.20 | 0.1602 | 905 |
| RAFFT-RGD | 90.05 | 0.2311 | 869 | 89.85 | 0.2392 | 894 | 89.35 | 0.2281 | 890 |
| RAFFT-MR | 90.15 | 0.2299 | 890 | 90.10 | 0.2288 | 885 | 89.50 | 0.2209 | 884 |

Table 6: Performance comparison of different methods on LLaMA 3B+MPQA.

| | alpha = 5 | | | alpha = 3 | | | alpha = 1 | | |
|---|---|---|---|---|---|---|---|---|---|
| Method | Accuracy | Loss | Time | Accuracy | Loss | Time | Accuracy | Loss | Time |
| Federated_LoRA | 88.40 | 0.2249 | 3,351 | 88.65 | 0.2203 | 3,339 | 88.00 | 0.2362 | 3,229 |
| FedAdaLoRA | 83.60 | 0.3318 | 3,134 | 84.85 | 0.3343 | 3,136 | 83.45 | 0.3179 | 3,137 |
| P-tuning v2 | 88.60 | 0.4830 | 3,360 | 86.85 | 0.3565 | 3,360 | 88.50 | 0.4606 | 3,358 |
| FedPrompt | 86.70 | 0.4537 | 3,358 | 87.70 | 0.4110 | 3,387 | 87.70 | 0.4110 | 3,354 |
| FedPepTAO | 88.90 | 0.4001 | 3,345 | 87.20 | 0.3535 | 3,335 | 87.70 | 0.5189 | 3,354 |
| PromptFL | 88.90 | 0.4000 | 3,352 | 88.50 | 0.2580 | 3,352 | 88.85 | 0.4520 | 3,360 |
| PE_FL | 88.25 | 0.3837 | 3,357 | 88.60 | 0.2580 | 3,353 | 88.60 | 0.2580 | 3,356 |
| SLoRA | 84.55 | 0.3028 | 3,893 | 81.35 | 0.3215 | 3,912 | 81.73 | 0.3579 | 3,851 |
| HetLoRA | 88.80 | 0.2685 | 2,848 | 88.95 | 0.2501 | 2,842 | 88.60 | 0.2310 | 2,842 |
| FedLoRA | 84.55 | 0.3028 | 2,792 | 81.35 | 0.3215 | 2,801 | 81.65 | 0.3579 | 2,805 |
| FFA-LoRA | 85.25 | 0.2552 | 2,789 | 84.35 | 0.2745 | 2,813 | 84.15 | 0.2776 | 2,811 |
| Fedkseed | 88.81 | 0.3979 | 3,356 | 88.83 | 0.2865 | 3,937 | 88.55 | 0.4165 | 3,356 |
| FLoRA | 87.05 | 0.3469 | 2,915 | 84.80 | 0.3443 | 2,957 | 84.84 | 0.4316 | 3,105 |
| RAFFT | 91.50 | 0.2769 | 2,718 | 91.35 | 0.2330 | 2,728 | 91.00 | 0.2418 | 2,754 |
| RAFFT-RGD | 90.15 | 0.3123 | 2,681 | 89.50 | 0.2930 | 2,678 | 88.90 | 0.2741 | 2,683 |
| RAFFT-MR | 89.95 | 0.2962 | 2,699 | 88.90 | 0.2899 | 2,701 | 88.70 | 0.2775 | 2,691 |

Table 7: Performance comparison of different methods on Roberta+MRPC.

| | alpha = 5 | | | alpha = 3 | | | alpha = 1 | | |
|---|---|---|---|---|---|---|---|---|---|
| Method | Accuracy | Loss | Time | Accuracy | Loss | Time | Accuracy | Loss | Time |
| Federated_LoRA | 81.32 | 0.4122 | 1,407 | 80.77 | 0.4217 | 1,411 | 80.70 | 0.4519 | 1,411 |
| FedAdaLoRA | 81.13 | 0.4309 | 1,563 | 80.29 | 0.4373 | 1,554 | 79.16 | 0.4818 | 1,570 |
| P-tuning v2 | 78.48 | 0.4325 | 1,049 | 79.41 | 0.4116 | 1,057 | 77.59 | 0.3935 | 1,064 |
| FedPrompt | 75.87 | 0.6784 | 1,004 | 75.87 | 0.6346 | 979 | 74.98 | 3.8650 | 1,022 |
| FedPepTAO | 81.83 | 0.3691 | 1,066 | 80.24 | 0.3577 | 1,053 | 81.21 | 0.3722 | 1,066 |
| PromptFL | 75.84 | 0.5917 | 1,001 | 75.97 | 0.7182 | 977 | 75.29 | 0.7722 | 1,022 |
| PE_FL | 76.18 | 0.5868 | 1,024 | 74.98 | 3.8320 | 1,052 | 75.45 | 0.6071 | 1,022 |
| SLoRA | 80.43 | 0.4559 | 1,044 | 80.81 | 0.4152 | 1,052 | 81.29 | 0.4075 | 1,043 |
| HetLoRA | 80.52 | 0.4470 | 1,086 | 80.33 | 0.4404 | 1,168 | 79.51 | 0.3834 | 1,146 |
| FedLoRA | 81.64 | 0.5644 | 1,124 | 82.99 | 0.4428 | 1,204 | 82.21 | 0.4141 | 1,193 |
| FFA-LoRA | 77.74 | 0.4846 | 1,149 | 78.22 | 0.4395 | 1,026 | 77.02 | 0.4180 | 1,070 |
| Fedkseed | 81.34 | 0.7509 | 1,083 | 81.29 | 0.675 | 1,058 | 81.40 | 0.6975 | 1,036 |
| FLoRA | 81.70 | 0.6994 | 1,105 | 82.38 | 0.6346 | 1,037 | 81.29 | 0.6579 | 1,175 |
| RAFFT | 85.49 | 0.2758 | 818 | 84.09 | 0.3583 | 863 | 83.85 | 0.3623 | 890 |
| RAFFT-RGD | 82.8 | 0.4166 | 802 | 82.78 | 0.3928 | 822 | 82.12 | 0.4140 | 822 |
| RAFFT-MR | 82.25 | 0.4259 | 798 | 83.12 | 0.4039 | 819 | 81.95 | 0.4232 | 851 |

Table 8: Performance comparison of different methods on Roberta+SST2.

| | alpha = 5 | | | alpha = 3 | | | alpha = 1 | | |
|---|---|---|---|---|---|---|---|---|---|
| Method | Accuracy | Loss | Time | Accuracy | Loss | Time | Accuracy | Loss | Time |
| Federated_LoRA | 92.89 | 0.3394 | 1,883 | 93.35 | 0.3276 | 1,862 | 92.89 | 0.3166 | 1,877 |
| FedAdaLoRA | 88.07 | 1.7253 | 1,710 | 87.96 | 1.7722 | 1,711 | 87.16 | 1.6742 | 1,720 |
| P-tuning v2 | 89.44 | 0.6417 | 1,545 | 90.36 | 0.5675 | 1,504 | 90.60 | 0.4632 | 1,533 |
| FedPrompt | 89.68 | 0.7164 | 1,487 | 93.81 | 0.5829 | 1,460 | 89.33 | 0.5689 | 1,495 |
| FedPepTAO | 91.06 | 0.4388 | 1,614 | 91.74 | 0.4267 | 1,620 | 91.51 | 0.3499 | 1,581 |
| PromptFL | 92.20 | 0.5044 | 1,453 | 93.12 | 0.5096 | 1,444 | 93.92 | 0.3634 | 1,489 |
| PE_FL | 93.00 | 0.4628 | 1,503 | 93.00 | 0.4732 | 1,498 | 93.69 | 0.3523 | 1,470 |
| SLoRA | 92.66 | 0.2616 | 1,447 | 92.88 | 0.1956 | 1,473 | 90.25 | 0.2588 | 1,501 |
| HetLoRA | 93.46 | 0.2785 | 1,067 | 92.43 | 0.5086 | 1,095 | 93.46 | 0.2091 | 1,128 |
| FedLoRA | 93.35 | 0.3002 | 1,221 | 93.58 | 0.2877 | 1,192 | 93.69 | 0.2878 | 1,248 |
| FFA-LoRA | 92.77 | 0.3048 | 1,022 | 91.62 | 0.8016 | 1,087 | 92.43 | 0.4128 | 1,065 |
| Fedkseed | 93.23 | 0.3662 | 1,124 | 93.23 | 0.3633 | 1,251 | 93.00 | 0.3636 | 1,103 |
| FLoRA | 93.46 | 0.3175 | 1,158 | 93.46 | 0.3254 | 1,186 | 93.12 | 0.3307 | 1,251 |
| RAFFT | 95.07 | 0.1894 | 1,012 | 95.41 | 0.1720 | 1,012 | 95.18 | 0.1605 | 1,020 |
| RAFFT-RGD | 93.12 | 0.2654 | 957 | 92.88 | 0.3290 | 952 | 93.35 | 0.2026 | 961 |
| RAFFT-MR | 93.00 | 0.2921 | 962 | 92.88 | 0.3280 | 951 | 93.46 | 0.2337 | 958 |

Table 9: Performance comparison of different methods on LLaMA3B+MRPC.

| | alpha = 5 | | | alpha = 3 | | | alpha = 1 | | |
|---|---|---|---|---|---|---|---|---|---|
| Method | Accuracy | Loss | Time | Accuracy | Loss | Time | Accuracy | Loss | Time |
| Federated_LoRA | 82.07 | 0.3670 | 4,331 | 81.67 | 0.4179 | 4,255 | 81.36 | 0.4257 | 4,291 |
| FedAdaLoRA | 81.22 | 0.8810 | 4,086 | 81.22 | 0.8473 | 4,069 | 81.22 | 0.7275 | 4,078 |
| P-tuning v2 | 81.34 | 4.1410 | 4,023 | 81.34 | 4.0730 | 4,103 | 80.82 | 4.1940 | 4,062 |
| FedPrompt | 81.18 | 4.3970 | 4,120 | 81.46 | 0.5310 | 4,094 | 81.22 | 0.4466 | 4,109 |
| FedPepTAO | 81.34 | 4.1410 | 3,891 | 81.34 | 0.5334 | 4,093 | 81.22 | 0.4460 | 4,125 |
| PromptFL | 79.19 | 5.7040 | 4,120 | 81.34 | 0.5884 | 4,093 | 81.22 | 0.4490 | 4,125 |
| PE_FL | 73.99 | 6.8350 | 4,114 | 81.34 | 0.5792 | 4,101 | 81.22 | 0.4447 | 4,111 |
| SLoRA | 81.78 | 0.3714 | 4,955 | 81.89 | 0.3811 | 4,952 | 80.15 | 0.4276 | 4,966 |
| HetLoRA | 76.80 | 4.6050 | 3,994 | 78.22 | 6.8990 | 3,995 | 78.27 | 7.0250 | 4,012 |
| FedLoRA | 82.07 | 0.4880 | 4,093 | 82.14 | 0.4748 | 4,207 | 81.97 | 0.3731 | 4,017 |
| FFA-LoRA | 80.76 | 3.2140 | 4,186 | 79.03 | 7.0660 | 4,008 | 78.78 | 7.1700 | 3,991 |
| Fedkseed | 74.92 | 6.5395 | 4,114 | 82.00 | 0.5822 | 4,100 | 81.84 | 0.4495 | 4,110 |
| FLoRA | 81.64 | 2.0501 | 4,912 | 81.83 | 0.5054 | 4,985 | 81.68 | 0.4092 | 4,963 |
| RAFFT | 82.63 | 0.4869 | 3,904 | 82.41 | 0.5877 | 3,915 | 82.63 | 0.4738 | 3,892 |
| RAFFT-RGD | 82.07 | 0.5319 | 3,971 | 81.95 | 0.5170 | 3,978 | 81.95 | 0.5623 | 3,956 |
| RAFFT-MR | 82.20 | 0.5133 | 3,956 | 81.98 | 0.6992 | 3,985 | 81.98 | 0.6992 | 3,985 |

Table 10: Performance comparison of different methods on LLaMA3B+SST2.

| | alpha = 5 | | | alpha = 3 | | | alpha = 1 | | |
|---|---|---|---|---|---|---|---|---|---|
| Method | Accuracy | Loss | Time | Accuracy | Loss | Time | Accuracy | Loss | Time |
| Federated_LoRA | 94.61 | 0.1793 | 3,899 | 95.41 | 0.1268 | 3,897 | 94.38 | 0.1752 | 3,921 |
| FedAdaLoRA | 87.16 | 0.8543 | 3,532 | 88.12 | 0.9312 | 3,528 | 86.47 | 1.0330 | 3,548 |
| P-tuning v2 | 93.23 | 0.2659 | 3,891 | 94.15 | 0.2156 | 3,900 | 92.43 | 0.2635 | 3,888 |
| FedPrompt | 93.69 | 0.3066 | 3,881 | 94.15 | 0.2606 | 3,893 | 94.04 | 0.2540 | 3,894 |
| FedPepTAO | 93.12 | 0.2619 | 3,778 | 94.15 | 0.2162 | 3,896 | 94.04 | 0.2540 | 3,894 |
| PromptFL | 93.92 | 0.3336 | 3,906 | 94.15 | 0.2606 | 3,893 | 92.32 | 0.2612 | 3,893 |
| PE_FL | 93.92 | 0.3063 | 3,924 | 94.15 | 0.2588 | 3,901 | 93.92 | 0.2627 | 3,890 |
| SLoRA | 94.04 | 0.2177 | 5,878 | 94.27 | 0.1750 | 5,792 | 93.81 | 0.1809 | 5,924 |
| HetLoRA | 94.04 | 0.2637 | 3,893 | 93.92 | 0.2726 | 3,638 | 94.50 | 0.2174 | 3,634 |
| FedLoRA | 94.61 | 0.2022 | 3,664 | 94.72 | 0.1556 | 3,723 | 95.18 | 0.1804 | 3,704 |
| FFA-LoRA | 93.12 | 0.2330 | 3,789 | 93.12 | 0.2419 | 3,593 | 93.46 | 0.2061 | 3,606 |
| Fedkseed | 93.92 | 0.3074 | 3,918 | 94.69 | 0.2604 | 3,900 | 94.80 | 0.2649 | 3,890 |
| FLoRA | 94.36 | 0.2370 | 3,853 | 94.90 | 0.19 | 3,904 | 94.00 | 0.2198 | 3,922 |
| RAFFT | 95.64 | 0.2048 | 3,672 | 95.53 | 0.1458 | 3,733 | 95.64 | 0.2029 | 3,749 |
| RAFFT-RGD | 93.81 | 0.2365 | 3,596 | 94.15 | 0.2314 | 3,634 | 93.92 | 0.2604 | 3,671 |
| RAFFT-MR | 93.80 | 0.2389 | 3,604 | 94.03 | 0.2353 | 3,615 | 93.57 | 0.2529 | 3,648 |

Table 11: Performance comparison of different methods on LLaMA7B+MRPC.

| | alpha = 5 | | | alpha = 3 | | | alpha = 1 | | |
|---|---|---|---|---|---|---|---|---|---|
| Method | Accuracy | Loss | Time | Accuracy | Loss | Time | Accuracy | Loss | Time |
| Federated_LoRA | 80.32 | 0.3386 | 7,783 | 80.02 | 0.3900 | 7,691 | 80.09 | 0.3255 | 7,722 |
| FedAdaLoRA | 81.18 | 0.7412 | 7,522 | 81.07 | 0.7650 | 7,509 | 81.07 | 0.6333 | 7,518 |
| P-tuning v2 | 81.07 | 0.9424 | 7,329 | 81.05 | 0.9306 | 7,261 | 81.07 | 0.8343 | 7,257 |
| FedPrompt | 81.34 | 0.5585 | 7,735 | 81.35 | 0.5322 | 7,667 | 81.63 | 0.4787 | 7,685 |
| FedPepTAO | 81.22 | 0.8325 | 7,328 | 81.11 | 0.9207 | 7,270 | 81.07 | 0.8174 | 7,253 |
| PromptFL | 81.46 | 0.5137 | 7,735 | 81.34 | 0.5329 | 7,673 | 81.07 | 0.8174 | 7,253 |
| PE_FL | 81.46 | 0.5348 | 7,741 | 81.35 | 0.5334 | 7,666 | 81.53 | 0.4791 | 7,678 |
| SLoRA | 81.66 | 0.5086 | 7,400 | 81.93 | 0.4805 | 7,314 | 81.30 | 0.3968 | 7,342 |
| HetLoRA | 80.88 | 0.5677 | 7,400 | 80.47 | 0.5675 | 7,342 | 80.88 | 0.4960 | 7,349 |
| FedLoRA | 81.60 | 0.4918 | 7,328 | 81.75 | 0.4760 | 7,492 | 81.60 | 0.4917 | 7,303 |
| FFA-LoRA | 80.90 | 0.8238 | 7,394 | 80.37 | 0.8623 | 7,337 | 81.26 | 0.7849 | 7,331 |
| Fedkseed | 81.81 | 0.5464 | 7,740 | 82.06 | 0.5397 | 7,666 | 81.74 | 0.5715 | 7,285 |
| FLoRA | 81.74 | 0.6461 | 7,314 | 80.98 | 0.7247 | 7,311 | 79.16 | 0.6914 | 7,338 |
| RAFFT | 83.62 | 0.4950 | 7,285 | 82.58 | 0.6641 | 7,216 | 83.11 | 0.6454 | 7,298 |
| RAFFT-RGD | 80.85 | 0.7416 | 7,291 | 80.73 | 0.7416 | 7,188 | 80.89 | 0.8807 | 7,301 |
| RAFFT-MR | 81.55 | 0.5580 | 7,295 | 82.03 | 0.6274 | 7,246 | 81.64 | 0.7618 | 7,288 |

Table 12: Performance comparison of different methods on LLaMA7B+SST2.

| | alpha = 5 | | | alpha = 3 | | | alpha = 1 | | |
|---|---|---|---|---|---|---|---|---|---|
| Method | Accuracy | Loss | Time | Accuracy | Loss | Time | Accuracy | Loss | Time |
| Federated_LoRA | 94.61 | 0.1541 | 7,332 | 94.84 | 0.1400 | 7,442 | 95.18 | 0.1677 | 6,922 |
| FedAdaLoRA | 93.35 | 0.2736 | 7,129 | 93.58 | 0.2273 | 7,154 | 78.89 | 1.0824 | 6,811 |
| P-tuning v2 | 90.02 | 0.2629 | 6,790 | 85.32 | 0.2731 | 6,807 | 94.04 | 0.2220 | 6,825 |
| FedPrompt | 82.91 | 0.3996 | 6,797 | 85.89 | 0.2773 | 6,813 | 93.92 | 0.2249 | 6,810 |
| FedPepTAO | 90.14 | 0.2632 | 6,719 | 90.14 | 0.2215 | 6,822 | 94.50 | 0.2258 | 6,811 |
| PromptFL | 88.42 | 0.2809 | 6,827 | 84.98 | 0.2677 | 6,813 | 93.92 | 0.2220 | 6,816 |
| PE_FL | 86.93 | 0.3327 | 6,797 | 84.29 | 0.2869 | 6,809 | 93.92 | 0.2262 | 6,815 |
| SLoRA | 89.22 | 0.2458 | 6,770 | 81.94 | 0.4805 | 7,314 | 81.29 | 0.3968 | 7,342 |
| HetLoRA | 91.40 | 0.2757 | 6,818 | 90.25 | 0.2588 | 6,860 | 95.18 | 0.1805 | 6,818 |
| FedLoRA | 94.45 | 0.1840 | 6,979 | 94.38 | 0.1599 | 6,498 | 95.18 | 0.1805 | 6,454 |
| FFA-LoRA | 94.38 | 0.2463 | 6,810 | 92.66 | 0.2617 | 6,838 | 92.89 | 0.1956 | 6,817 |
| Fedkseed | 86.77 | 0.3502 | 6,799 | 85.40 | 0.2927 | 6,809 | 94.18 | 0.2298 | 6,814 |
| FLoRA | 92.66 | 0.2216 | 6,610 | 92.77 | 0.1940 | 6,637 | 93.96 | 0.2028 | 6,916 |
| RAFFT | 96.33 | 0.1982 | 6,681 | 95.53 | 0.1949 | 6,618 | 95.41 | 0.2015 | 6,744 |
| RAFFT-RGD | 92.78 | 0.2951 | 6,731 | 93.69 | 0.2795 | 6,731 | 93.12 | 0.3003 | 6,738 |
| RAFFT-MR | 94.15 | 0.2758 | 6,724 | 93.92 | 0.2323 | 6,692 | 93.69 | 0.3629 | 6,819 |

Table 13: Performance comparison of different methods on ViT+CIFRA100.

| | alpha = 5 | | | alpha = 3 | | | alpha = 1 | | |
|---|---|---|---|---|---|---|---|---|---|
| Method | Accuracy | Loss | Time | Accuracy | Loss | Time | Accuracy | Loss | Time |
| Federated_LoRA | 46.43 | 1.7763 | 3,340 | 46.32 | 1.8492 | 3,394 | 43.43 | 2.0657 | 3,314 |
| FedAdaLoRA | 46.15 | 1.7674 | 3,548 | 46.10 | 1.8546 | 3,488 | 42.81 | 2.1023 | 3,454 |
| SLoRA | 44.10 | 1.9510 | 3,372 | 43.34 | 1.9870 | 3,306 | 41.39 | 2.1920 | 3,362 |
| HetLoRA | 46.31 | 1.8132 | 3,347 | 45.68 | 1.8629 | 3,321 | 43.53 | 2.0552 | 3,305 |
| FedLoRA | 50.08 | 1.5120 | 3,404 | 44.94 | 1.8940 | 3,290 | 42.40 | 2.1020 | 3,371 |
| FFA-LoRA | 45.99 | 1.8065 | 3,363 | 46.06 | 1.8210 | 3,363 | 43.19 | 1.9970 | 3,334 |
| FLoRA | 40.39 | 1.5424 | 3,288 | 45.36 | 1.6339 | 3,326 | 41.93 | 1.811 | 3,418 |
| RAFFT | 48.44 | 1.3240 | 3,273 | 48.36 | 1.3390 | 3,295 | 45.82 | 1.5210 | 3,314 |
| RAFFT-RGD | 47.11 | 1.5020 | 3,308 | 46.96 | 1.5480 | 3,280 | 43.33 | 1.6940 | 3,297 |
| RAFFT-MR | 47.21 | 1.4959 | 3,625 | 46.47 | 1.5746 | 3,301 | 43.75 | 1.7250 | 3,309 |

Table 14: Performance comparison of different methods on ViT+IamgeNet.

| Method | alpha = 5 | | | alpha = 3 | | | alpha = 1 | | |
|---|---|---|---|---|---|---|---|---|---|
| | Accuracy | Loss | Time | Accuracy | Loss | Time | Accuracy | Loss | Time |
| Federated_LoRA | 26.92 | 2.9963 | 11,497 | 26.18 | 3.0743 | 11,139 | 24.34 | 3.2956 | 11,260 |
| FedAdaLoRA | 27.10 | 3.0361 | 12,278 | 26.72 | 3.0535 | 11,820 | 24.38 | 3.2249 | 11,908 |
| SLoRA | 26.76 | 3.2740 | 11,176 | 25.76 | 3.3610 | 11,755 | 24.18 | 3.6510 | 11,878 |
| HetLoRA | 26.78 | 3.0303 | 11,487 | 25.90 | 3.0713 | 11,317 | 24.14 | 3.2865 | 11,278 |
| FedLoRA | 26.80 | 3.2570 | 11,643 | 26.24 | 3.3519 | 11,720 | 24.32 | 3.6429 | 11,960 |
| FFA-LoRA | 26.42 | 3.2642 | 11,700 | 26.02 | 3.3664 | 11,787 | 24.06 | 3.6111 | 11,797 |
| FLoRA | 23.96 | 3.5034 | 11,564 | 23.56 | 3.5504 | 11,508 | 21.82 | 3.8373 | 11,755 |
| RAFFT | 28.82 | 2.9140 | 11,236 | 27.88 | 2.9350 | 11,195 | 25.12 | 3.1270 | 11,225 |
| RAFFT-RGD | 27.74 | 3.0150 | 11,159 | 26.90 | 3.0470 | 11,598 | 24.08 | 3.2850 | 11,591 |
| RAFFT-MR | 27.16 | 3.0480 | 10,938 | 27.18 | 3.0370 | 11,245 | 24.58 | 3.2260 | 10,957 |

Table 15: Performance comparison on LLaMA2-13B + QNLI (10 rounds), $\alpha = 0.5$

| **Method** | **Accuracy (%)** | **Loss** | **Time (s)** |
|---|---|---|---|
| Federated LoRA | 90.15 | 0.4704 | 18,337 |
| RFedSVRG | 90.19 | 0.5172 | 15,272 |
| NLFHD | 89.57 | 0.6240 | 14,925 |
| GeoLoRA | 90.81 | 0.6290 | 13,369 |
| AdaLoRA | 87.23 | 0.9891 | 16,633 |
| SLoRA | 90.54 | 0.5770 | 14,841 |
| HetLoRA | 89.15 | 0.5290 | 12,583 |
| FedLoRA | 89.67 | 0.6385 | 12,692 |
| FFA-LoRA | 90.05 | 0.8524 | 12,018 |
| RAFFT | **91.96** | **0.3437** | **11,532** |

**Accuracy of classification using Riemannian manifolds on different numbers of clients.**To comprehensively investigate the applicability of our RAFFT method for classification tasks under different client numbers, we evaluated the method with 40, 60, 80, and 100 clients while keeping other settings constant. Tables 16-21 present the classification accuracy on three datasets using Riemannian manifold techniques. We observed consistent results, indicating that the three variants of our RAFFT method achieved the best accuracy in most experiments. This demonstrates the superior performance of RAFFT under varying client numbers. A plausible explanation is that the rigorous mathematical analysis based on Riemannian manifold theory significantly enhances the effectiveness and applicability of our RAFFT method across different scenarios.

Table 16: Performance comparison of different methods on Roberta+MPQA with varying numbers of clients (N).

| Method | N = 40 | | | N = 60 | | | N = 80 | | | N = 100 | | |
|---|---|---|---|---|---|---|---|---|---|---|---|---|
| | Accuracy | Loss | Time | Accuracy | Loss | Time | Accuracy | Loss | Time | Accuracy | Loss | Time |
| Federated_LoRA | 91.70 | 0.1511 | 1,481 | 90.95 | 0.1604 | 1,489 | 91.40 | 0.2203 | 1,472 | 89.65 | 0.2510 | 1,433 |
| FedAdaLoRA | 89.60 | 0.2471 | 1,669 | 89.15 | 0.2639 | 1,730 | 88.05 | 0.3008 | 1,710 | 85.85 | 0.4136 | 1,763 |
| P-tuning v2 | 89.25 | 0.2481 | 1,588 | 88.10 | 0.2930 | 1,610 | 87.60 | 0.3337 | 1,631 | 87.45 | 0.3563 | 1,581 |
| FedPrompt | 87.90 | 0.4247 | 1,485 | 87.15 | 0.4846 | 1,584 | 85.25 | 0.5106 | 1,495 | 86.00 | 0.5352 | 1,463 |
| FedPepTAO | 89.95 | 0.1627 | 1,586 | 89.60 | 0.2348 | 1,683 | 89.20 | 0.2421 | 1,583 | 89.20 | 0.2854 | 1,608 |
| PromptFL | 87.70 | 0.4394 | 1,479 | 86.50 | 0.4824 | 1,575 | 84.90 | 0.5149 | 1,499 | 85.75 | 0.5358 | 1,696 |
| PE_FL | 88.05 | 0.3954 | 1,507 | 86.15 | 0.4736 | 1,489 | 85.65 | 0.4727 | 1,529 | 85.50 | 0.5331 | 1,663 |
| SLoRA | 91.15 | 0.1598 | 1,410 | 90.70 | 0.2509 | 1,463 | 91.00 | 0.2743 | 1,469 | 90.05 | 0.2544 | 1,488 |
| HetLoRA | 88.10 | 0.3145 | 1,154 | 86.80 | 0.3668 | 1,221 | 84.00 | 0.4775 | 1,276 | 87.70 | 0.3377 | 1,207 |
| FedLoRA | 91.30 | 0.1522 | 1,493 | 90.75 | 0.2478 | 1,539 | 91.10 | 0.2744 | 1,571 | 89.95 | 0.2473 | 1,399 |
| FFA-LoRA | 87.55 | 0.3448 | 1,065 | 86.00 | 0.4245 | 1,098 | 84.45 | 0.3580 | 1,119 | 87.50 | 0.3580 | 1,193 |
| Fedkseed | 88.80 | 0.3138 | 1,114 | 86.90 | 0.4047 | 1,141 | 84.95 | 0.5082 | 1,168 | 82.75 | 0.5833 | 1,176 |
| FLoRA | 89.05 | 0.2966 | 1,202 | 87.75 | 0.3707 | 1,151 | 85.65 | 0.4662 | 1,129 | 84.25 | 0.5227 | 1,154 |
| RAFFT | 91.80 | 0.1065 | 842 | 92.00 | 0.1285 | 905 | 91.70 | 0.1469 | 885 | 91.45 | 0.1692 | 905 |

Table 17: Performance comparison of different methods on Roberta+MRPC with varying numbers of clients (N).

| | N = 40 | | | N = 60 | | | N = 80 | | | N = 100 | | |
|---|---|---|---|---|---|---|---|---|---|---|---|---|
| Method | Accuracy | Loss | Time | Accuracy | Loss | Time | Accuracy | Loss | Time | Accuracy | Loss | Time |
| Federated_LoRA | 85.21 | 0.2362 | 1,416 | 83.55 | 0.3623 | 1,395 | 83.72 | 0.3956 | 1,443 | 81.32 | 0.4122 | 1,407 |
| FedAdaLoRA | 83.37 | 0.2942 | 1,545 | 83.62 | 0.3217 | 1,506 | 83.75 | 0.3641 | 1,514 | 81.13 | 0.4309 | 1,563 |
| P-tuning v2 | 80.63 | 0.2974 | 1,037 | 78.13 | 0.4139 | 1,088 | 79.11 | 0.4611 | 1,059 | 78.48 | 0.4325 | 1,049 |
| FedPrompt | 76.29 | 0.5435 | 1,003 | 75.29 | 0.6265 | 1,003 | 75.13 | 0.7028 | 992 | 75.87 | 0.6784 | 1,004 |
| FedPepTAO | 84.98 | 0.2090 | 1,042 | 81.40 | 0.2732 | 1,080 | 81.68 | 0.3586 | 1,120 | 80.85 | 0.3982 | 1,049 |
| PromptFL | 75.55 | 0.6329 | 1,022 | 74.98 | 0.6772 | 1,045 | 75.34 | 0.7687 | 972 | 75.84 | 0.5917 | 1,001 |
| PE_FL | 83.26 | 0.2482 | 1,045 | 80.75 | 0.2792 | 1,087 | 81.27 | 0.3896 | 1,037 | 76.18 | 0.5686 | 1,024 |
| SLoRA | 85.43 | 0.3257 | 1,029 | 83.57 | 0.3722 | 1,066 | 81.39 | 0.3846 | 1,021 | 80.43 | 0.4559 | 1,044 |
| HetLoRA | 81.68 | 0.4203 | 1,035 | 78.83 | 0.4678 | 1,143 | 76.77 | 0.5138 | 1,150 | 80.52 | 0.4470 | 1,086 |
| FedLoRA | 85.07 | 0.4072 | 1,083 | 84.11 | 0.4674 | 1,114 | 82.92 | 0.5052 | 1,075 | 81.64 | 0.5645 | 1,095 |
| FFA-LoRA | 81.06 | 0.3960 | 1,116 | 80.87 | 0.4550 | 1,033 | 78.30 | 0.5054 | 1,036 | 77.74 | 0.4846 | 1,060 |
| Fedkseed | 81.32 | 0.6024 | 1,075 | 81.28 | 0.6224 | 1,084 | 81.34 | 0.6945 | 1,041 | 81.40 | 0.6975 | 1,153 |
| FLoRA | 82.38 | 0.5507 | 1,153 | 81.52 | 0.6001 | 1,031 | 81.38 | 0.6627 | 1,052 | 81.29 | 0.6579 | 1,188 |
| RAFFT | 86.80 | 0.2629 | 994 | 85.55 | 0.2914 | 1,005 | 85.70 | 0.3949 | 997 | 84.75 | 0.3519 | 1,097 |

Table 18: Performance comparison of different methods on Roberta+SST2 with varying numbers of clients (N).

| | N = 40 | | | N = 60 | | | N = 80 | | | N = 100 | | |
|---|---|---|---|---|---|---|---|---|---|---|---|---|
| Method | Accuracy | Loss | Time | Accuracy | Loss | Time | Accuracy | Loss | Time | Accuracy | Loss | Time |
| Federated_LoRA | 94.83 | 0.2296 | 1,149 | 94.38 | 0.2550 | 1,133 | 94.38 | 0.2523 | 1,157 | 92.89 | 0.3394 | 1,883 |
| FedAdaLoRA | 93.81 | 0.2471 | 1,269 | 93.69 | 0.2498 | 1,270 | 93.46 | 0.2424 | 1,223 | 88.07 | 1.7253 | 1,710 |
| P-tuning v2 | 90.02 | 0.6433 | 1,562 | 88.07 | 0.7700 | 1,527 | 87.27 | 0.7822 | 1,534 | 89.44 | 0.6417 | 1,545 |
| FedPrompt | 93.69 | 0.4831 | 1,501 | 90.13 | 0.6522 | 1,490 | 90.37 | 0.7105 | 1,472 | 89.68 | 0.7164 | 1,487 |
| FedPepTAO | 91.28 | 0.4281 | 1,592 | 90.83 | 0.5123 | 1,623 | 90.71 | 0.5028 | 1,603 | 91.06 | 0.4388 | 1,614 |
| PromptFL | 92.78 | 0.4751 | 1,469 | 91.86 | 0.5922 | 1,472 | 90.48 | 0.6318 | 1,432 | 92.20 | 0.5044 | 1,453 |
| PE_FL | 94.50 | 0.4647 | 1,512 | 92.43 | 0.5441 | 1,492 | 91.85 | 0.5617 | 1,478 | 93.00 | 0.4628 | 1,503 |
| SLoRA | 95.64 | 0.2084 | 1,185 | 95.30 | 0.2302 | 1,215 | 95.18 | 0.2233 | 1,239 | 81.65 | 3.4859 | 1,447 |
| HetLoRA | 93.69 | 0.2472 | 1,071 | 93.23 | 0.2734 | 1,143 | 93.12 | 0.3029 | 1,054 | 93.46 | 0.2785 | 1,067 |
| FedLoRA | 95.41 | 0.2875 | 1,178 | 95.05 | 0.2962 | 1,206 | 94.95 | 0.2701 | 1,215 | 93.35 | 0.3002 | 1,221 |
| FFA-LoRA | 93.00 | 0.3431 | 1,032 | 92.32 | 0.4621 | 995 | 92.77 | 0.5617 | 1,015 | 93.46 | 0.3048 | 1,022 |
| Fedkseed | 94.03 | 0.2437 | 1,258 | 93.58 | 0.2739 | 1,314 | 93.69 | 0.2736 | 1,142 | 93.00 | 0.2724 | 1,046 |
| FLoRA | 94.38 | 0.2389 | 1,192 | 93.69 | 0.2623 | 1,207 | 93.69 | 0.2544 | 1,103 | 93.12 | 0.3307 | 1,045 |
| RAFFT | 95.76 | 0.1561 | 922 | 95.30 | 0.1665 | 944 | 95.30 | 0.1396 | 969 | 95.07 | 0.1894 | 1012 |

Table 19: Performance comparison of different methods on ViT+CIFRA10 with varying numbers of clients (N).

| | N = 40 | | | N = 60 | | | N = 80 | | | N = 100 | | |
|---|---|---|---|---|---|---|---|---|---|---|---|---|
| Method | Accuracy | Loss | Time | Accuracy | Loss | Time | Accuracy | Loss | Time | Accuracy | Loss | Time |
| Federated_LoRA | 71.95 | 0.6527 | 3,278 | 71.77 | 0.6565 | 3,321 | 71.48 | 0.6874 | 3,286 | 71.90 | 0.7170 | 3,329 |
| FedAdaLoRA | 72.34 | 0.6616 | 3,518 | 72.12 | 0.6467 | 3,627 | 71.83 | 0.6873 | 3,590 | 71.76 | 0.6936 | 3,535 |
| SLoRA | 72.76 | 0.6372 | 3,301 | 72.39 | 0.6652 | 3,294 | 71.77 | 0.6634 | 3,330 | 71.75 | 0.6843 | 3,309 |
| HetLoRA | 72.22 | 0.6614 | 3,310 | 71.81 | 0.6831 | 3,312 | 71.30 | 0.7046 | 3,350 | 71.76 | 0.6939 | 3,355 |
| FedLoRA | 72.35 | 0.6800 | 3,269 | 71.64 | 0.6867 | 3,343 | 71.53 | 0.6873 | 3,301 | 71.56 | 0.7149 | 3,282 |
| FFA-LoRA | 71.79 | 0.6435 | 3,269 | 71.91 | 0.6848 | 3,362 | 71.53 | 0.6993 | 3,310 | 71.47 | 0.7135 | 3,321 |
| FLoRA | 72.59 | 0.5949 | 3,409 | 72.25 | 0.6060 | 3,373 | 71.03 | 0.5980 | 3,350 | 70.95 | 0.7266 | 3,401 |
| RAFFT | 75.71 | 0.5021 | 3,279 | 75.67 | 0.5252 | 3,286 | 74.61 | 0.5232 | 3,301 | 74.54 | 0.5757 | 3,304 |

Table 20: Performance comparison of different methods on ViT+CIFRA100 with varying numbers of clients (N).

| | N = 40 | | | N = 60 | | | N = 80 | | | N = 100 | | |
|---|---|---|---|---|---|---|---|---|---|---|---|---|
| Method | Accuracy | Loss | Time | Accuracy | Loss | Time | Accuracy | Loss | Time | Accuracy | Loss | Time |
| Federated_LoRA | 45.69 | 1.7550 | 3,267 | 45.88 | 1.7610 | 3,295 | 45.46 | 1.8640 | 3,251 | 46.43 | 1.7763 | 3,340 |
| FedAdaLoRA | 44.28 | 1.8590 | 3,535 | 44.53 | 1.8950 | 3,489 | 43.54 | 1.9040 | 3,538 | 46.15 | 1.7674 | 3,548 |
| SLoRA | 44.78 | 1.8630 | 3,304 | 45.16 | 1.8620 | 3,237 | 44.52 | 1.9560 | 3,311 | 44.10 | 1.9510 | 3,372 |
| HetLoRA | 45.80 | 1.7540 | 3,278 | 45.90 | 1.7990 | 3,315 | 45.50 | 1.8280 | 3,334 | 46.31 | 1.8132 | 3,347 |
| FedLoRA | 46.13 | 1.7310 | 3,335 | 45.72 | 1.7500 | 3,286 | 44.95 | 1.8430 | 3,289 | 45.26 | 1.5120 | 3,404 |
| FFA-LoRA | 45.75 | 1.7200 | 3,331 | 45.85 | 1.7780 | 3,280 | 45.28 | 1.8550 | 3,404 | 45.99 | 1.8065 | 3,363 |
| FLoRA | 48.11 | 1.6190 | 3,329 | 48.09 | 1.6210 | 3,494 | 46.76 | 1.6030 | 3,344 | 40.39 | 1.5424 | 3,288 |
| RAFFT | 48.94 | 1.1740 | 3,193 | 48.85 | 1.2130 | 3,122 | 48.27 | 1.3310 | 3,284 | 48.44 | 1.3240 | 3,273 |

Table 21: Performance comparison of different methods on ViT+IamgeNet with varying numbers of clients (N).

| | N = 40 | | | N = 60 | | | N = 80 | | | N = 100 | | |
|---|---|---|---|---|---|---|---|---|---|---|---|---|
| Method | Accuracy | Loss | Time | Accuracy | Loss | Time | Accuracy | Loss | Time | Accuracy | Loss | Time |
| Federated_LoRA | 28.46 | 3.0426 | 11,604 | 26.34 | 3.1904 | 11,737 | 26.82 | 3.2050 | 11,546 | 26.92 | 2.9963 | 11,497 |
| FedAdaLoRA | 28.86 | 2.9607 | 12,264 | 26.50 | 3.1529 | 12,481 | 26.64 | 3.1230 | 12,433 | 27.10 | 3.0361 | 12,278 |
| SLoRA | 28.32 | 3.0342 | 11,583 | 26.40 | 3.2080 | 11,834 | 26.92 | 3.2540 | 11,734 | 26.76 | 3.2740 | 11,176 |
| HetLoRA | 28.50 | 2.9923 | 11,838 | 26.58 | 3.2077 | 12,349 | 27.00 | 3.2010 | 12,045 | 26.78 | 3.0303 | 11,487 |
| FedLoRA | 28.30 | 2.9999 | 11,855 | 26.48 | 3.1991 | 12,008 | 26.84 | 3.2300 | 11,922 | 26.80 | 3.2570 | 11,643 |
| FFA-LoRA | 28.44 | 3.0310 | 11,789 | 26.40 | 3.2059 | 11,810 | 26.78 | 3.2140 | 11,941 | 26.42 | 3.2642 | 11,700 |
| FLoRA | 26.96 | 3.499 | 11,586 | 26.68 | 3.4914 | 11,716 | 25.76 | 3.5060 | 11,516 | 23.96 | 3.5034 | 11,564 |
| RAFFT | 29.66 | 2.6210 | 11,038 | 27.36 | 2.9390 | 11,142 | 29.24 | 2.8190 | 11,349 | 28.82 | 2.9140 | 11,236 |

**Accuracy of classification using Riemannian manifolds on different initial rank values.**To comprehensively investigate the applicability of our RAFFT method for classification tasks with different initial rank values, we set the initial ranks to 2, 4, 8, and 16 while keeping other settings constant. Tables 22-27 present the classification accuracy on three datasets using Riemannian manifold techniques. We observed consistent results, indicating that the three variants of our RAFFT method achieved the best accuracy in most experiments. A plausible explanation is that the rigorous mathematical analysis based on Riemannian manifold theory significantly enhances the effectiveness and applicability of our RAFFT method across different scenarios.

Table 22: Performance comparison of different methods on Roberta+MPQA with varying rank values (r).

| | r = 2 | | | r = 4 | | | r = 8 | | | r = 16 | | |
|---|---|---|---|---|---|---|---|---|---|---|---|---|
| Method | Accuracy | Loss | Time | Accuracy | Loss | Time | Accuracy | Loss | Time | Accuracy | Loss | Time |
| Federated_LoRA | 90.6 | 0.2157 | 1,040 | 90.55 | 0.2153 | 1,038 | 89.65 | 0.2510 | 1,442 | 90.55 | 0.2075 | 1,011 |
| FedAdaLoRA | 82.46 | 0.8709 | 1,237 | 81.80 | 0.8581 | 1,195 | 85.85 | 0.4136 | 1,774 | 82.10 | 0.8887 | 1,228 |
| SLoRA | 90.10 | 0.2219 | 1,034 | 90.10 | 0.2213 | 1,065 | 90.05 | 0.2545 | 1,473 | 90.10 | 0.2222 | 1,073 |
| HetLoRA | 86.60 | 0.3707 | 1,318 | 83.20 | 0.5256 | 1,203 | 87.70 | 0.3377 | 1,207 | 89.60 | 0.2552 | 1,186 |
| FedLoRA | 90.20 | 0.2170 | 1,095 | 90.30 | 0.2175 | 1,049 | 89.95 | 0.2473 | 1,416 | 90.20 | 0.2177 | 1,140 |
| FFA-LoRA | 87.95 | 0.3290 | 1,158 | 88.55 | 0.3251 | 1,139 | 87.50 | 0.3580 | 1,193 | 87.85 | 0.3413 | 1,140 |
| FLoRA | 84.15 | 0.5238 | 1,159 | 84.10 | 0.5257 | 1,180 | 84.25 | 0.5227 | 1,197 | 84.30 | 0.5250 | 1,186 |
| RAFFT | 91.00 | 0.1900 | 849 | 91.05 | 0.1806 | 848 | 91.45 | 0.1692 | 905 | 91.55 | 0.1500 | 918 |

Table 23: Performance comparison of different methods on Roberta+MRPC with varying rank values (r).

| | r = 2 | | | r = 4 | | | r = 8 | | | r = 16 | | |
|---|---|---|---|---|---|---|---|---|---|---|---|---|
| Method | Accuracy | Loss | Time | Accuracy | Loss | Time | Accuracy | Loss | Time | Accuracy | Loss | Time |
| Federated_LoRA | 82.27 | 0.3894 | 1,417 | 82.49 | 0.3853 | 1,385 | 81.32 | 0.4122 | 1,402 | 81.86 | 0.3862 | 1,401 |
| FedAdaLoRA | 79.98 | 0.4240 | 1,516 | 82.34 | 0.3992 | 1,528 | 81.14 | 0.4309 | 1,563 | 81.66 | 0.4020 | 1,572 |
| SLoRA | 82.27 | 0.3864 | 1,039 | 82.08 | 0.3794 | 1,012 | 80.43 | 0.4559 | 1,044 | 81.38 | 0.3824 | 1,074 |
| HetLoRA | 75.40 | 0.5103 | 1,045 | 74.78 | 0.5767 | 1,033 | 80.52 | 0.4470 | 1,086 | 74.78 | 0.9160 | 1,082 |
| FedLoRA | 81.45 | 0.5971 | 1,047 | 81.37 | 0.5958 | 1,022 | 81.64 | 0.5645 | 1,056 | 81.33 | 0.5974 | 1,018 |
| FFA-LoRA | 74.81 | 0.5438 | 1,003 | 74.98 | 0.5441 | 1,014 | 77.74 | 0.4846 | 1,060 | 74.91 | 0.5549 | 1,048 |
| FLoRA | 81.16 | 0.6580 | 1,037 | 81.17 | 0.6591 | 1,084 | 81.29 | 0.6579 | 1,010 | 81.67 | 0.6592 | 1,024 |
| RAFFT | 85.16 | 0.3345 | 813 | 84.57 | 0.3000 | 825 | 85.39 | 0.2758 | 818 | 86.04 | 0.3453 | 830 |

Table 24: Performance comparison of different methods on Roberta+SST2 with varying rank values (r).

| | r = 2 | | | r = 4 | | | r = 8 | | | r = 16 | | |
|---|---|---|---|---|---|---|---|---|---|---|---|---|
| Method | Accuracy | Loss | Time | Accuracy | Loss | Time | Accuracy | Loss | Time | Accuracy | Loss | Time |
| Federated_LoRA | 93.35 | 0.2529 | 1,040 | 93.19 | 0.2613 | 1,001 | 92.89 | 0.3394 | 1,883 | 93.12 | 0.2614 | 1,076 |
| FedAdaLoRA | 89.44 | 1.5001 | 1,237 | 89.79 | 1.4422 | 1,195 | 88.07 | 1.7253 | 1,710 | 89.56 | 1.5087 | 1,184 |
| SLoRA | 93.18 | 0.2571 | 1,034 | 92.30 | 0.2595 | 1,065 | 81.65 | 3.4859 | 1,447 | 95.18 | 0.1595 | 1,105 |
| HetLoRA | 93.35 | 0.2531 | 1,032 | 93.00 | 0.3403 | 1,085 | 93.46 | 0.2785 | 1,067 | 92.20 | 0.7275 | 1,093 |
| FedLoRA | 93.92 | 0.2559 | 1,095 | 90.30 | 0.2175 | 1,049 | 93.92 | 0.2548 | 1,221 | 93.92 | 0.2559 | 1,086 |
| FFA-LoRA | 91.74 | 0.6232 | 1,017 | 91.97 | 0.5818 | 1,042 | 92.77 | 0.3048 | 1,022 | 91.86 | 0.7081 | 1,036 |
| FLoRA | 92.26 | 0.2368 | 1,224 | 93.34 | 0.2369 | 1,206 | 93.12 | 0.3307 | 1,232 | 94.27 | 0.2369 | 1,249 |
| RAFFT | 94.15 | 0.2316 | 994 | 95.18 | 0.1790 | 992 | 95.07 | 0.1894 | 1012 | 95.30 | 0.2130 | 1,014 |

Table 25: Performance comparison of different methods on ViT+CIFRA10 with varying rank values (r).

| | r = 2 | | | r = 4 | | | r = 8 | | | r = 16 | | |
|---|---|---|---|---|---|---|---|---|---|---|---|---|
| Method | Accuracy | Loss | Time | Accuracy | Loss | Time | Accuracy | Loss | Time | Accuracy | Loss | Time |
| Federated_LoRA | 71.14 | 0.7078 | 3,256 | 72.08 | 0.6924 | 3,241 | 71.90 | 0.717 | 3,329 | 70.69 | 0.7221 | 3,318 |
| FedAdaLoRA | 71.06 | 0.717 | 3,600 | 71.62 | 0.7060 | 3,510 | 71.76 | 0.6936 | 3,535 | 71.47 | 0.7127 | 3,622 |
| SLoRA | 71.54 | 0.6927 | 3,269 | 72.12 | 0.6871 | 3,337 | 71.75 | 0.6843 | 3,309 | 72.03 | 0.7002 | 3,357 |
| HetLoRA | 71.50 | 0.7071 | 3,358 | 70.66 | 0.7172 | 3,333 | 71.76 | 0.6939 | 3,355 | 70.91 | 0.7045 | 3,361 |
| FedLoRA | 71.87 | 0.7133 | 3,277 | 71.28 | 0.7287 | 3,300 | 71.56 | 0.7149 | 3,282 | 71.83 | 0.7111 | 3,306 |
| FFA-LoRA | 71.90 | 0.6900 | 3,316 | 72.10 | 0.7000 | 3,291 | 71.47 | 0.7135 | 3,321 | 71.22 | 0.7167 | 3,341 |
| FLoRA | 71.75 | 0.5803 | 3,840 | 72.38 | 0.6042 | 3,913 | 70.95 | 0.7266 | 3,901 | 71.34 | 0.5885 | 3,970 |
| RAFFT | 73.67 | 0.5615 | 3,282 | 74.23 | 0.5953 | 3,244 | 74.54 | 0.5757 | 3,304 | 73.97 | 0.579 | 3,301 |

Table 26: Performance comparison of different methods on ViT+CIFRA100 with varying rank values (r).

| | r = 2 | | | r = 4 | | | r = 8 | | | r = 16 | | |
|---|---|---|---|---|---|---|---|---|---|---|---|---|
| Method | Accuracy | Loss | Time | Accuracy | Loss | Time | Accuracy | Loss | Time | Accuracy | Loss | Time |
| Federated_LoRA | 44.45 | 1.8870 | 3,212 | 44.32 | 1.9000 | 3,333 | 46.43 | 1.7763 | 3,340 | 44.64 | 1.8830 | 3,399 |
| FedAdaLoRA | 44.24 | 1.9410 | 3,519 | 43.76 | 1.9600 | 3,507 | 46.15 | 1.7674 | 3,548 | 43.41 | 1.9920 | 3,559 |
| SLoRA | 43.81 | 1.9670 | 3,382 | 43.42 | 2.0000 | 3,317 | 44.10 | 1.9510 | 3,372 | 43.00 | 1.9810 | 3,437 |
| HetLoRA | 44.87 | 1.8690 | 3,314 | 44.83 | 1.8740 | 3,358 | 46.31 | 1.8132 | 3,347 | 44.46 | 1.9110 | 3,440 |
| FedLoRA | 44.41 | 1.9140 | 3,365 | 44.56 | 1.9090 | 3,351 | 45.26 | 1.8920 | 3,260 | 44.53 | 1.8830 | 3,337 |
| FFA-LoRA | 44.62 | 1.9000 | 3,389 | 44.60 | 1.9220 | 3,375 | 45.99 | 1.8065 | 3,363 | 44.00 | 1.8880 | 3,464 |
| FLoRA | 45.05 | 1.6170 | 3,873 | 45.23 | 1.6100 | 3,813 | 40.39 | 1.5424 | 3,888 | 46.91 | 1.6500 | 3,839 |
| RAFFT | 48.76 | 1.3330 | 3,305 | 48.13 | 1.3220 | 3,255 | 48.44 | 1.3240 | 3,273 | 48.94 | 1.3000 | 3,296 |

Table 27: Performance comparison of different methods on ViT+IamgeNet with varying rank values (r).

| | r = 2 | | | r = 4 | | | r = 8 | | | r = 16 | | |
|---|---|---|---|---|---|---|---|---|---|---|---|---|
| Method | Accuracy | Loss | Time | Accuracy | Loss | Time | Accuracy | Loss | Time | Accuracy | Loss | Time |
| Federated_LoRA | 27.02 | 3.2640 | 11,425 | 27.20 | 3.2700 | 11,383 | 26.92 | 2.9963 | 11,497 | 26.64 | 3.2910 | 11,542 |
| FedAdaLoRA | 26.58 | 3.2550 | 12,272 | 26.28 | 3.2700 | 12,256 | 27.10 | 3.0362 | 12,278 | 26.36 | 3.2980 | 12,294 |
| SLoRA | 26.82 | 3.2590 | 11,102 | 26.84 | 3.2520 | 11,145 | 26.76 | 3.2740 | 11,176 | 26.16 | 3.2850 | 11,191 |
| HetLoRA | 26.80 | 3.2540 | 11,502 | 27.08 | 3.2500 | 11,394 | 26.78 | 3.0303 | 11,487 | 27.10 | 3.2540 | 11,674 |
| FedLoRA | 26.56 | 3.2610 | 11,523 | 27.26 | 3.2190 | 11,401 | 26.80 | 3.2570 | 11,643 | 26.28 | 3.2890 | 11,723 |
| FFA-LoRA | 27.00 | 3.2530 | 11,685 | 26.92 | 3.2660 | 11,504 | 26.42 | 3.2642 | 11,700 | 26.68 | 3.2630 | 11,894 |
| FLoRA | 24.36 | 3.477 | 11,817 | 24.48 | 3.4890 | 11,905 | 23.96 | 3.5033 | 11,564 | 23.44 | 3.4843 | 12,218 |
| RAFFT | 29.24 | 2.9230 | 11,295 | 28.40 | 2.9040 | 11,012 | 28.82 | 2.9140 | 11,236 | 28.42 | 2.9330 | 11,096 |

**Impact of select rank threshold** Based on Table 28-29, we evaluate the performance effect of setting the selection ranking threshold to 0.6, 0.7, 0.8, 0.9, and 1. We observe that as the threshold increases, the performance improves slightly initially and performs best at a threshold of 0.9. Beyond this point, performance starts to degrade. This trend suggests that a threshold of 0.9 is optimal, probably because it strikes a balance between filtering out irrelevant information and retaining useful information. When the threshold is set to 1, it means there is no level truncation which may introduce too much noise or redundant information, leading to performance degradation.

Table 28: Performance comparison of different models with varying Theta values (ACC).

| **Model** | **ACC** | | | | |
|---|---|---|---|---|---|
| | $\Theta = 0.6$ | $\Theta = 0.7$ | $\Theta = 0.8$ | $\Theta = 0.9$ | $\Theta = 1$ |
| Roberta+SST-2 | 95.30 | 95.30 | 95.41 | 95.07 | 93.00 |
| Roberta+MRPC | 84.22 | 83.22 | 85.67 | 84.75 | 82.25 |
| Roberta+MPQA | 91.15 | 91.30 | 91.55 | 91.45 | 90.15 |
| LLaMA 7B+SST-2 | 95.41 | 95.53 | 95.41 | 95.64 | 94.15 |
| LLaMA 7B+MRPC | 82.77 | 82.77 | 82.77 | 83.62 | 81.55 |
| LLaMA 7B+MPQA | 91.40 | 91.45 | 91.70 | 92.00 | 90.80 |
| ViT+CIFAR10 | 74.07 | 73.53 | 73.95 | 73.89 | 72.88 |
| ViT+CIFAR100 | 49.16 | 48.22 | 47.97 | 48.44 | 47.21 |
| ViT+ImageNet | 28.92 | 28.64 | 28.66 | 28.82 | 27.16 |

Table 29: Performance comparison of different models with varying Theta values (Time).

| Model | Time (s) | | | | |
|---|---|---|---|---|---|
| | $\Theta = 0.6$ | $\Theta = 0.7$ | $\Theta = 0.8$ | $\Theta = 0.9$ | $\Theta = 1$ |
| Roberta+SST-2 | 976 | 981 | 968 | 1,012 | 962 |
| Roberta+MRPC | 853 | 850 | 843 | 838 | 798 |
| Roberta+MPQA | 865 | 886 | 883 | 905 | 890 |
| LLaMA 7B+SST-2 | 6,848 | 6,848 | 6,852 | 6,988 | 6,961 |
| LLaMA 7B+MRPC | 7,595 | 7,504 | 7,513 | 7,558 | 7,541 |
| LLaMA 7B+MPQA | 4,840 | 5,025 | 4,916 | 5,010 | 5,021 |
| ViT+CIFAR10 | 3,591 | 3,611 | 3,587 | 3,555 | 3,687 |
| ViT+CIFAR100 | 3,553 | 3,695 | 3,638 | 3,585 | 3,625 |
| ViT+ImageNet | 13,260 | 13,073 | 13,388 | 12,706 | 13,164 |

Table 30: Performance comparison of different models with varying Learning Rates (ACC).

| Model | ACC | | | | |
|---|---|---|---|---|---|
| | LR=0.0001 | LR=0.0005 | LR=0.001 | LR=0.005 | LR=0.01 |
| Roberta+SST-2 | 86.24 | 93.81 | 94.84 | 95.30 | 95.64 |
| Roberta+MRPC | 74.78 | 77.33 | 81.93 | 84.40 | 87.04 |
| Roberta+MPQA | 79.55 | 90.10 | 91.20 | 91.55 | 91.70 |
| LLaMA 7B+SST-2 | 95.18 | 96.10 | 96.33 | 61.70 | 50.92 |
| LLaMA 7B+MRPC | 81.52 | 82.70 | 83.62 | 81.22 | 81.22 |
| LLaMA 7B+MPQA | 91.10 | 92.00 | 91.90 | 67.60 | 67.70 |
| ViT+CIFAR10 | 74.54 | 69.28 | 54.97 | 27.90 | 23.73 |
| ViT+CIFAR100 | 48.44 | 44.07 | 29.38 | 6.55 | 6.18 |
| ViT+ImageNet | 28.82 | 16.80 | 15.40 | 9.28 | 2.72 |

Table 31: Performance comparison of different models with varying Learning Rates (Time).

| Model | Time (s) | | | | |
|---|---|---|---|---|---|
| | LR=0.0001 | LR=0.0005 | LR=0.001 | LR=0.005 | LR=0.01 |
| Roberta+SST-2 | 979 | 981 | 990 | 980 | 967 |
| Roberta+MRPC | 862 | 847 | 832 | 826 | 825 |
| Roberta+MPQA | 905 | 914 | 920 | 907 | 952 |
| LLaMA 7B+SST-2 | 6,971 | 6,953 | 6,988 | 6,812 | 6,937 |
| LLaMA 7B+MRPC | 7,511 | 7,508 | 7,558 | 7,612 | 7,545 |
| LLaMA 7B+MPQA | 4,886 | 4,906 | 4,878 | 4,988 | 4,949 |
| ViT+CIFAR10 | 3,555 | 3,647 | 3,783 | 3,642 | 3,671 |
| ViT+CIFAR100 | 3,585 | 3,704 | 3,651 | 3,598 | 3,543 |
| ViT+ImageNet | 12,706 | 13,041 | 13,215 | 13,192 | 13,264 |

Table 32: Performance comparison of different models with varying Training Epochs (ACC).

| **Model** | **ACC** | | | | |
|---|---|---|---|---|---|
| | **Epoch 1** | **Epoch 5** | **Epoch 10** | **Epoch 15** | **Epoch 20** |
| Roberta+SST-2 | 87.79 | 93.81 | 94.72 | 95.18 | 95.07 |
| **Epoch 10** | **Epoch 20** | **Epoch 30** | **Epoch 40** | **Epoch 50** | |
| Roberta+MRPC | 76.60 | 79.82 | 81.81 | 83.40 | 85.67 |
| **Epoch 10** | **Epoch 20** | **Epoch 30** | **Epoch 40** | **Epoch 50** | |
| Roberta+MPQA | 88.85 | 90.15 | 90.70 | 91.20 | 91.45 |
| **Epoch 2** | **Epoch 4** | **Epoch 6** | **Epoch 8** | **Epoch 10** | |
| LLaMA 7B+SST-2 | 89.91 | 94.84 | 95.41 | 95.41 | 95.64 |
| **Epoch 5** | **Epoch 10** | **Epoch 15** | **Epoch 20** | **Epoch 25** | |
| LLaMA 7B+MRPC | 81.29 | 81.29 | 82.28 | 82.28 | 83.62 |
| **Epoch 5** | **Epoch 10** | **Epoch 15** | **Epoch 20** | **Epoch 25** | |
| LLaMA 7B+MPQA | 89.45 | 90.90 | 91.25 | 91.25 | 92.00 |
| **Epoch 40** | **Epoch 80** | **Epoch 120** | **Epoch 160** | **Epoch 200** | |
| ViT+CIFAR10 | 57.69 | 64.74 | 69.42 | 71.85 | 74.54 |
| **Epoch 40** | **Epoch 80** | **Epoch 120** | **Epoch 160** | **Epoch 200** | |
| ViT+CIFAR100 | 29.51 | 37.72 | 42.42 | 45.43 | 48.44 |
| **Epoch 50** | **Epoch 100** | **Epoch 200** | **Epoch 300** | **Epoch 400** | |
| ViT+ImageNet | 13.16 | 17.68 | 22.48 | 25.48 | 28.82 |

Table 33: Performance comparison of different models with varying Training Epochs (Time).

| **Model** | **Time (s)** | | | | |
|---|---|---|---|---|---|
| | **Epoch 1** | **Epoch 5** | **Epoch 10** | **Epoch 15** | **Epoch 20** |
| Roberta+SST-2 | 84 | 324 | 638 | 949 | 1,012 |
| **Epoch 10** | **Epoch 20** | **Epoch 30** | **Epoch 40** | **Epoch 50** | |
| Roberta+MRPC | 173 | 341 | 517 | 655 | 843 |
| **Epoch 10** | **Epoch 20** | **Epoch 30** | **Epoch 40** | **Epoch 50** | |
| Roberta+MPQA | 186 | 360 | 528 | 701 | 905 |
| **Epoch 2** | **Epoch 4** | **Epoch 6** | **Epoch 8** | **Epoch 10** | |
| LLaMA 7B+SST-2 | 1,380 | 2,642 | 4,043 | 5,462 | 6,988 |
| **Epoch 5** | **Epoch 10** | **Epoch 15** | **Epoch 20** | **Epoch 25** | |
| LLaMA 7B+MRPC | 1,547 | 2,994 | 4,602 | 6,012 | 7,558 |
| **Epoch 5** | **Epoch 10** | **Epoch 15** | **Epoch 20** | **Epoch 25** | |
| LLaMA 7B+MPQA | 5,071 | 5,063 | 5,102 | 4,972 | 5,010 |
| **Epoch 40** | **Epoch 80** | **Epoch 120** | **Epoch 160** | **Epoch 200** | |
| ViT+CIFAR10 | 736 | 1,450 | 2,143 | 2,935 | 3,555 |
| **Epoch 40** | **Epoch 80** | **Epoch 120** | **Epoch 160** | **Epoch 200** | |
| ViT+CIFAR100 | 722 | 1,460 | 2,203 | 2,911 | 3,585 |
| **Epoch 200** | **Epoch 250** | **Epoch 300** | **Epoch 350** | **Epoch 400** | |
| ViT+ImageNet | 1,645 | 3,288 | 6,728 | 9,691 | 12,706 |

**Accuracy of classification using Riemannian manifolds on different parameters.** As shown in Table

34-35, RAFFT demonstrates superior performance and stability in extreme non-IID data environments across diverse tasks. For instance, in the LLaMA 7B + MPQA task with $\alpha = 0.5$, RAFFT achieves the highest accuracy of 90.80, outperforming all baseline methods. Similarly, in the ViT + CIFAR-10 task with $\alpha = 0.1$, RAFFT achieves the best accuracy of 61.22, surpassing all other methods. These results highlight RAFFT's robustness and effectiveness in handling high data heterogeneity, further supported by its Riemannian framework, which mitigates both aggregation noise and rank-drift issues and ensures stability across diverse data distributions. As illustrated in Figure 3, the distribution of samples per class for each client in the MPQA dataset reflects the highly heterogeneous nature of the data.

Table 34: Performance comparison of methods on LLaMA 7B + MPQA (25 rounds) with $\alpha = 0.5$.

| **Method** | **Accuracy (%)** | **Loss** | **Time (s)** |
|---|---|---|---|
| Federated_LoRA | 82.9000 | 0.2834 | 5432 |
| FedAdaLoRA | 32.7500 | 10.5591 | 5503 |
| P-tuning v2 | 85.2000 | 0.2912 | 5664 |
| FedPrompt | 87.3500 | 0.2639 | 5393 |
| FedPepTAO | 87.6000 | 0.2584 | 5475 |
| PromptFL | 87.4000 | 0.2574 | 5586 |
| PE_FL | 87.2500 | 0.2661 | 5263 |
| SLoRA | 84.1000 | 0.3372 | 5622 |
| HetLoRA | 84.2300 | 0.3035 | 5229 |
| FedLoRA | 87.7400 | 0.1664 | 5308 |
| FFA-LoRA | 80.0000 | 0.3496 | 5358 |
| Fedkseed | 82.4500 | 0.2918 | 5452 |
| FLoRA | 79.1900 | 0.3016 | 5293 |
| RAFFT | 90.8000 | 0.2766 | 5198 |
| RAFFT-RGD | 86.2100 | 0.2947 | 5151 |
| RAFFT-MR | 86.7300 | 0.3004 | 5177 |

Table 35: Performance comparison of methods on ViT + CIFAR-10 with $\alpha = 0.1$.

| **Method** | **Accuracy (%)** | **Loss** | **Time (s)** |
|---|---|---|---|
| Federated_LoRA | 60.4800 | 1.0437 | 3578 |
| FedAdaLoRA | 60.9200 | 1.1428 | 3260 |
| SLoRA | 58.8900 | 0.8824 | 3402 |
| HetLoRA | 59.6300 | 1.0270 | 3387 |
| FedLoRA | 59.1100 | 0.9824 | 3310 |
| FFA-LoRA | 60.2100 | 0.9651 | 3412 |
| FLoRA | 59.3100 | 1.0490 | 3249 |
| RAFFT | 61.2200 | 0.8544 | 3222 |
| RAFFT-RGD | 60.6200 | 0.9478 | 3288 |
| RAFFT-MR | 59.9100 | 1.0032 | 3265 |

Figure 3: Client class distribution on MPQA dataset for different $\alpha$ values. Each plot shows the number of samples per class across clients, illustrating the heterogeneity in data distribution.

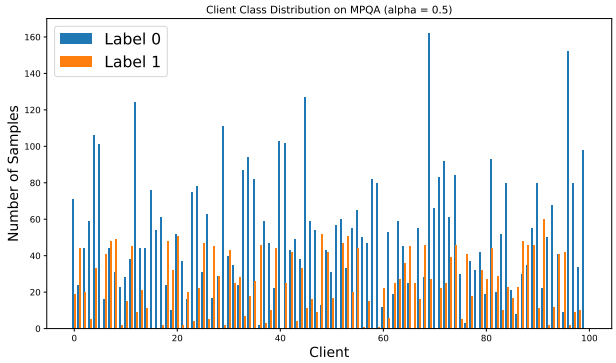


(a) $\alpha = 0.5$

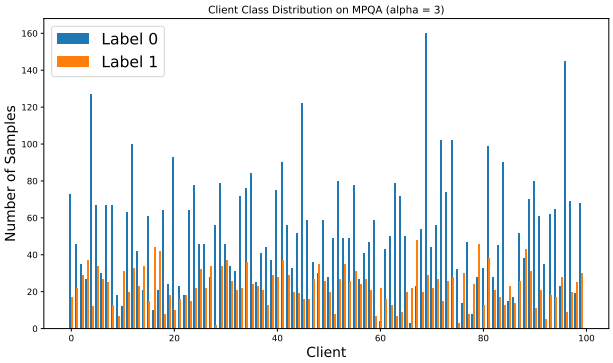


(c) $\alpha = 3$

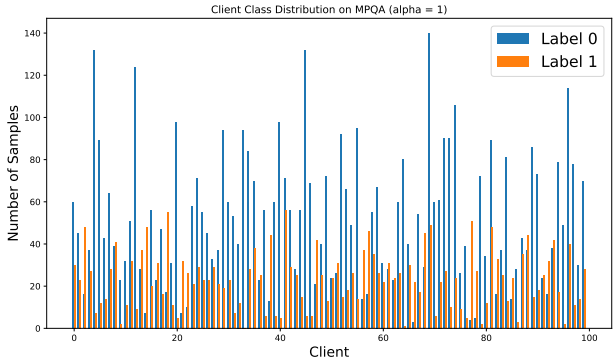


(b) $\alpha = 1$

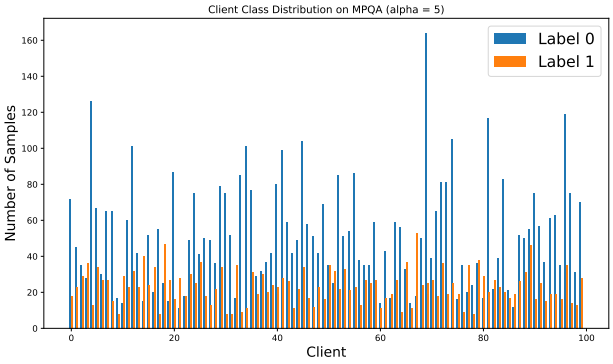


(d) $\alpha = 5$

**Resource Efficiency Analysis Using Riemannian Optimization.** The resource usage of our method is comprehensively quantified across multiple dimensions, including FLOPS (measuring computational complexity), throughput (processing rate), communication volume (data transfer during training), training time, and accuracy, as shown in our experimental results. Definitions of these metrics are provided in Bai et al. (2024a).

As shown in Table 36, the resource usage of 16 federated parameter-efficient fine-tuning methods is evaluated on the LLaMA 7B + MPQA task. Our method, RAFFT, achieves the highest throughput of 6229.19 tokens/sec with lower FLOPS (72.73 GFLOPS) compared to other methods (72.76 GFLOPS). This reduction in FLOPS is achieved because the server selects the optimal rank and sets the remaining ranks and their corresponding parameters to zero, thereby reducing unnecessary computations. Additionally, RAFFT significantly reduces the communication volume to 3146112 bytes, the lowest among LoRA-based methods, and achieves the highest accuracy of 0.908. Similarly, on the ViT + CIFAR-10 task, RAFFT achieves the best accuracy of 61.22, with the shortest training time of 3222 seconds and a communication volume of 98352 bytes. These results highlight RAFFT's ability to balance computational and communication efficiency effectively. A plausible explanation for this superior performance is that the Riemannian parameter matching and Riemannian gradient optimization enable faster convergence and improved accuracy, while the adaptive rank selection reduces redundant computation, making RAFFT a highly practical and efficient approach for real-world federated learning scenarios.

Table 36: Performance comparison of methods on LLaMA 7B + MPQA.

| Method | FLOPS (GFLOPS) | Throughput (tokens/sec on H100) | Communication Volume (Bytes) | Training Time (s) | Accuracy (%) |
|---|---|---|---|---|---|
| Federated_LoRA | 72.7557 | 5701.2920 | 4,194,304 | 5432 | 82.90 |
| FedAdaLoRA | 72.7557 | 6052.1700 | 4,194,816 | 5503 | 32.75 |
| P-tuning v2 | 72.3243 | 5563.1500 | 524,288 | 5664 | 85.20 |
| FedPrompt | 72.3243 | 5100.2800 | 524,288 | 5393 | 87.35 |
| FedPepTAO | 72.3243 | 5829.5450 | 524,288 | 5475 | 87.60 |
| PromptFL | 72.3243 | 5546.1950 | 524,288 | 5586 | 87.40 |
| PE_FL | 72.3243 | 5710.5881 | 524,288 | 5263 | 87.25 |
| SLoRA | 72.7557 | 6199.1755 | 4,194,304 | 5622 | 84.10 |
| HetLoRA | 72.7557 | 5019.9379 | 4,194,304 | 5229 | 84.23 |
| FedLoRA | 72.7557 | 5100.2800 | 6,742,618,112 | 5308 | 87.74 |
| FFA-LoRA | 72.7557 | 5034.1700 | 4,194,304 | 5358 | 80.00 |
| FLoRA | 72.7557 | 4728.9951 | 4,194,304 | 5293 | 79.19 |
| RAFFT | 72.6401 | 6229.1855 | 3,146,112 | 5151 | 90.80 |
| RAFFT-RGD | 72.8020 | 5525.9890 | 4,194,816 | 5198 | 86.21 |
| RAFFT-MR | 72.7557 | 6392.1002 | 3,146,112 | 5177 | 86.73 |

Table 37: Performance comparison of methods on ViT + CIFAR-10.

| Method | FLOPS (GFLOPS) | Throughput (images/sec on 2080Ti) | Communication Volume (Bytes) | Training Time (s) | Accuracy (%) |
|---|---|---|---|---|---|
| Federated_LoRA | 41.9654 | 5730.05 | 98,304 | 3578 | 60.48 |
| FedAdaLoRA | 41.9654 | 4722.30 | 98,352 | 3260 | 60.92 |
| SLoRA | 41.9654 | 5739.46 | 98,304 | 3402 | 58.89 |
| HetLoRA | 41.9654 | 5781.50 | 98,304 | 3387 | 59.63 |
| FedLoRA | 41.9654 | 5663.19 | 5,322,240 | 3310 | 59.11 |
| FFA-LoRA | 41.9654 | 5625.11 | 98,304 | 3412 | 60.21 |
| FLoRA | 41.9654 | 5646.20 | 98,304 | 3249 | 59.31 |
| RAFFT | 41.6335 | 5721.55 | 78,962 | 3222 | 61.22 |
| RAFFT-RGD | 41.9927 | 5315.95 | 98,304 | 3288 | 60.62 |
| RAFFT-MR | 41.9654 | 5681.28 | 78,962 | 3265 | 59.91 |

**Accuracy of classification using Riemannian manifolds on different parameters.** In order to comprehensively study the applicability of our RAFFT method to classification tasks with different parameter values, in addition to the select rank threshold in section 5 we also evaluate the following parameters: training epoch, learning rate (LR), while keeping other settings unchanged. Table 29-33 shows the classification accuracy using Riemannian manifold techniques on data sets for different models. We observe consistent results, showing that the three variants of our RAFFT method achieve the best accuracy in most experiments. A reasonable explanation is that rigorous mathematical analysis based on Riemannian manifold theory significantly enhances the effectiveness and applicability of our RAFFT method in different scenarios.

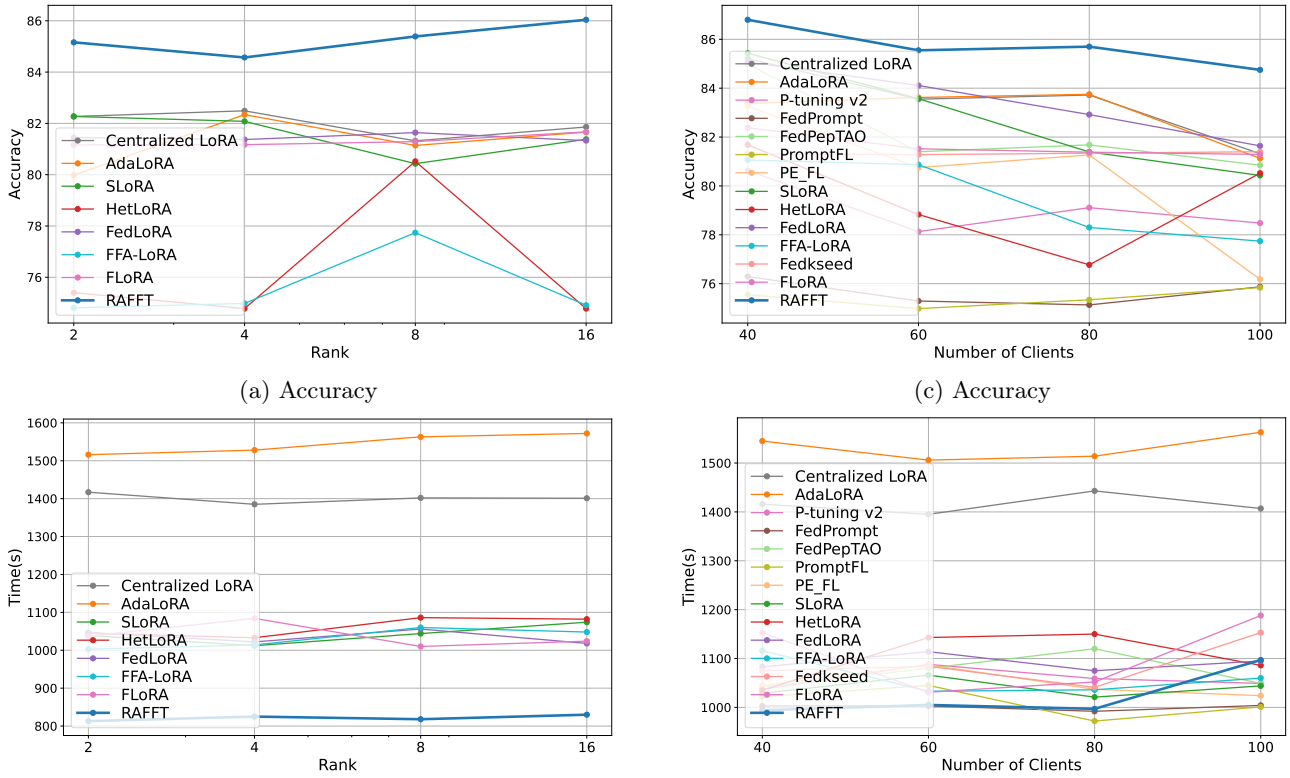


(a) Accuracy (c) Accuracy

(b) Time (d) Time

Figure 4: Accuracy and Time (s) with various LoRA ranks and client numbers on Roberta-MRPC

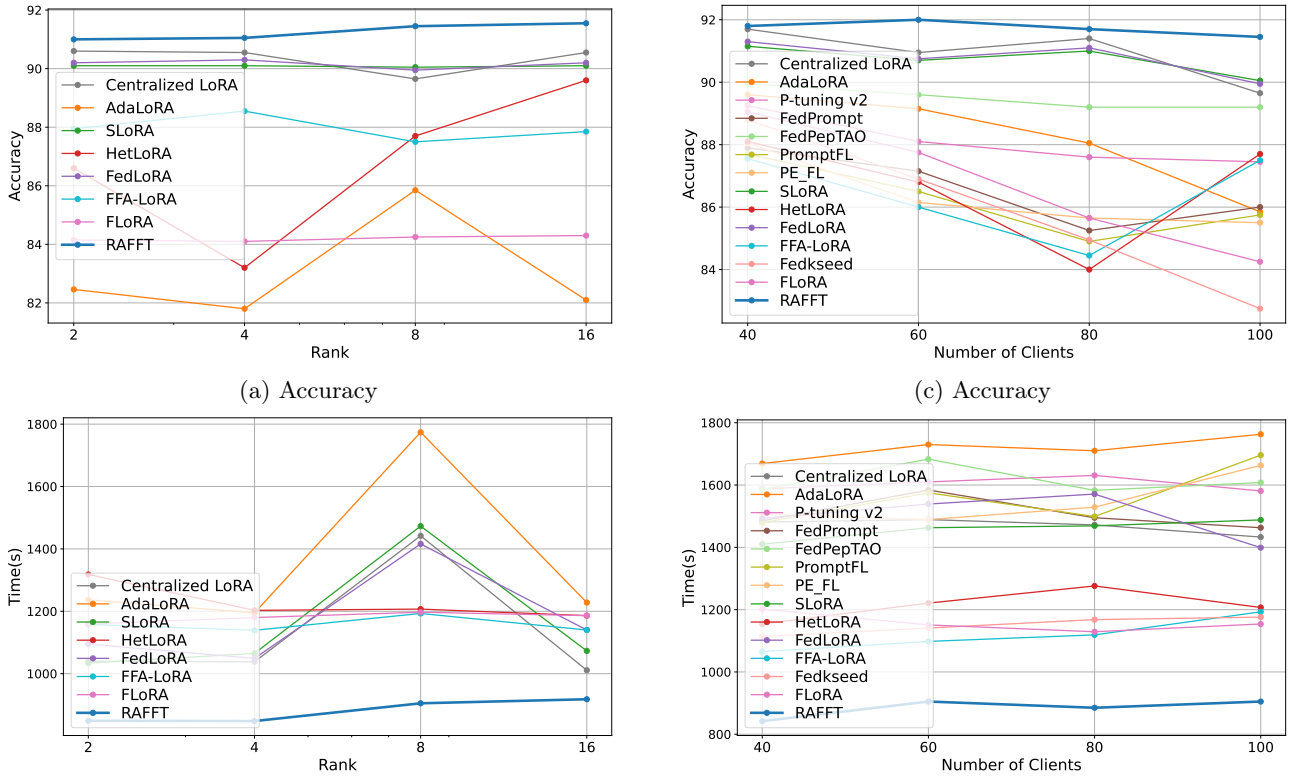


(a) Accuracy (c) Accuracy

(b) Time (d) Time

Figure 5: Accuracy and Time (s) with various LoRA ranks and client numbers on Roberta-MPQA

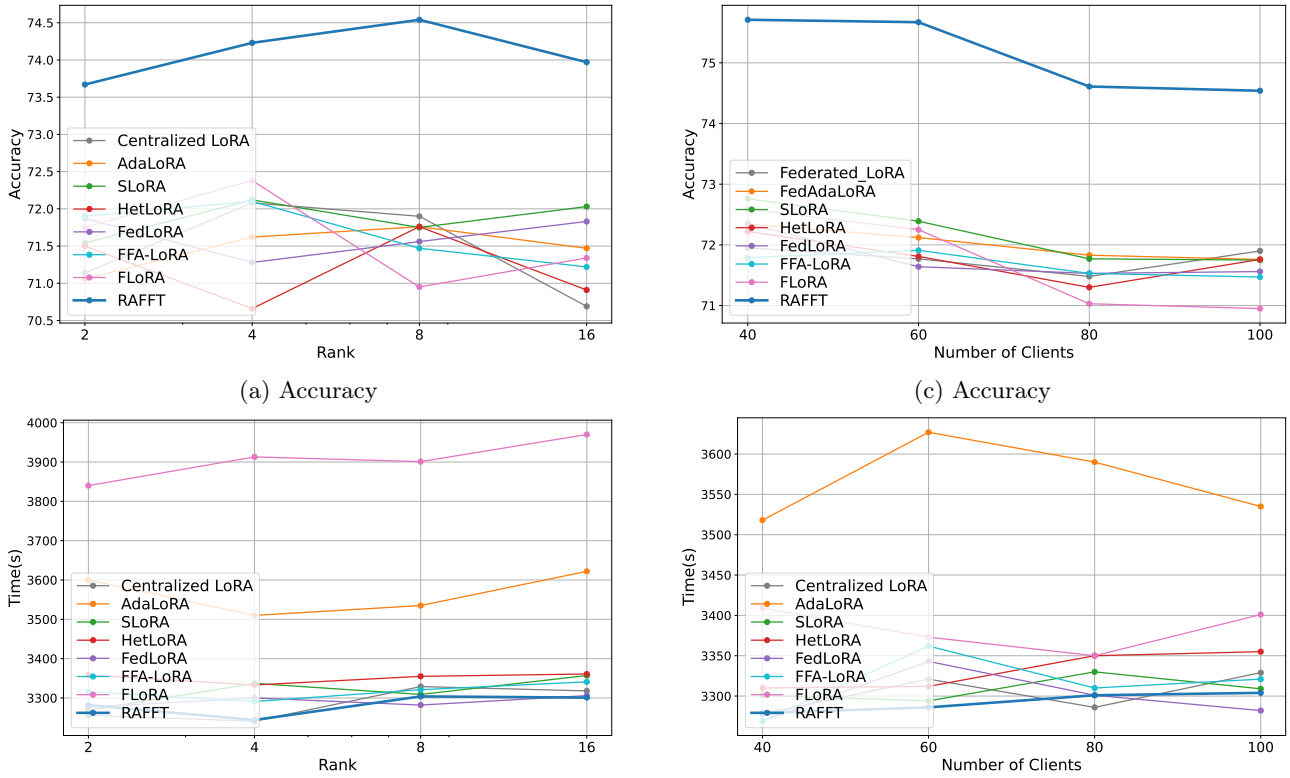


(a) Accuracy

(c) Accuracy

(b) Time

(d) Time

Figure 6: Accuracy and Time (s) with various LoRA ranks and client numbers on ViT-CIFAR-10

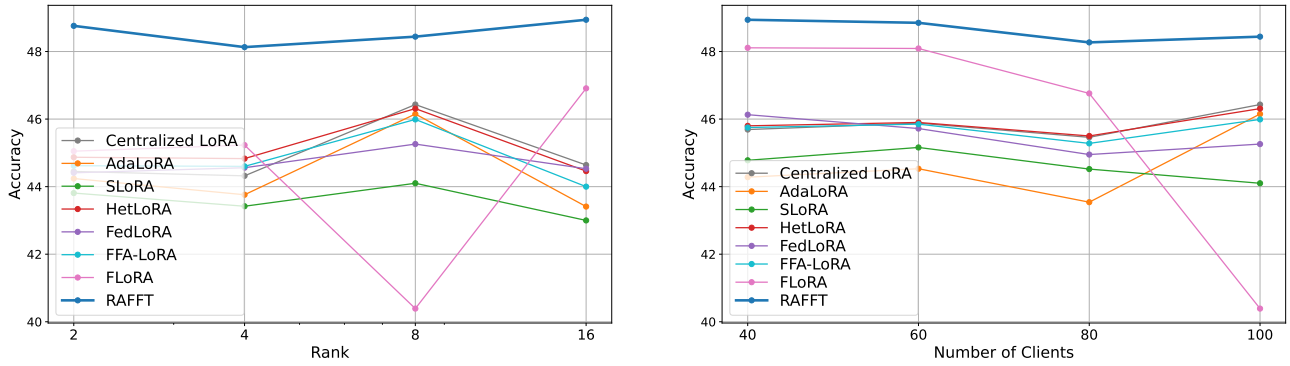


(a) Accuracy (c) Accuracy

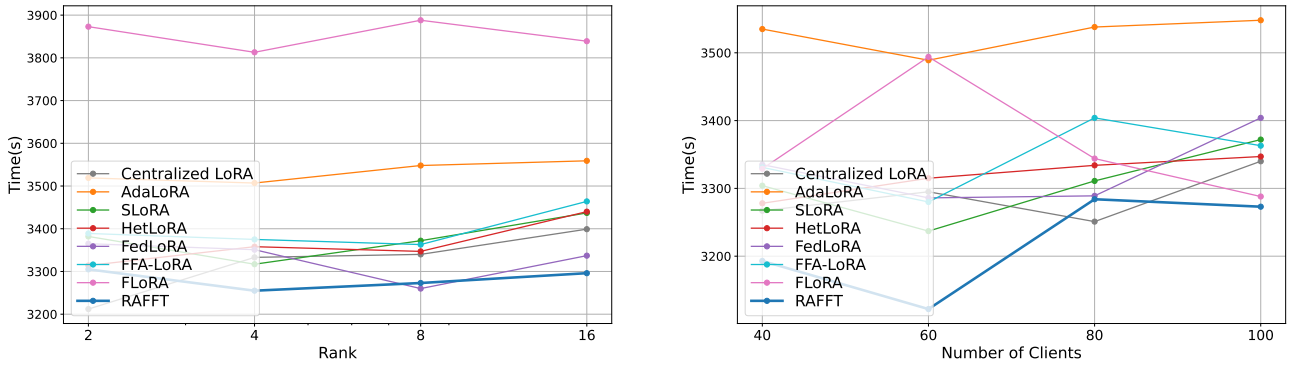


(b) Time (d) Time

Figure 7: Accuracy and Time (s) with various LoRA ranks and client numbers on ViT-CIFAR-100

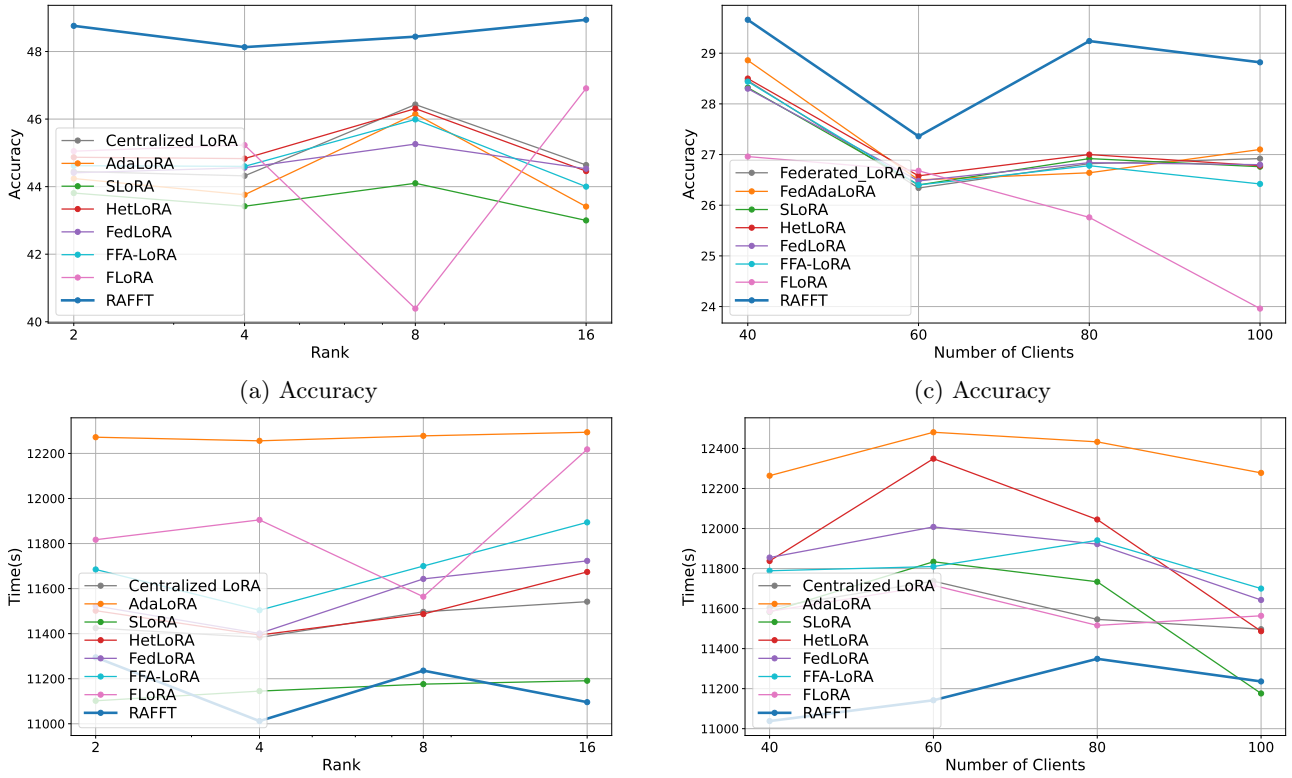


(a) Accuracy (c) Accuracy

(b) Time (d) Time

Figure 8: Accuracy and Time (s) with various LoRA ranks and client numbers on ViT-Tiny-ImageNet

### A.9 Potential Negative Societal Impacts and Limitations

In this work, the three large language datasets Socher et al. (2013); Dolan and Brockett (2005); Wiebe et al. (2005) and the three image classification datasets are open-release datasets allowing researchers to use them for non-commercial research and educational purposes. These three datasets are widely used for training/evaluating text classification. All baseline code is open access from GitHub and is licensed under the MIT License, requiring only that the copyright and license notices be retained, and containing permissions for commercial use, modification, distribution, and private use. To the best of our knowledge, this work is the first to theoretically verify the possibility of solving aggregation noise and ranking drift through Riemannian manifold theory. Compared with existing FedPEFT technology, this work explores the equivalence between the theoretical LoRA-based ranking adaptive federated learning method for base model fine-tuning and the standard federated base model federated fine-tuning method. Our model can be used for various large model fine-tuning tasks that require low latency and energy consumption in resource-intensive scenarios. This paper is primarily of a theoretical nature. We expect our findings to produce positive environmental impact, i.e., significantly improve the efficiency and scalability of federated large model fine-tuning by reducing the time and space requirements of large model fine-tuning in federated learning scenarios during training and testing. To our best knowledge, we do not envision any immediate negative societal impacts of our results, such as security, privacy, and fairness issues. An important product of this paper is the theoretical exploration to verify the feasibility of addressing aggregation noise and rank drift through Riemannian manifold theory. Given the large scale of neural networks in practical scenarios and the limitations of current computational hardware, we employ approximate methods for Riemannian distance. This ensures that the rank-adaptive federated learning method based on LoRA for fine-tuning foundation models is equivalent to the standard federated fine-tuning of foundation models on a fully parameterized FedAvg matrix. Our theoretical framework can inspire further improved development and implementations on FedPEFT with better applicability and efficiency from the academic institutions and industrial research labs.

### A.10 Notation Definition

Below, we provide detailed definitions of the notations used in the main text:

Table 38: Definitions of Notations

| Notation | Explanation |
|---|---|
| $\mathbf{W} \in \mathbb{R}^{m\times n}$ | Full parameter matrix of the foundation model |
| $\mathbf{W}^k \in \mathbb{R}^{m\times n}$ | Local model parameter matrix for client $K$. |
| $\mathbf{W}_0 \in \mathbb{R}^{m\times n}$ | Pre-trained foundation model parameters |
| $\Delta\mathbf{W} \in \mathbb{R}^{m\times n}$ | Adapter parameters, used for fine-tuning |
| $\Delta\mathbf{W}^k \in \mathbb{R}^{m\times n}$ | Adapter parameter matrix for client $K$ |
| $\mathbf{U}^k \in \mathbb{R}^{m\times r}$,$\mathbf{V}^k \in \mathbb{R}^{r\times n}$ | Matrices representing the left and right singular vectors of $\Delta\mathbf{W}^k$ |
| $\mathbf{\Sigma}^k \in \mathbb{R}^{r\times r}$ | Diagonal matrix containing the singular values of $\Delta\mathbf{W}^k$ |
| $\mathbf{B} \in \mathbb{R}^{r\times n}$,$\mathbf{A} \in \mathbb{R}^{m\times r}$ | Low-rank matrices representing adapter parameters$\Delta\mathbf{W} = \mathbf{BA}$ |
| $r \in \mathbb{R}^{r\times r}$ | Rank of decomposition, much smaller than $m$ and $n$ |
| $D = \{D_1, \cdots, D_K\}$ | The set of local training data from $K$ clients |
| $K$ | The total number of clients involved in federated learning |
| $n^k$ | The size of the local dataset $D_k$, i.e., $n^k = \lvert D_k\rvert$. |
| $n$ | The size of the total training data $\mathbf{D}$, i.e., $n = n_1 + \cdots + n_K$. |
| $\mathcal{L}(\mathbf{W})$ | The global loss function to be minimized, aggregated over all clients. |
| $L^k(\mathbf{W})$ | The loss function for client $K$. |
| $l_i(\mathbf{W})$ | The loss function for a single data sample $\{x_i, y_i\}$ |
| $S$ | The set of orthogonal matrices on Riemann manifold |
| $S_p$ | The procrustes representation space on manifold $S$ |
| $\mathbf{R}^k \in \mathbb{R}^{r\times r}$,$\mathbf{S}^k \in \mathbb{R}^{r\times r}$ | The symmetric positive matrix for Riemannian parameter matching. |
| $\mathbf{P}^k \in \mathbb{R}^{m\times r}$,$\mathbf{\Lambda}^k \in \mathbb{R}^{r\times r}$, $\mathbf{Q}^k \in \mathbb{R}^{r\times n}$ | Matrices obtained from the SVD of $(\mathbf{U}^1)^T\mathbf{U}^k$ |
| $\mathbf{Y}^k$, $\mathbf{Z}^k$ | Auxiliary variables introduced to reformulate the Riemann problem. |
| $\tilde{\mathbf{U}}^k \in \mathbb{R}^{m\times r}$,$\tilde{\mathbf{V}}^k \in \mathbb{R}^{r\times n}$ | Matrices representing the aligned parameters after Riemannian matching |
| $\tilde{\mathbf{\Sigma}}^k$ | Modified version of diagonal matrix $\mathbf{\Sigma}^k$ for ensuring consistency |
| $\lambda_{R_{\min}}, \lambda_{R_{\max}}$ | Minimum and maximum eigenvalues of the matrix $\mathbf{R}^k$ |
| $\lambda_{S_{\min}}, \lambda_{S_{\max}}$ | Minimum and maximum eigenvalues of the matrix$\mathbf{S}^k$ |
| $H, N$ | Constants bounding the Frobenius norms of matrices $\lambda_{R_{\min}}$ and $\lambda_{S_{\min}}$ |
| $\Theta(r)$ | Singular value contribution rate |
| $\varphi$ | Threshold value for determining rank |
| $R(\mathbf{U}^k, \mathbf{V}^k)$ | Regularization term to enforce orthogonality of $\mathbf{U}^k$ and $\mathbf{V}^k$ |
| $M$ | The set of fixed rank matrices on Riemann manifold |
| $T_M$ | Tangent space of the Riemannian manifold $M$ at the point $\Delta\mathbf{W}$ |
| $\mathbf{G} \in \mathbb{R}^{r\times r}, \mathbf{U}_p^k \in \mathbb{R}^{m\times r}, \mathbf{V}_p^k \in \mathbb{R}^{n\times r}$ | The tangent vector at $\Delta\mathbf{W}$ |
| $\mathbf{U}_\perp^k$,$\mathbf{V}_\perp^k$ | The orthogonal complements of $\mathbf{U}^k$ and $\mathbf{V}^k$ |
| $\nabla L^k(\Delta\mathbf{W}^k)$ | Gradient of the local objective function $L^k$ in Euclean space |
| $\Gamma L^k(\Delta\mathbf{W}^k)$ | Riemannian gradient of the local objective function $L^k$ |
| $P$ | Orthogonal projection |
| $\Gamma_{\mathbf{U}^k} L^k$, $\Gamma_{\mathbf{\Sigma}^k} L^k$, $\Gamma_{\mathbf{V}^k} L^k$ | The components of the Riemannian gradient at$\Delta\mathbf{W}^k$ |
| $\eta_t$ | Learning rate |
| $f()$ | Retraction function |
| $t$ $(0 \le t \le C)$ | Federated learning round |
| $c_g$ | Geodesic smoothness constant for the function $L^k$ |
| $\zeta$ | Key geometric constant that captures the impact of the manifold's curvature |